Università di Napoli "Federico II"

Applied and fundamental physics

PhD Thesis

XXII Cycle

Aircraft noise predictions in realistic operative conditions

Tutors:

D. Casalino,

Senior Research Engineer at CIRA

P. Maddalena,

Professor at Federico II University

Candidate:

Francesco P. Adamo

Researcher Dott. at CIRA

November 22, 2010

Contents

Introduction

Aeroacoustics is the unification of fluid dynamic and acoustic phenomena. Acoustics can be considered as the small pertubation limit of fluid dynamics because the unsteady motion of a compressible fluid often includes small amplitude unsteady disturbances. These perturbations decay very slowly with distance from the region where the flow is significantly different from its ambient state. Far from their "source", where the term source means a more or less clearly defined region where the fluid dynamic processes which generate the sound are confined, these disturbances are irrotational and isentropic, and propagate at a certain fixed velocity with respect to an uniform ambient fluid. These distubances can be detected by a microphone, and, within a certain frequency range, by the human ear.
The field of aerodynamic sound has evolved around two fundamental problems raised by the above empirical observation. The first is to derive a physically accurate and mathematically rigorous definition of what is "sound". The second one is to predict the amount of sound produced by the fluid dynamic processes, trying to unify different scales: the acoustic scale characterized by small pertubation and long range, and the fluid-dynamic scale with large pertubation and confined region.
The necessity of developing a science which explain the production and the generation of sound was born because aircraft and aero-engine manufacturers are exposed to a continuously growing demand for quieter aircraft. This is

due on one hand to the increased community expectation for quality of life, and on the other side to the necessity to compensate both the growth in air traffic and the encroachment of airport-neighboring communities.

Since the first theoretical work by James Lighthill in 1952 on sound generated aerodynamically[1][2] that led to the first predictive model of jet noise, many progresses have been made in the physical understanding of several aeroacoustic mechanisms and their mathematical representation.

The growth in the theoretical description of many aeroacustics mechanisms in the past fifty years has been accompanied by a progressive reduction of aircraft noise. Since the Sixties the historical aircraft noise trend shows a reduction of about 20 EPNdB[1], mostly due to the progressive introduction into service of high-bypass turbofans and more effective nacelle acoustic treatments. Since the Eighties, however, the noise reduction trend has not been so significant. Therefore, any further noise reduction is very difficult to be achieved without affecting the aircraft operating cost.

Due to the progresses achieved in reducing the propulsive noise and due to the expected reduction with the entry into service of ultra high-bypass ratio turbofans and novel noise control devices, on modern civil aircraft the engine noise is expected to be comparable and even lower than the airframe noise generated by the high-lift devices and by the undercarriage.

From these considerations it is clear that aircraft manufacturers have to comply with a new emerging necessity: the enviromental concern, in terms of acoustic and chemical pollution, must be considered as a driving factor in the design and operation of any new commercial aircraft. In other words, the preliminary design of an aircraft is the result of re-defined tradeoffs between operating costs and environmental performances, in a multi-disciplinary framework involving aircraft operational factors, aircraft/engine performances, airframe/powerplant noise modeling, powerplant emission modelling, and oper-

[1]Effective Perceived Noise Levels.

ational costs.
Since multi-disciplinary/multi/objective optimization processes relies on fast numerical methods, a great deal of interest have been devoted during the last years to the re-discovery and improvement of analytical models for both airframe and powerplant noise prediction.
The goal of this thesis is to provide a literary review on the subject of different aircraft noise sources using analytical, semi-analytical or empirical models. In fact, though significant progress has been made in computational power and numerical simulation methodologies in recent years, the solution of flow field, and hence, the computing of the noise field, often is still not a practically feasible task. An analytical/semi-analytical or empirical treatment is, hence, very useful.
In this work we have focused our analysis on three different aircraft noise sources: the jet noise (turbulence problem), the propeller noise (tonal noise) and the landing gear noise (airframe noise). This thesis is divided into five chapters. In chapter 1 an overview of the main kind of aircraft noise sources is provided. In chapter 2 we will give the mathematical instruments needed for a noise analysis (Navier-Stokes equations and acoustic analogy). In chapter 3 we will perform the noise analysis of a jet, in subsonic and supersonic regime. The analysis is performed with two semi-analytical model for subsonic jet and a semi-analytical model in supersonic regime. In chapter 4 we will perform an analytical treatment of the propeller noise, focusing our attention on a typical regional propeller, as requested by an international project named Pplane (Personal plane). In chapter 5 an empirical model for the landing gear and based on Boeing data is treated. Finally, in last chapter, we will have the concluding remarks.

Chapter 1

Aircraft noise sources

1.1 Introduction

In this chapter an overview of main aircraft noise sources is provided. The noise sources treated are: airframe noise, consisting of trailing-edge noise, flap-side edge noise, slat/flap cove noise and landing gear noise; the propeller noise and jet noise in subsonic and supersonic regime[4].

1.2 Airframe noise

The aerodynamic noise generated by all the non-propulsive components of an aircraft is classified as airframe noise. For modern high-by pass engine powered commercial aircraft, the airframe noise represents the main contribution to the overall flyover noise levels during landing approach phases, when the high-lift devices and the landing gear are deployed. Five main mechanisms are recognized to contribute significantly to the airframe noise: (i) the wing trailing-edge scattering of boundary-layer turbulent kinetic energy into acoustic energy, (ii) the vortex shedding from slat/main body trailing-edges and the possible gap tone excitation through nonlinear coupling in the slat/flap

coves, (iii) the flow unsteadiness in the recirculation bubble behind the slat leading-edge, (iv) the roll-up vortex at flap side edge, (v) the landing-gear multi-scale vortex dynamics and the consequent multi-frequency unsteady force applied to the gear components. All these mechanisms have been addressed both experimentally and theoretically since the Seventies. In the following paragraphs we describe the physical origin of all these sources and we give a brief overview of the state of the art.

1.2.1 Trailing-edge noise

The main source of airframe noise is represented by the wing trailing-edge noise. A solid surface immersed in a turbulent flow has a dual influence on the radiated acoustic field. On one hand, it affects the structure of the flow field and, consequently, of the aeroacoustic sources. On the other hand, it constitutes an acoustic impedance discontinuity which affects the scattering of the acoustic waves. The noise from a trailing-edge is a singular problem for which a wrong separation of these two effects can lead to wrong theoretical results.

A trailing-edge in a fluctuating flow field generates an unsteady vortical wake. This phenomenon can be regarded as an unsteady boundary-layer separation due to the fluid viscosity. An inviscid model of the vortex shedding process consists in prescribing an edge condition. Since the vortex shedding smears the singular behavior of the flow at the trailing-edge, a Kutta[1] condition is commonly imposed at the trailing-edge, which requires that the flow velocity is finite at the edge. The physical relation between the smoothing effect due to the vortical wake and the Kutta condition is not completely clear. The experimental works of Archibald[5] and Satyanarayana and Davis[6],

[1]The Kutta condition states that a body with a sharp trailing edge which is moving through a fluid create on itself a circulation of sufficient strength to hold the rear stagnation point at the trailing edge.

for example, show that the Kutta condition is only partially fulfilled at the trailing-edge of an airfoil in a high-frequency perturbed field. A viscous flow, in fact, has a characteristic relaxation time over which the flow reacts to an imposed disturbance. If this relaxation time is greater than the characteristic period of the perturbation field, the flow would not have enough time to fully satisfy the Kutta condition. From these preliminary considerations it follows that the aeroacoustic sources are significantly affected by the hypothesis made on the behavior of the flow at a trailing-edge.

This is a first difficulty in modeling the trailing-edge noise. Another difficulty lies on the fact that an edge does not distinguish between an acoustic and a vortical disturbance. As a result, the unsteady pressure field induced by the wake itself can couple with the vortex shedding process causing an increase of the noise levels. A further difficulty is related to the refraction effect of a boundary shear flow. This imposes some restrictions on the applicability of an acoustic analogy model that requires a clear separation between the vortical aeroacoustic sources and the diffracting effects due to the edge. Depending on the strategy used to face these difficulties, different theoretical results have been obtained in the past. Crighton[7], following the work of Orszag and Crow[8], investigated the interaction between an acoustic incident field, an unstable shear layer and a flat-plate trailing-edge. He showed that, at low Mach numbers, a Kutta condition induces a change in the flow velocity dependence of the acoustic intensity from U_∞^4 to U_∞^2 , provided that the vortex-sheet is unstable. Jones[9] investigated the diffraction of the acoustic field generated by a source near the edge of a semi-infinite flat-plate. He concluded that the Kutta condition generates an intense beaming effect along the plane of the plate. Crighton and Leppington[10] did not obtained significant effects on the acoustic radiation due to the Kutta condition. Davis[11] investigated the effect of the Kutta condition on the flat-plate problem and concluded that, without a Kutta condition, the far-field noise

exhibits a $sin^2(\theta/2)$ directivity pattern and a U_∞^3 acoustic power law. Conversely, with a Kutta condition, a beaming effect along the wake takes place and the noise intensity level increases as U_∞. Howe[14], in his comprehensive review work, pointed out that both Crighton[7] and Davis[11] analysis were erroneous since not compatible with a far-field wave radiation condition. Howe[12] demonstrated that the imposition of the Kutta condition removes the flow singularity at a sharp edge. As a consequence, it always leads to a reduction of the noise levels. The wake intensity, in fact, is related, both in amplitude and phase, to the incident vortical disturbances and generates a sound field which cancels the one generated by the incident turbulent field.
A different view of the trailing-edge problem consists in focusing separately on the acoustic scattering properties of the edge, and the fluctuating pressure field close to the edge. Ffowcs Williams and Hall[16] and Crighton and Leppington [18][19] examined the scattering problem in the context of Lighthill' s acoustic analogy theory. They related the acoustic far field to the turbulent quadrupole sources. Chase[20] and Chandiramani[21] proposed a procedure to relate the far-field acoustic spectrum to measurable statistical properties of the hydrodynamic pressure field in proximity of the edge. These properties are formally synthesized by the wavenumber/frequency spectrum of the driving pressure field. Rienstra[22] examined the half-plane scattering problem of an acoustic incident field in the presence of a vortex-sheet shed from the trailing-edge. He showed that the vortex shedding process extracts energy from both the incident acoustic field and the mean flow, thus reducing the far-field noise intensity. However, the interaction between the trailing-edge and the unsteady pressure field induced by the wake generates a noise radiation whose energy may exceed that absorbed by the wake.
Crighton[7], using the method of matched asymptotic expansions, determined the noise radiated by a line-vortex convected past the edge of a semi-infinite flat-plate under the influence of its image vortex. The intensity of the acous-

tic field driven by the vortex-induced hydrodynamic field was demonstrated to have a $sin^2(\theta/2)$ directivity pattern and a third power dependence on the flow velocity. The latter result was in agreement with the general result obtained by Ffowcs Williams and Hall[16] and Crighton and Leppington[18] according to which the effect of the interaction between a fluctuating turbulent flow and the edge of a semi-infinite plate is to increase the far-field acoustic intensity by a factor M_∞^3. In fact, the acoustic energy radiated by a vortex filament in free space or in the presence of an infinite rigid plate follows a sixth power law.

Amiet[23] related the acoustic spectrum to the wall pressure spectrum through an airfoil response function. In order to use a wall pressure distribution with the same characteristics it would have in the absence of the trailing-edge, he assumed that the turbulence was statistically stationary when convected past the trailing-edge. A concentrated dipole sources induced by the turbulent flow near the trailing-edge was used to model the noise radiation. The airfoil response function used by Amiet was obtained under the assumption that, at high frequency, as relevant for a trailing-edge noise problem, the leading- and trailing-edge noise scattering can be taken into account separately in an iterative converging procedure. In recent years trailing-edge broadband noise models of Amiet type, involving iterative leading- trailing-edge corrections, have been developed and validated against experimental data in practical cases representative of airframes, wing turbines, helicopter blades and fan cooling systems by Roger and Moreau[24] [25].

Howe[13] investigated the general problem of the noise from an airfoil interacting with a frozenly convected turbulent eddy. By supposing a small flow Mach number $M_\infty^2 \ll 1$, he assumed an incompressible potential flow. The acoustic problem was then formulated in terms of Howe's[12] acoustic analogy theory describing the noise generated by vorticity and entropy gradients. In the limit of a frozen convection hypothesis Howe showed that, when

a line-vortex is convected past the edge of a half-plane, a Kutta condition results in a vortex shedding that exactly cancels the sound generated by the vortex-edge interaction. Furthermore, in the case of an acoustically compact airfoil, the effect of the vortex shedding is to cancel the field diffracted by the trailing-edge. Since the fulfillment level of the Kutta condition decreases as the frequency of the perturbation flow increases, the effectiveness of the vortical wake in reducing the radiated noise decreases at higher frequency. As a consequence, a trailing-edge in a turbulent flow acts as a source of high-frequency noise. Howe[14] revisited the problem of the trailing-edge noise and formulated a generalized theory. This includes, as special cases, the models developed by Ffowcs Williams and Hall[16], Crighton[7], Chase[20] and Chandiramani[21]. All these models were shown to give essentially the same results when properly interpreted. In particular, the so-called cardioid $sin^2(\theta/2)$ directivity law and the fifth power scaling law of the acoustic intensity on the free-stream velocity were recovered. Moreover, Howe investigated the influence of the Kutta condition on the noise levels by assuming a wake convection velocity w which differs from the convection velocity v of the vortical disturbances within the boundary-layer. He found that the effect of the Kutta condition is to reduce the sound pressure level by a factor $(1 - w/v)^{-2}$, which diverges when the Kutta condition is fully satisfied (w = v). A first experimental validation of the trailing-edge noise theory by Howe was carried-out by Brooks and Hodgson[26] who measured the noise generated by a NACA-0012 airfoil in a low Mach number flow at several angles of attack and with different degrees of edge bluntness. The airfoil was provided of roughness trips on both its sides in order to ensure a well developed turbulent boundary-layer. In order to investigate the vortex shedding process in terms of wake convection velocity w, as proposed by Howe[14], Brooks and Hodgson carried-out coherence measurements between a cross hot wire just downstream of the edge and a wall pressure transducer close to the edge. No

vortex shedding was detected. From this result and the verified consistency of the evanescent wave model proposed by Chase[20] in the edge region, they concluded that a vanishing wake velocity can be used in the trailing-edge noise model. In addition a good agreement with the theoretical U_∞^5 acoustic power law and the $sin^2(\theta/2)$ directivity pattern was found.

1.2.2 Flap side-edge noise

One of the most effective sources of airframe noise at takeoff and landing conditions is due to the vortical flow around the side edge of a deployed flap. The physical mechanism of flap side-edge noise generation can be described as follows. The pressure jump across the upper and lower surfaces of the flap creates a recirculating flow around the side edge. The shear layer detaches at the side edge of the flap and rolls up to a single vortical structure. This is responsible for two noise generation mechanisms: the first is due to a direct interaction between the shear layer fluctuations and the sharp edge, the second is due to the induction of unstable oscillation modes in the vortical structure. In addition, vortex breakdown has been observed at high flap angles as an additional noise source mechanism.

The problem of sound generation by the vortex roll-up about a deflected side-edge has been investigated analytically by Hardin[27] and by Howe[15]. The model put forward by Hardin is based on the analogy according to which, the transient streamwise vortex roll-up can be seen, in a plane normal to the edge and the flow direction, as a two-dimensional vortex that is swept around the edge of half-plane under the effect of self induction. The model presents strong analogies with the trailing-edge noise model proposed by Crighton[7] and therefore suggested the same U_∞^5 acoustic power law and the same $sin^2(\theta/2)$ directivity pattern. A drawback of this analytical model is that, not only the hydrodynamic field, but also the driven acoustic field is as-

sumed to be two-dimensional. A different model was proposed by Howe[15]. By using an acoustic analogy approach, he separated the sound generation mechanisms from the acoustic edge scattering problem. Thus he represented all the involved vortex dynamic processes in terms of a prescribed statistical surface pressure distribution, and focused on the Greens function of a simplified geometrical configuration. In particular, he obtained analytical expression for a finite chordwise slot in a wing with an otherwise straight trailing-edge, both in the low- and high-frequency limit. The most important result obtained by Howe is that the radiation efficiency of the side-edge sources is greater for low values of the dimensionless frequency referred to the slot clearance and the spanwise flow velocity. This is because, at low frequency the sound generation mechanism is well represented by a dipole type source, whereas at high frequency the sound generation mechanism is dominated by a monopole-type source that reproduces the mass flux through the slot.

1.2.3 Slat/flap cove and trailing-edge noise

While the dominant sound generated by a slat wing component is of broadband nature and due to the flow recirculating bubble behind the leading-edge and to turbulence convected past the trailing-edge through the gap, there exists a certain experimental evidence of tonal noise radiation. This is commonly attributed to the vortex shedding from the blunt trailing-edge. In certain cases, however, a surprisingly high tone have been observed, that disappears when the slat deflection angle is slightly modified. This behavior was attributed by Khorrami et al.[28] to a feedback loop between the slat trailing-edge and the main wing surface which drives the vortex shedding frequency. A numerical demonstration of the gap whistle generation has been pursued by Tam and Pastouchenko[29]. The predicted tone frequencies was

shown to agree fairly well with a simple algebraic model of feed-back loop based on the principle of causeeffect phase compatibility.

1.2.4 Landing-gear noise

The sound generation mechanism from a landing-gear is due to the vortex-force generated by the quasi-periodic unsteady flow separation behind the different structural components. The mechanism is similar to the so-called Aeolian tones generation from circular cylinders, but complicated by the simultaneous shedding from bodies of different size and shape, and by the mutual vortex interactions. The resulting noise is of broadband nature, spanning over a wide interval in the audibility range. The dipolar character of the source mechanism results in U_∞^6 acoustic power scaling law. However, due to acoustic installation effects, a destructive interference of sound generated by dipoles in the vertical plane, i.e. generated by vorticity vector components parallel to the reflecting airframe panels, may occur, thus resulting in a quadrupole source degeneration and a corresponding U_∞^8 acoustic power scaling law. Several semiempirical models have been developed by aircraft manufactures both in the US and Europe. The Airbus model, for instance, has been recently applied to evaluate the impact of a low noise gear on the overall airframe noise[30]. A further installation aspect that should be addressed in landing-gear noise modeling is the excitation of some cavity mode in the wheel wells. Three different mechanisms of tonal noise response of a cavity flow exist. The first one is due to a feedback cycle generated by the coupling between the waves generated when the shear layer vortical fluctuations impinge on the downstream edge, and the vortex shedding from the upstream edge. The second mechanism involves a volume mode fluctuation of the recirculating bubble induced by a coupling with a standing wave across the width or along the length of the cavity. The third mechanism

is a Helmholtz resonation occurring when the flux mass across the cavity neck balance the fluid volume stiffness. A complete review of self-sustaining mechanisms in cavity flows is a Helmholtz resonation occurring when the flux mass across the cavity neck balance the fluid volume stiffness.
In the chapter 5 we will use a semi empirical method, the Guo model, in order to give an estimation of the noise from landing gear.

1.3 Propeller noise

A propeller can be generally described as an open (unshrouded), rotating, bladed device. Although there are many differences in details among various designs and applications, such as number of blades, blade shape, and airfoil section, the noise-generating process is basically the same for all. The major propeller noise components are thickness noise (due to the volume displacement of the blades), steady-loading noise (due to the steady forces on the blades), unsteady-loading noise (due to circumferentially nonuniform loading), quadrupole (nonlinear) noise, and broadband noise. Although the relative importance of these sources depends on design and operating conditions, defining them will completely describe the acoustic signature of a propeller.

One important consideration is the effect of installation on the noise produced by a propeller. This effect is essentially the difference between the laboratory environment and the real world. It is generally assumed that in a laboratory environment conditions are ideal, that is, the propeller is operating in perfectly uniform flow. For an operational propeller, this is never the case. Propellers are always operating in a flow field that has some distortion. This can be from the wing upwash, the pylon wake, the airplat angle of attack, or the inflow turbulence. Since this distortion leads to additional noise, it is a factor which must be considered in defining the total noise of

an operational propeller.

In this chapter the characteristics of propellers and their noise-generating mechanisms are described.

1.3.1 General Characteristics of propellers

A propeller is an open rotor having fixed or adjustable-pitch blades. The blades are designed to produce a region of low pressure on one side and high pressure on the other. The resulting forces induce air from the front and push it back, resulting in thrust. Because propellers impart a relatively small amount of velocity to a large mass of air, their efficiencies are high. However, the efficiencies of conventional propellers tend to fall off at high speed. This has led to a variation of the propeller called the propfan. The propfan is also an open rotor, but compared with conventional propellers it has a smaller diameter for a given thrust and has more blades, which are swept. To improve efficiency further a second rotor can be added behind a propeller, resulting in a counterrotating propeller.

A typical high-performance, modern propeller in widespread use on commuter airplanes is shown on the left-upper side of figure (1.1). These propellers have two to six relatively straight, narrow blades. Although this type of propeller is well-suited for moderate flight speed (below a Mach number of about 0.65), its performance decreases at higher , flight speeds. The primary limitation of this propeller is associated with high drag at high speed due to blade thickness and large relative blade section speed.

The propfan, shown on right-upper side of figure (1.1), has been developed to extend the practical flight envelope of the propeller. Compared with conventional propellers, the propfan has more blades (from 6 to 12), uses thin airfoils and swept blades to provide good aerodynamic performance at high speed, and operates at much higher power loading to reduce the diameter.

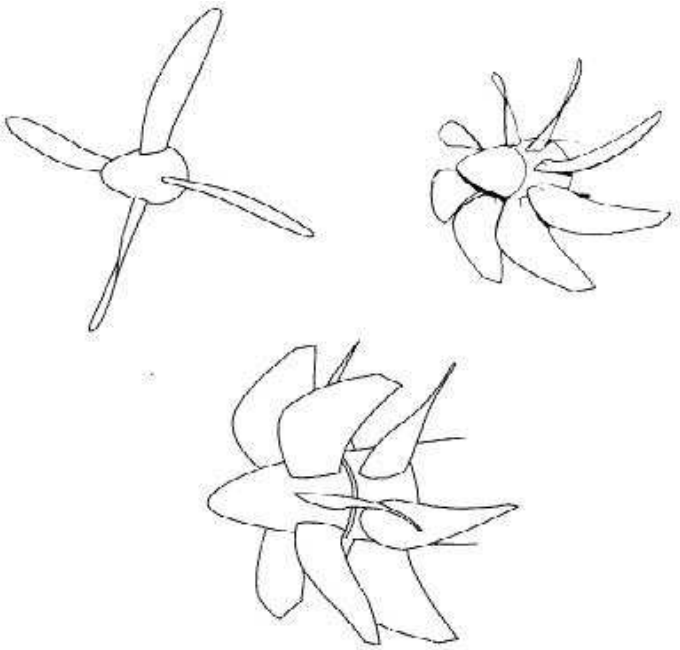

Figure 1.1: On upper side, on the left there is an high-performance low noise propeller for moderate flight-speed commuter airplane propulsion; on the right a propofan propulsion system for high subsonic cruise speed application. On the bottom a counterrotating propfan propulsion system for high subsonic cruise speed application.

One factor leading to loss of efficiency in propellers is swirl in the wake resulting from engine torque. Generation of swirl uses energy but does not contribute to thrust. The amount of swirl is related to the power loading. One concept to recover the swirl losses is to add a second blade row behind the first. This is shown on lower part of figure (1.1) for the propfan. The second blade row rotates in the direction opposite to that of the first, thus cancelling its swirl. This cancellation can result in performance increases of 8 to 10 percent compared with that of single rotation propellers[3].

1.3.2 Propeller Noise Characteristics

Propeller noise can be classified into three categories: harmonic noise, broadband noise, and narrow-band random noise.

Harmonic noise is the periodic component, that is, its time signature can be represented by a pulse which repeats at a constant rate. If an ideal propeller with B blades is operating at constant rotational speed N, then the resulting noise appears as a signal with fundamental frequency BN. The blade-passage period is $1/BN$. Typically the generated pulse is not a pure sinusoid, so that many harmonics exist. These occur at integer multiples of the fundamental frequency. The first harmonic is the fundamental, the second harmonic occurs at twice the fundamental frequency, and so on. Figure (1.2) illustrates the characteristics of harmonic noise in both the time and frequency domains.

Broadband noise is random in nature and contains components at all frequencies. A typical broadband noise signal for propellers is shown in figure (1.3). The frequency spectrum in continuous, although there may be a "shape" to it because not all frequencies have the same amplitude.

Narrow-band random noise is almost periodic. However, examination of the harmonics reveals that the energy is not concentrated at isolated frequen-

cies, but rather it is spread out. As illustrated in figure (1.4) the signal may appear periodic, but certain components do nolt repeat exactly with time. The frequency spectrum shows o discrete components, but these spread out, particularly at the higher frequencies.

1.3.3 Propeller Noise-Generating Mechanisms

The mechanisms which lead to the generation of the spectral characteristics discussed above are described in this section.

Steady Sources

Steady sources are those which would appear constant in time to an observer oil the rotating blade. They produce periodic noise because of their rotation. Noise sources are usually divided into three categories: linear thickness, linear loading, and (nonlinear) quadrupole

Thickness noise arises from the transverse periodic displacement of the air by the volume of a passing blade element. The amplitude of this noise component is proportional to the blade volume, with frequency characteristics dependent on the shape of the blade cross section (airfoil shape) and rotational speed. Thickness noise can be represented by a monopole source distribution and becomes important at high speeds. Thin blade sections and planform sweep are used to control this noise.

Loading noise is a combination of thrust and torque (or lift and drag) components which result from the pressure field that surrounds each blade as a consequence of its motion. This pressure disturbance moving in the medium propagates as noise. Loading is an important mechanism at low to moderate speeds.

For moderate blade section speed, the thickness and loading sources are linear and act on the blade surfaces. When flow over the blade sections is

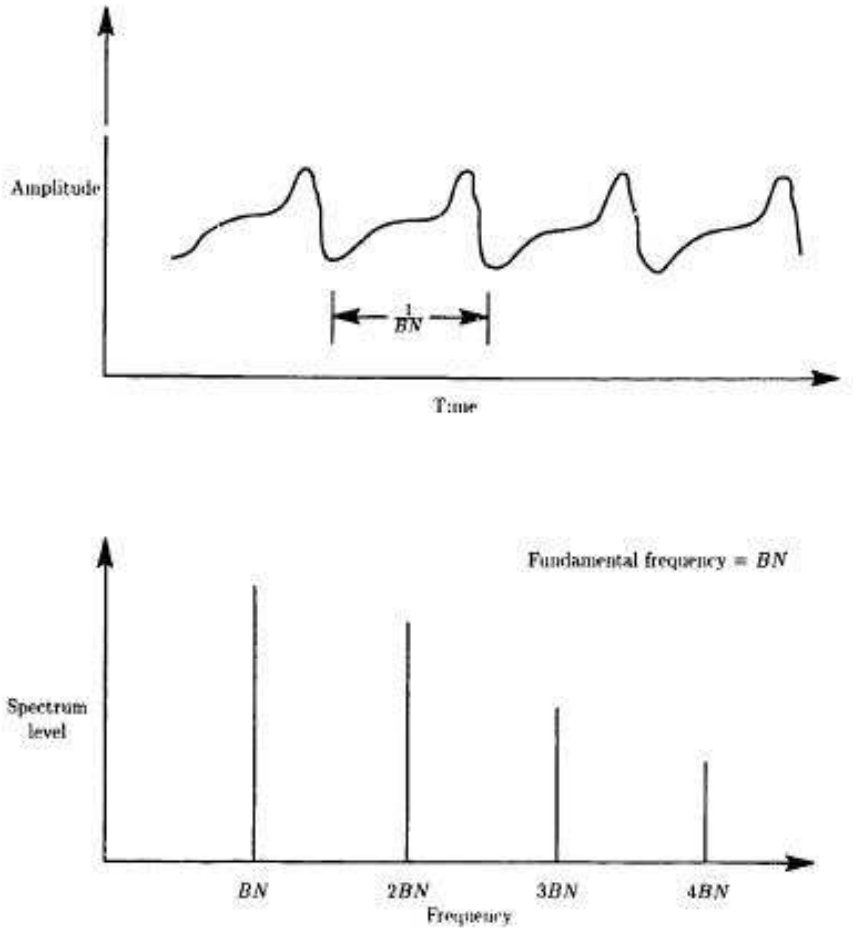

Figure 1.2: Characteristics of propeller rotational noise.

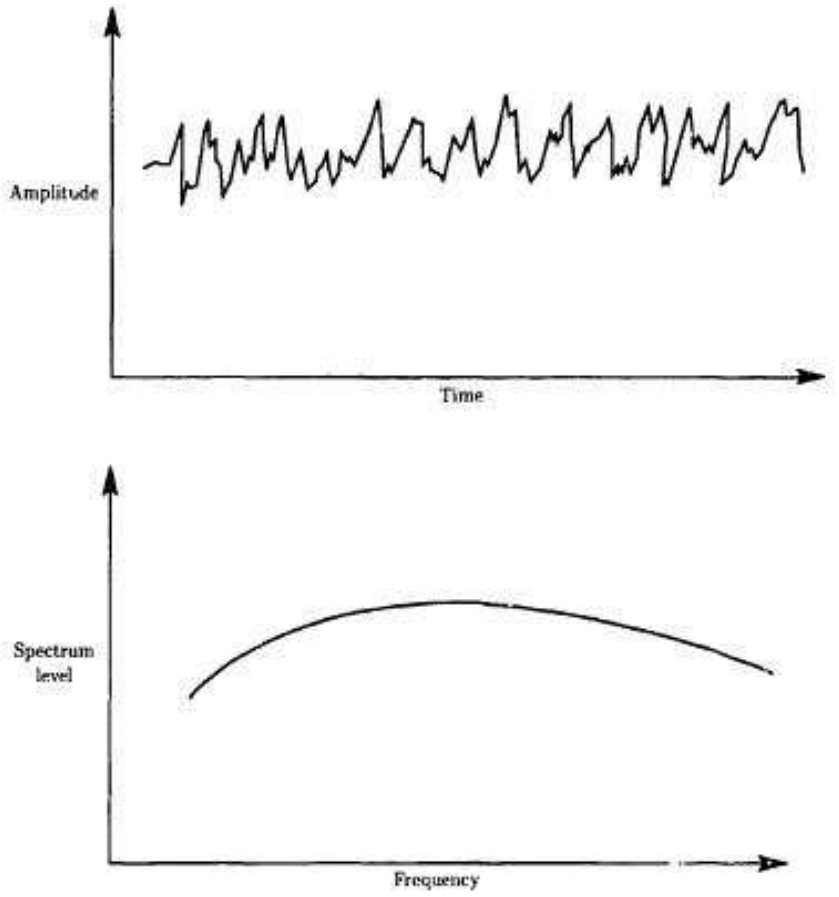

Figure 1.3: Characteristics of propeller broadband noise.

transonic, nonlinear effects can become significant. In aeroacoustic theory these can be modeled with quadrupole sources distributed in the volume surrounding the blades.

In principle, the quadrupole could be used to account for all the viscous and propagation effects not covered by the thickness and loading sources. However, the only practical application of this term to propeller acoustics has been its evaluation in the nonviscous flow close to the blade surface. At transonic blade section speeds the quadrupole enhances the linear thickness

and loading sources and causes a noise increase for unswept, high-tip-speed propellers and helicopter rotors.

Unsteady Sources

Unsteady sources are time dependent in the rotating-blade frame of reference. They include periodic and random variation of loading on the blades.

A typical example of periodic blade loading in propellers is the effect of shaft angle of attack. When the propeller axis is tilted relative to the inflow, each blade sees a cyclic change in local angle of attack. As a consequence, the loading on the blade vanes during a revolution. The loading change may be once per revolution or several times per revolution, depending on the source of inflow distortion. All inflow distortion which is invariant with time results in blade-loading changes which repeat exactly for every propeller revolution. The resulting periodic unsteady-loading noise occurs at harmonics of blade-passage frequency.

Depending on the circumferential location of the loading disturbance relative to the observer, unsteady-loading noise can add or subtract from the steady-loading noise. The noise directivity is no longer axisymmetric and a third coordinate is needed to define it. The circumferential directivity exhibits lobes-peaks and valleys-with the number of lobes dependent on the order of the distortion and unrelated to the number of blades. For example, a propeller behind a wing might show two circumferential directivity lobes regardless of the number of blades on the propeller.

Unsteady loading is an important source in the counterrotating propeller. Although the counterrotating propeller does not contain any additional or unique sources of noise, the aerodynamic interference between the two rotors gives rise to significant levels of unsteady-loading noise which are particularly significant at low flight speeds, such as during takeoff and landing. Each front rotor blade leaves a wake which convects into the rear rotor. (This wake can

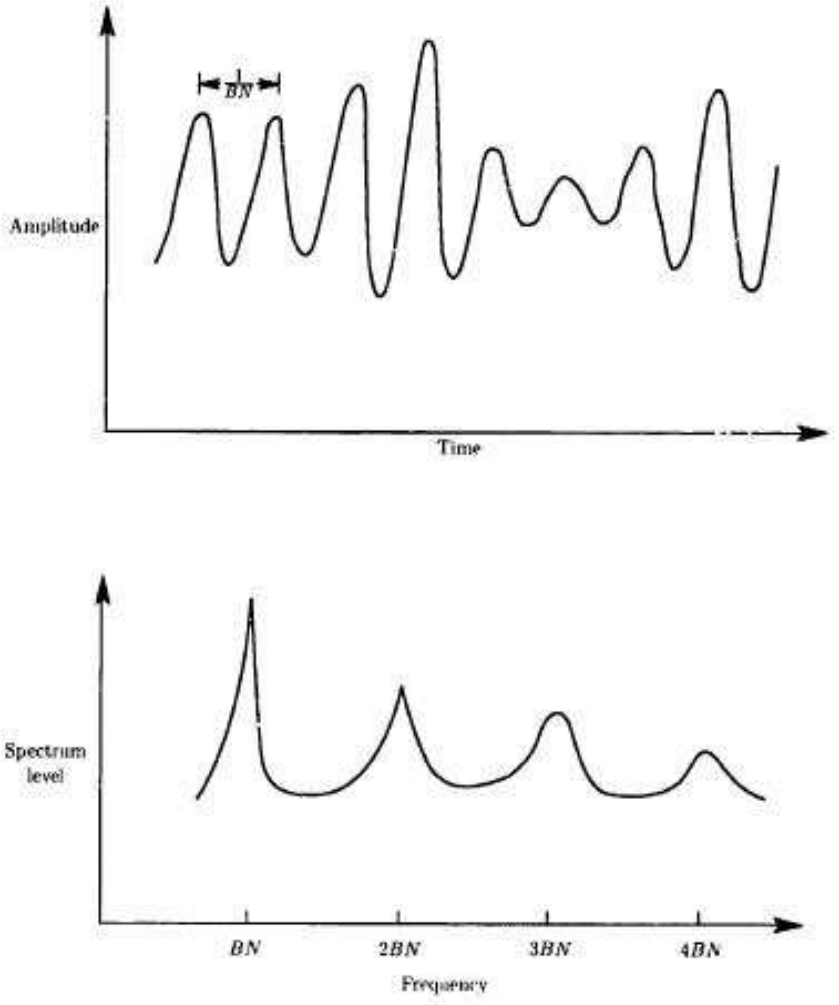

Figure 1.4: Characteristics of propeller narrow-band random noise.

be complex, consisting of downwash due to the lift on the blades, velocity deficits due to the drag of the sections, and tip vortices.) This convection results in a sequence of lift pulses on the rear rotor blades. Another mechanism is the potential field (due to blade loading,) of the rear rotor creating a disturbance which is felt by the aft part of the front rotor blades. The magnitudo of this source depends on the level of loading on the rear rotor and the spacing between the two rotors.

Because the wakes are periodic, the generated noise is also periodic. If the two rotors have the same number of blades and are operating at the same rotational speed, then the components of the steady sources and the unsteady sources are at the same frequencies and the noise spectra contain only harmonics of blade-passage frcquency. However, if the number of blades of the front rotor is different from that of the rear rotor or the two rotors operate at different rotational rates, then the individual interaction components (modes) are distinct in the noise spectra.

Figure (1.5) shows the importance of the aerodynamic interaction in a counterrotating propeller. On the upper side, the figure shows the spectra of single-rotating-propeller (SRP) noise at a forward directivity, near the plane of rotation, and at an aft directivity. It is readily apparent that there are no significant higher frequency harmonics. For comparison, noise spectra for a counterrotating propeller (CRP) are shown on the bottom of the figure. It is apparent that the counterrotating propeller has significantly higher levels of higher frequency harmonics. Figure (1.5) shows a direct comparison between the noise from the two types of propellers. In this comparison the two propellers were operating at equal tip speeds and power per rotor. Three decibels were added to the SRP noise levels to simulate the total power of the counterrotating propeller. If the two rotors of the counterrotating propeller were uncoupled, then the two spectra would be identical. In fact, the levels at the blade-passage frequency are very close. At the higher harmonics, the

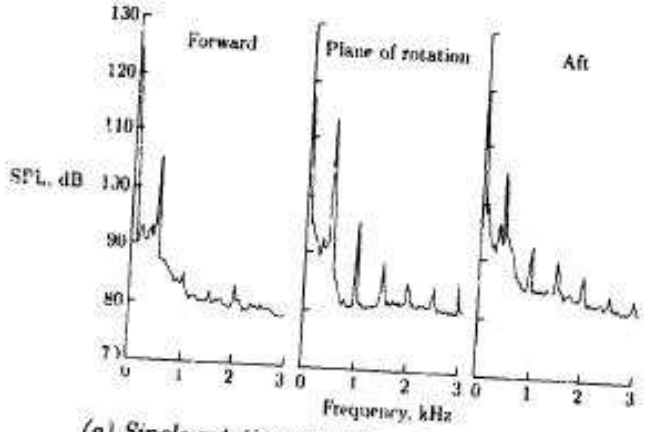

(a) Single-rotating-propeller noise spectra

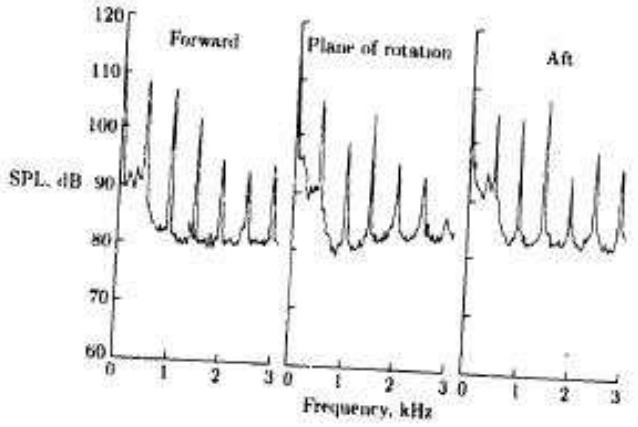

(b) Counterrotating-propeller noise spectra.

Figure 1.5: Aerodynamic interaction noise in a counterrotating propeller.

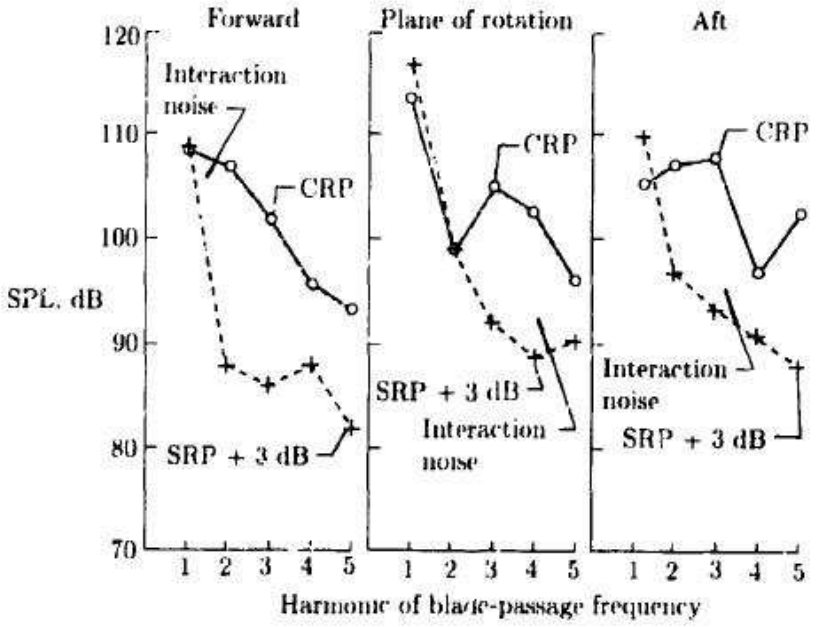

Figure 1.6: Aerodynamic interaction noise.

counter-rotating propeller shows significantly higher levels. This is a direct indication of the aerodynamic interaction effects on noise in counterrotating propellers.

Aerodynamic interaction is a significant source of noise for low-speed operation. At higher flight speeds, such as during cruise, the aerodynamic interaction becomes less important because the steady sources (thickness, steady loading, and quadrupole) become dominant.

Under certain conditions blade loading which is nearly periodic can occur. An example of this is the ingestion of a vortex, which could be induced by the propeller and attached to the fuselage or to the ground ahead of the propeller. In this example, a local distortion is induced by and drawn into the propeller. The blades chop through tne distortion and a blade-loading pulse is produced. Because the distortion can persist for several propeller revolutions,

the unsteady-loading noise can appear at blade-passage frequency harmonics. However, as conditions change, the location of the distortion changes and the amplitude and phase of the unsteady-loading noise change. These changes broaden the noise spectrum, as previously described for narrow-band random noise.

Random Sources

Random sources give rise to broadband noise. For propellers there are two sources which may be important, depending on the propeller design and operating conditions.

The first broadband noise source is the interaction of inflow turbulence with the blade leading edges. Because the inflow is turbulent, the resulting noise is random. The importance of this noise source depends on the magnitude of the inflow turbulence but it can be quite significant underconditions of high turbulence at low speeds.

In the second broadband mechanism, noise is generated near the blade trailing edge. A typical propeller develops a turbulent boundary layer over the blade surfaces, which can result in fluctuating blade loading at the trailing edge. The noise is characterized by the boundary-layer properties. A related mechanism occurs at the blade tips, where turbulence in the core of the tip vortex interacts with the trailing edge. It has been determined for full-scale propellers in flight that the broadband noise sources are relatively unimportant and do not contribute significantly to the total noise[3].

1.4 Jet noise

The main difficulty in the prediction of jet noise is due to the lack of a general theory describing the turbulent fluctuations in a jet flow. For this reason, a first principle jet noise theory is not yet available. The understanding of

jet noise as a study in aerodynamic noise had its foundations, however, in the work of Lighthill[1][2] on "sound generated aerodynamically." That work was complemented by several experimental studies[3]. These experimental studies not only verified Lighthill's eighth power law, but also confirmed the other broad features of the theory relating to convective amplification with Mach number and consequent changes in directivity and spectra.

In subsonic jets, the small-scale turbulence is believed to be the dominant source of noise. Even though large-scale coherent turbulent structures and instability waves have been observed in a wide range of Reynolds numbers, these structures are not effective aeroacoustic sources. However, they play a crucial indirect role on the jet noise generation, by enhancing the turbulent mixing and the consequent jet spreading.

In supersonic jets, even though a direct empirical evidence is difficult to be achieved, large-scale coherent turbulent structures and instability waves are believed to be very effective aeroacoustic sources.

The universal character of the small-scale turbulent fluctuations contributes to the success of predictive models based on the acoustic analogy theory. This models describe the mechanisms of mixing noise generation in subsonic jets. The same mechanisms are present in supersonic jets, but in this case other phenomena predominate. The convection of instability waves or coherent turbulent structures at supersonic speed is responsible for the generation of Mach waves. In addition, when shock cells are present in the jet plume, the interaction between shear layer vortical disturbances and the shocks generate a broadband shock associated noise. Finally, upstream propagating shock associated pressure disturbances can excite instability waves in the shear layer through receptivity mechanisms at the nozzle lip. As a consequence, a feedback coupling can occur with tonal noise selection and generation of the so-called screech noise.
Following we give an overview of the main sources cathegorized as jet noise.

Mixing Noise

From the publication of the first aeroacoustic theory by Lighthill in 1952 until the earlier Seventies, most of the analytical work on jet noise was focused on Lighthills acoustic analogy. The main result of Lighthills theory was the so-called eighth power law of the jet noise intensity versus the jet velocity. This law was confirmed through extensive experimental campaigns [183]. Further analytical improvements of Lighthills theory were mainly concerned with the extension to moving jets, the modeling of the turbulence correlation tensors and consequent removal of the Doppler singularity, the analysis of the mean flow convective effects and the description of the so-called Mach wave radiation occurring when vortical disturbances are convected at supersonic phase speed. Several reviews on this subject can be found in the references on literature[3]. A commonly accepted feature of the mixing noise from high-speed jet is that it consists of two components. The first one is associated with large-scale vortical fluctuations in the jet plume and is predominant in the aft quadrant close to the jet axis. The second component is associated with fine-scale turbulence and is predominant in the forward quadrant and at near-normal angles to the jet-axis. Due to the more universal character of small-scale turbulent fluctuations, this second mixing noise component can be predicted on the base of statistical turbulence models and acoustic analogy formulations.

Broadband Shock-Associated Noise

When a supersonic jet nozzle operates at adapted ambient conditions, no shock cells are generated in the plume. In this case, the only noise generation mechanisms is associated with the small-scale turbulence mixing noise and Mach wave radiation. The mixture of these two mechanisms is commonly referred to as supersonic turbulent mixing noise[3]. Two commonly observed

features of this noise generation mechanism are: the first is the high directionality, with downstream predominant radiation between 25° and 45° from the jet flow direction. Figure 6(a) shows a typical directional distribution of the SPL of turbulent mixing noise for cold supersonic jets (ratio of jet temperature to ambient temperature $T_j/T_0$of 0.73). As shown, the predominant part of the noise is radiated in the downstream direction. The peak value is about 25° from the jet flow direction. This maximum directivity angle θ varies as a function of Mach number and jet temperature.
The second characteristic is a broadband power spectral density spanning over about two frequency orders, with a very smooth peak separating a variation law as the square of the frequency on the left, from a variation law as the inverse of the frequency on the right. Figure 6(a) shows the directivity of the overall SPL of a fully expanded jet at a Mach number of 1.37 and a temperature ratio of 0.73[3].

The jet is practically shock-free so that this is the directivity of turbulent mixing noise. Also plotted in this figure is the directivity of overall SPL of an under expanded supersonic jet with the same full expanded Mach number and jet operating conditions. The noise from this underexpanded jet contains both turbulent mixing noise and broadband shock-associated noise. The differences in these two directivities, therefore, would provide a good estimate of the distribution of shockassociated noise. It is clear from this figure that shock-associated noise is important mainly in the forward direction of the jet.

When a supersonic jet is not operated at perfectly expanded conditions, a quasi-periodic shock cell pattern appears in the jet plume. The interaction between the vortical disturbances in the jet stream and the shock fronts generates additional noise, referred to as shock associated noise. The main property of this noise component is that its spectral peak frequency decreases

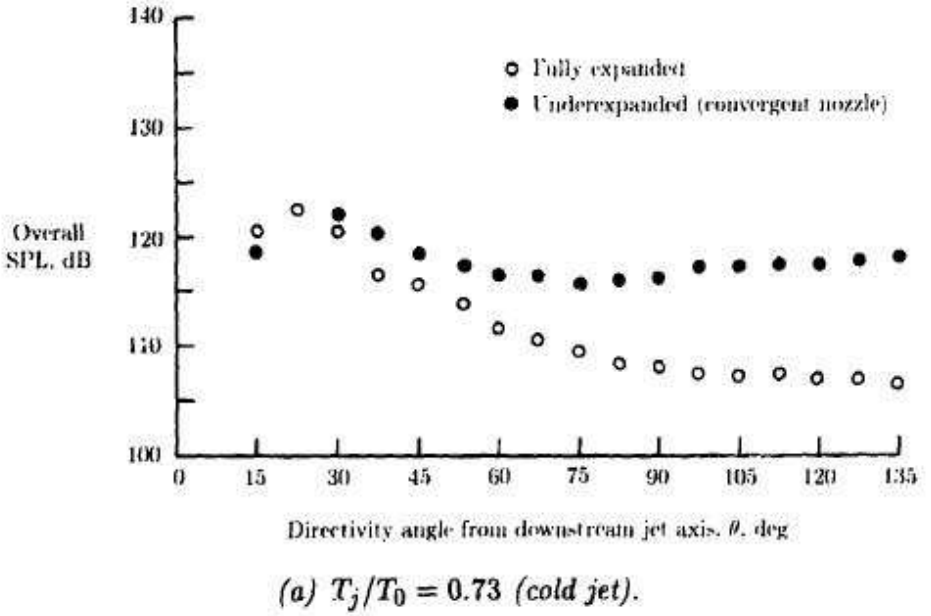

(a) $T_j/T_0 = 0.73$ *(cold jet).*

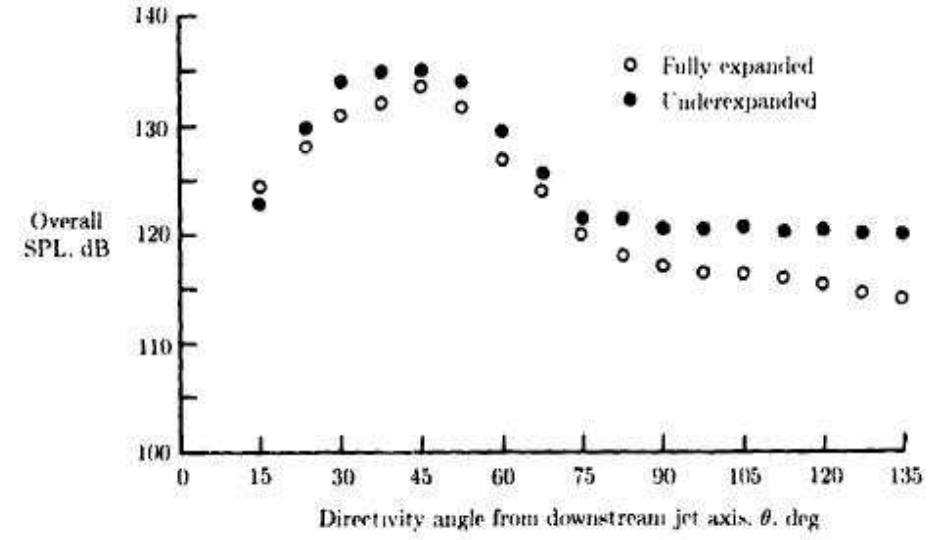

Figure 1.7: Directivity of overall sound pressure level with Mach number 1.37.

away from the downstream flow direction. In addition, the associated acoustic power level exhibits an opposite directivity behavior with respect to the mixing noise. As a consequence, the acoustic radiation in the jet rear arc, at observation angles greatest than 90°, is commonly dominated by the shock associated noise. This behavior has been described by a simple and elegant phased point-source array model by Harper-Bourne and Fisher[43], that we will discuss in great details in next chapters.

Mach wave radiation

Vortical disturbances frozenly convected through a sheared jet flow do not radiate sound until their phase velocity is supersonic. The phase velocity of a compact turbulent eddy is well represented by the eddy convection velocity. The pressure fluctuations driven by turbulent structures convected at supersonic phase speed interfere constructively in the direction of the angle between the normal to the Mach cone attached to the eddies and the direction of the convective motion, usually denoted as sonic angle. As described by Ffowcs Williams and Maidanik[31], the acoustic power associated with the Mach wave radiation scales as the cube of the jet velocity. As a consequence, a saturation process occurs when the jet velocity is increased from low subsonic values, at which the acoustic intensity scales as the eight power of the jet velocity, to high supersonic values, at which the acoustic intensity scales as the cube of the jet velocity.

ScreechTones

Unless a supersonic jet issuing from a convergent-divergent nozzle is operated very close to the nozzle design condition, its noise spectrum invariably consists of discrete and broadband components. The discrete components are

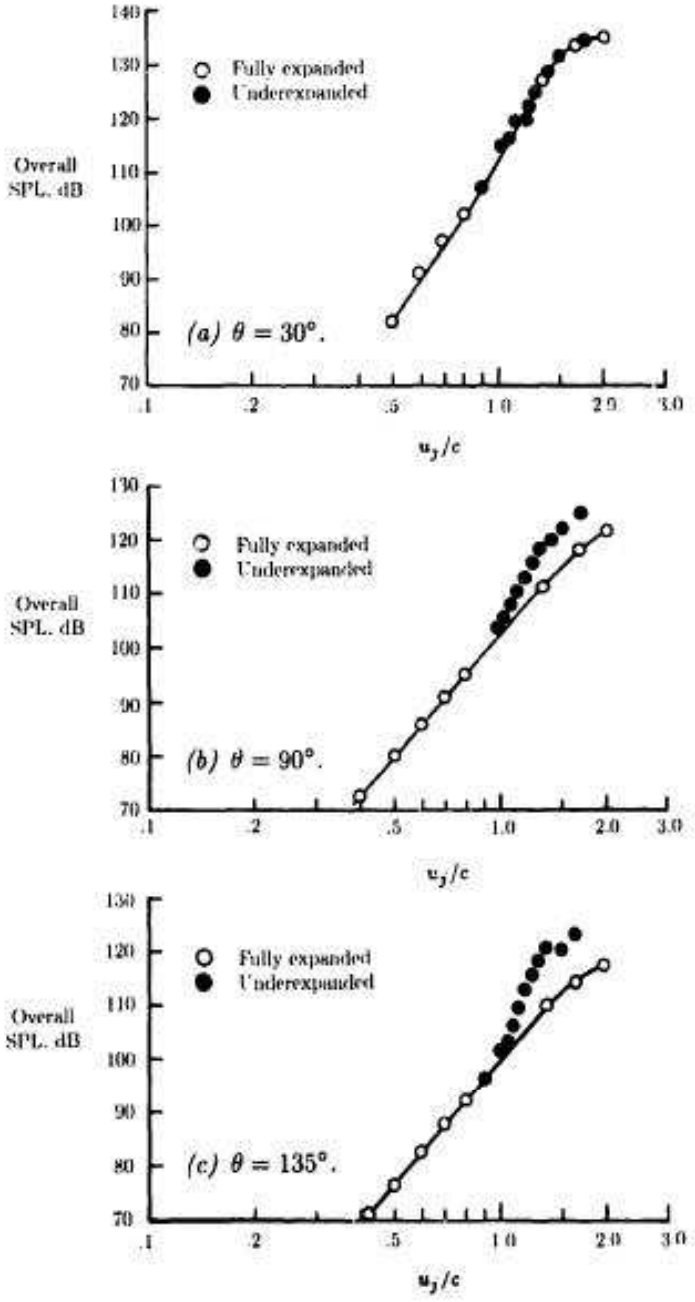

Figure 1.8: Overall sound pressure level broadband shock-associated noise.

generally referred to as screech tones. For imperfectly expanded supersonic jets with rather strong shock cells, the screech tone is often accompanied by its harmonics. In some cases, such as underexpanded jets from convergent nozzles, as many as four harmonics have been observed. The screech component disappears when the jet is perfectly expanded. The fundamental tone arises at the same frequency all along the observation arc. This frequency appears to be a lower bound for the central frequency peak of the shock associated noise. This suggested a relationship between screech tones and shock associated noise. In fact, as illustrated by Tam[3], the screech tone frequency corresponds to the phased array frequency at an observation angle of 180°. The shock associated waves propagating in the upstream direction are those enforced by a feedback loop involving instability waves generated in the shear layer close to the nozzle. The occurrence of harmonics of the fundamental screech tone is attributed to nonlinear propagation effects in the jet plume.

1.5 Final remarks

In this chapter we have used a bibliographic approach to describe qualitatively the underlying mechanisms involved in the generation of aerodynamic noise in modern aircraft for civil transportation. We have summarized all the kind of noise sources in three main cathegories: the aircraft noise, the propeller noise and the jet noise. We have provided a description of each one of these kind of noise sources and for each one we have distinguished all the subcategories of noise generation. We have cited, for example, the trailing-edge noise and landing-gear noise as two of main sources classified as airframe noise; the mixing noise and the mach wave radiation classified as jet noise and we have given an overview of all the main mechanisms of noise generation by a propeller. These noise will be discussed in next chapters

with an analytical treatment.

Chapter 2

Navier-Stokes equations and Acoustic Analogies

2.1 The Governing Equations

All of the physics of both the generated sound and the sound generation process are described by the compressible Navier-Stokes equations, including equations of conservation of mass and energy, an equation of state, and appropriate boundary and initial conditions. We write the dimensional equations in the following conservative Cartesian tensor notation:

$$\begin{aligned}
&\frac{\partial \rho^d}{\partial t^d} + \frac{\partial}{\partial x_j^d}(\rho^d u_j^d) = 0 \\
&\frac{\partial \rho^d u_i^d}{\partial t^d} + \frac{\partial}{\partial x_j^d}(\rho^d u_i^d u_j^d + p_{ij}) = 0 \\
&\frac{\partial e^d}{\partial t^d} + \frac{\partial}{\partial x_j^d}(e^d u_j^d) + \frac{\partial}{\partial x_j^d}(u_k^d p_{jk}) + \frac{\partial q_j}{\partial x_j^d} = 0
\end{aligned} \tag{2.1}$$

where ρ^d is the density, u_i^d are the velocity components, p_{ij} is the compressive stress tensor, q_j is the heat flux vector, and e^d is the energy defined

by:

$$e^d = \rho^d(E^d + \frac{1}{2}u_i^d u_i^d) \tag{2.2}$$

where E^d is the internal energy per unit mass. We assume a Newtonian perfect gas. In a perfect gas, the molecular viscosity and thermal conductivity are functions of the temperature. In flows without significant temperature gradients, the molecular viscosity and thermal conductivity can be assumed constant with little loss of accuracy.
Temperature gradients are likely to be small if the initial and boundary conditions do not force large temperature gradients, and the Mach number is low. in this case the molecular properties can be assumed to be constant and the compressive stress tensor and heat flux vector are given by:

$$\begin{aligned} p_{ij} &= p^d\delta_{ij} - \mu\Big(\frac{\partial u_i^d}{\partial x_j^d} + \frac{\partial u_j^d}{\partial x_i^d} - \frac{2}{3}\frac{\partial u_k^d}{\partial x_k^d}\delta_{ij}\Big) \\ q_j &= -k\frac{T^d}{x_j^d} \end{aligned} \tag{2.3}$$

where p^d is the pressure, μ and k are the (constant) viscosity and thermal conductivity, and $T^d$is the temperature given by the perfect gas law:

$$p^d = \rho^d R T^d \tag{2.4}$$

where R is the gas constant.
The superscript "d"in the equations indicates that the quantities involved are dimensional. A fully compressible non-dimensionalization is used as follows:

$$\rho = \frac{\rho^d}{\rho_\infty}$$

$$
\begin{aligned}
u_i &= \frac{u_i^d}{a_\infty} \\
e &= \frac{e^d}{\rho_\infty a_\infty^2} \\
p &= \frac{p^d}{\rho_\infty a_\infty^2} \\
T &= \frac{T^d c_p}{a_\infty^2} \\
x_i &= \frac{x_i^d}{L} \\
t &= \frac{t^d a_\infty}{L}
\end{aligned} \tag{2.5}
$$

where ρ_∞ and a_∞ are the reference density and sound speed and L is some length scale; c_p is the (assumed constant) specific heat at constant pressure. L, a_∞ and ρ_∞ are defined differently for the different flows which we consider; they will be defined later for each particular flow. Typically, a_∞ and ρ_∞ are equal to the ambient values far from the region of non-uniform flow. Inserting Equations (2.5)into Equations (2.1) through (2.4), gives the following non-dimensional equations:

$$
\begin{aligned}
&\rho + \frac{\partial}{\partial x_i}(\rho u_j) = 0 \\
&\rho u_i + \frac{\partial}{\partial x_i}(\rho u_i u_j + p\delta_{ij}) = \frac{1}{Re}\frac{\partial}{\partial x_j}\Big(\frac{\partial u_i}{\partial x_j} + \frac{\partial u_j}{\partial x_i} - \frac{2}{3}\frac{\partial u_k}{\partial x_k}\delta ij\Big) \\
&e + \frac{\partial}{\partial x_i}\Big((e+p)u_j\Big) = \frac{1}{Re}\frac{\partial}{\partial x_j}\Big(u_i(\frac{\partial u_i}{\partial x_j} + \frac{\partial u_j}{\partial x_i} - \frac{2}{3}\frac{\partial u_k}{\partial x_k}\delta ij)\Big) + \frac{1}{RePr}\frac{\partial^2 T}{\partial x_k \partial x_k} \\
&p = \frac{\gamma - 1}{\gamma}\rho T
\end{aligned} \tag{2.6}
$$

where

$$
Re_\alpha = \frac{\rho_\infty a_\infty L}{\mu}
$$

$$Pr = \frac{c_p \mu}{k} \tag{2.7}$$

are the Reynolds and Prandtl numbers respectively. Note that the speed of sound is used in defining the Reynolds number based on a velocity in the flow, say U, is $Re_u = \rho_\infty UL/\mu$ and is related to the "acoustic" Reynolds number by:

$$Re_u = MRe \tag{2.8}$$

where M is the Mach number defined as $M = U/a_\infty$. U will be defined later for each particular flow considered.
The Prandtl number is taken to be 1. Temperature gradients will be small in the flows considered, thus the Prandtl number is relatively unimportant, and the results are not exptected to be significantly different than for air at standard conditions for which $Pr = 0.7$. The ratio of specific heats, γ, is taken to be 1.4.

2.2 Derivation of Acoustic Analogies

The acoustic analogy approach consists of solving a simplified wave equation in place of the full non-linear Navier-Stokes problem. This approach was originated by Lighthill[1]. Starting with the exact conservation equations for continuity and momentum, first two of Equations (2.6), Lighthill first rearranged the second of (2.6) as:

$$\rho u_i + a_\infty^2 \frac{\partial \rho}{\partial x_i} = -\frac{\partial T_{ij}}{\partial x_j} \tag{2.9}$$

where

$$T_{ij} = \rho u_i u_j + (p - a_\infty^2 \rho)\delta_{ij} + \frac{1}{Re}\Big(\frac{\partial u_i}{\partial x_j} + \frac{\partial u_j}{\partial x_i} - \frac{2}{3}\frac{\partial u_k}{\partial x_k}\delta ij\Big) \tag{2.10}$$

Eliminating ρu_i between (2.9) and the first of (2.6) then gives:

$$\frac{\partial^2 \rho}{\partial t^2} - a_\infty^2 \frac{\partial^2 \rho}{\partial x_i \partial x_i} = \frac{\partial^2 T_{ij}}{\partial x_i \partial x_j} \tag{2.11}$$

Equation (2.11) then represents the wave propagation in a *fictitious* acoustic medium, with sound speed a_∞[1], acted on by an external stress distribution T_{ij}. By a fictitious we mean that such a region may not exists in the real flow.

The analogy is *exact*, in the sense that no approximations to the exact equations have been made. However, the analogy is not complete unless the following conditions are met:

- $T_{ij} = 0$ in the region where the sound is to be predicted (that is to say, that the postulated fictitious acoustic medium is identical to a region of the real flow where a_∞^2 is constant and there is no mean flow).
- There exists a way to compute T_{ij} indipendently of Equation (2.11).

The first of these stipulations is obeyed for a variety of flows, the foremost example being the jet. Co-flowing jets and mixing layers, on the other hand violate this condition, since they have a finite uniform flow extending to infinity. The second condition, that T_{ij} is known indipendently, is more difficult to achieve. There are several possibilities:T_{ij} could be determined experimentally; or, T_{ij} could be determined from numerical solutions of the Navier-Stokes equations. The first of these is likely to be useful only in very

[1]In the non-dimensionalization given above, $a_\infty^2 = 1$ if a_∞ is taken as the sound speed of the acoustic medium.

simplified flows and it is certainly not possible in the case of turbulent shear flows. Experimentally, it is not yet feasible to measure the instantaneous T_{ij} over the entire flow region. However, computing T_{ij} from numerical solutions to the governing equations (DNS) is possible, especially at low Reynolds numbers where computational resolution requirements are not too limiting.

So, except for the possibility of using DNS to compute T_{ij} which will be discussed in greater detail below, additional assumptions about T_{ij} must be invoked to make specific predictions from Equation (2.11). For example, Lighthill's (1954) scaling law for the sound produced by a single produced by a single compact eddy in a turbulent field can be derived by the assuming that $\rho u_i u_j$ is the dominant contribution to T_{ij}. Further, the density ρ in the above can be replaced by the density of the surrounding quiescent medium, ρ_∞, and each eddy produces sound with wavelength much longer than its eddy length scale (true if the velocity scale of the eddy is very much smaller than the ambient sound speed, a_∞). Then acoustic waves with frequency (as seen by a stationary observer in the surrounding medium) equal to the typical eddy frequency (i.e. the velocity scale of the eddy divide by the length scale).

Now consider the possibility of using DNS data to compute T_{ij}. An important question is how accurately must T_{ij} be computed so that the solutions to Equation (2.11) gives reliable predictions. For example, consider a subsonic cold jet. In the jet region there is mean subsonic flow plus turbulent fluctuations plus sound waves. Away from the jet mean flow decays to a quiescent state given by ρ_∞ and a_∞, and the fluctuations decay to isentropic acoustic waves of very small amplitude. The first term of T_{ij} contains the following interactions: mean-mean, mean-turbulence,turbulence-tubulence,mean-sound,turbulence-sound and sound-sound. Errors in the mean-mean, mean-turbulence and turbulence-tubulence interactions could completely swamp the mean-sound turbulence-sound and sound-sound interactions.

It is important to retain, in as much as is possibile, scattering and refraction termn on the left-hand side of the acoustic analogy, i.e. in the wave propagation operator. Infact, if one explicitly linearized Lighthill's Equation about the mean flow then, to first order, the Raylegh equations should be recovered (with the addition of viscous and heat conduction terms). Unless there is no mean flow everywhere (including the source region) the linearized Lighthill equation does not have this property. The resulting equation is incomplete; it is a single equation for all the first order perturbation of ρ, u_i and p.
The lack of proper treatment of refraction terms in Lighthill's equation was noted by Phillips[32], who proposed a different acoustic analogy equation, which is derived as follows. For simplicity, we will assume that viscous and heat conduction effects are negligible. It is convenient to define a logarithmic pressure variable:

$$\Pi = \frac{1}{\gamma} ln p \tag{2.12}$$

So, combining the first and the third of (2.6) we have:

$$\begin{aligned} &\frac{\mathrm{D}\rho}{\mathrm{D}t} + \rho \frac{\partial u_j}{\partial x_j} = 0 \\ &\frac{\mathrm{D}u_i}{\mathrm{D}t} + a^2 \frac{\partial \Pi}{\partial x_i} = 0 \\ &\frac{\mathrm{D}\Pi}{\mathrm{D}t} + \frac{\partial u_j}{\partial x_j} = 0 \end{aligned} \tag{2.13}$$

where $a^2 = \gamma p/\rho$ is the (variable) speed of sound, and $\frac{D}{Dt} = \frac{\partial}{\partial t} + u_j \frac{\partial}{\partial x_j}$. Operating on the third of (2.13) with $\frac{D}{Dt}$ and using the second gives:

$$\frac{D^2\Pi}{Dt^2} - \frac{\partial}{\partial x_j}(a^2 \frac{\partial \Pi}{\partial x_j}) = \frac{\partial u_k}{\partial x_j} \frac{\partial u_j}{\partial x_k} \tag{2.14}$$

where the identity

$$\frac{\mathrm{D}}{\mathrm{D}t} = (\frac{\partial u_i}{\partial x_j}) = \frac{\partial}{\partial x_j}(\frac{\mathrm{D}u_i}{\mathrm{D}t}) - \frac{\partial u_k}{\partial x_j}\frac{\partial u_i}{\partial x_k} \tag{2.15}$$

has been used.

Equation (2.14) is known as Phillips equation[32]. Phillips interpreted the terms on the left-hand side of the equation as "those of a wave equation in a moving medium with a variable speed of sound". However, if Phillips equation is linearized about the mean flow, the right hand side once again contains terms which are linear in the perturbation quantity, unless the mean flow is uniform. Thus, Phillips equation only generalizes Lighthill's equation to include a non-zero uniform mean flow away from the source. Thus Phillips equation could be used for a flow with non-zero uniform velocity far from the source, such as a mixing layer or co-flowing jet, but it may lead to errors because certain scattering and refraction terms are still concealed in the source term.

Lilley[33] generalized the acoustic analogy one step further. He found that by operating on (2.14) again with $\frac{\mathrm{D}}{\mathrm{D}t}$ that the following equation results:

$$\frac{\mathrm{D}}{\mathrm{D}t}\Big(\frac{\mathrm{D}^2\Pi}{\mathrm{D}t^2} - \frac{\partial}{\partial x_j}(a^2\frac{\partial \Pi}{\partial x_j})\Big) + 2\frac{\partial u_k}{\partial x_j}\frac{\partial}{\partial x_k}(a^2\frac{\partial \Pi}{\partial x_j}) = -2\frac{\partial u_j}{\partial x_k}\frac{\partial u_i}{\partial x_j}\frac{\partial u_k}{\partial x_i} \tag{2.16}$$

where the second of (2.13) and (2.15) have been used.

If we proceed to linearize Lilley's equation, (2.16), about the mean flow, then only terms which are linear in the logarithmic pressure fluctuation appear so long as the mean flow is unidirectional and only transversely sheared. In fact, as can be demonstrated by comparison to the equation derived by Pridmore-Brown (1958), the linearized Lilley's equation is the correct equation describing wave propagation in a unidirectional transversely sheared mean flow.

For example, consider the following two dimensional flow. Only the u_1 component of the mean velocity is non-zero, and the mean flow is only a function of x_2.Let[2]:

$$\begin{aligned} u_1(x_1, x_2, t) &= \bar{u}_1(x_2) + u_1'(x_1, x_2, t) \\ u_2(x_1, x_2, t) &= u_2'(x_1, x_2, t) \\ \Pi(x_1, x_2, t) &= \bar{\Pi} + \Pi'(x_1, x_2, t) \\ a^2(x_1, x_2, t) &= \bar{a}^2(x_2) + a'^2(x_1, x_2, t) \end{aligned} \tag{2.17}$$

When Equations (2.17) are inserted into Equation (2.14) terms which are linear in both the pressure fluctuation and velocity fluctuations appear in the result. Thus even when the flow is parallel and transversely sheared the Phillip' s equation is incomplete. Inserting Equations (2.17) into Equation (2.16) gives:

$$L(\Pi') = \frac{\bar{D}}{Dt}\Big(\frac{\bar{D}^2\Pi'}{Dt^2} - \frac{\partial^2\Pi'}{\partial x_j \partial x_j}\Big) + 2\frac{\partial U}{\partial x_2}\frac{\partial^2\Pi'}{\partial x_1 \partial x_2} = \Gamma \tag{2.18}$$

where, since only low Mach number mixing layers where the temperature of both free streams are equal are considered, $\bar{a}^2$ varies little across the shear layer and thus has been set to a constant, $\bar{a}^2 = 1$, given the nondimensionalization. Note that variations in the speed of sound (both mean and fluctuations) are accounted for in the source terms given below while has been neglected the effect of the nonuniform mean speed of sound on the propagation of the generated waves. In Equation (2.18) $\frac{\mathrm{D}}{\mathrm{D}t}$ is the convective derivative following the parallel flow:

$$\frac{\bar{D}}{Dt} = +U(x_2)\frac{\partial}{\partial x_1} \tag{2.19}$$

[2]Note that in the third of (2.17) $\bar{\Pi} = \frac{1}{\gamma} ln(\frac{1}{\gamma})$ because of the non-dimensionalization.

and the source term, Γ is given by:

$$L(\Pi') = \Gamma^{(1)} = \frac{\bar{D}}{Dt}\Big(\underbrace{\frac{\partial^2 u_i' u_j'}{\partial x_i \partial x_j}}_{\text{Term Ia}} - \underbrace{\frac{\partial^2 u_i' u_k'}{\partial x_i \partial x_k}}_{\text{Term IIa}} + \underbrace{\frac{\partial}{\partial x_j}(a'^2 \frac{\partial \Pi'}{\partial x_j})}_{\text{Term IIIa}} + \underbrace{a^2 \frac{\partial \Pi'}{\partial x_i}\frac{\partial \Pi'}{\partial x_i}}_{\text{Term IVa}} + \underbrace{\frac{\partial \Pi'}{\partial x_j}(u_i' \frac{\partial u_j'}{\partial x_i}) + u_j' \frac{\partial}{\partial x_j}(u_i' \frac{\partial \Pi'}{\partial x_i})}_{\text{Term Va}} \Big)$$
$$-2\frac{dU}{dx_2}\Big(\underbrace{\frac{\partial^2 u_2' u_j'}{\partial x_1 \partial x_j}}_{\text{Term Ib}} - \underbrace{\frac{\partial^2 u_2' u_k'}{\partial x_1 \partial x_k}}_{\text{Term IIb}} + \underbrace{\frac{\partial}{\partial x_1}(a'^2 \frac{\partial \Pi'}{\partial x_2})}_{\text{Term IIIb}} + \underbrace{a^2 \frac{\partial \Pi'}{\partial x_1}\frac{\partial \Pi'}{\partial x_2}}_{\text{Term IVb}} + \underbrace{\frac{\partial \Pi'}{\partial x_1}(u_2' \frac{\partial u_i'}{\partial x_i}) + u_i' \frac{\partial}{\partial x_1}(u_2' \frac{\partial \Pi'}{\partial x_i})}_{\text{Term Vb}} \Big) \tag{2.20}$$

The superscript (1) is used on the expression for the source Γ because the right hand side is not unique; the (2.17) can be used to express the right hand side in different ways, and we have labeled each of the terms on the right hand side for ease of future reference.

When the fluctuations are small and the left hand side of (2.20) is negligible compared to the right, Equation (2.20) reduces to the Pridmore-Brown equation for fluctuations propagating in an unidirectional transversely sheared flow. The products of fluctuations on the right hand side, the, truly represent the sources of sound in an unidirectional transversely sheared flow, and for that case there is no longer any ambiguity associated with the acoustic analogy approach: it is consistent with a perturbation expansion of the basic flow equations. Note that as written Equation (2.20) is still exact.

In practice, unfortunately the mean of turbulent shear flows is neither unidirectional (there is a mean u_2 velocity due to entrainment), nor solely transversely sheared, since the flow spreads as a function of the streamwise coordinate, x_1. If the flow is decomposed into its true mean flow plus fluctuations

and inserted into Equation (2.16) then once again a single equation in several dependent variables is obtained.

Since the spreading of the mean flow (or more specifically the derivatives of mean quantities with respect to x_1) is generally small compared to the shear, Equation (2.16) has been used for jet flow predictions in both low and high speed jets. The only effects unaccounted for in the left-hand side of Equation (2.20) are refraction of the sound waves by the spreading part of the mean flow, and scattering of the sound waves by turbulent fluctuations and by the generated sound itself. It has been argued that these propagation effects are quite small compared to the refraction by the part of the velocity field which is steady, unidirectional and transversely sheared(Goldstein[ref]).

Many investigators have attempted to make jet noise predictions (for both high and low speed jets) based on solutions of Lilley's equation. Research has been primarily focused on solutions to Lilley's equation in the high and low frequency limits. Even for the approximate solutions it is necessary, in the general case, to solve at least an Ordinary Differential Equation numerically. Solutions are generally obtained for point quadrupole sources moving through parallel shear flows.

For low Mach number cold (i.e. no large temperature fluctuations) flows, Goldstein[34] concluded that terms proportional to the dilation (divergence of velocity) and certain terms involving products of the pressure and other variables might be neglected on the right-hand side of (2.20) as described below. Under these assumptions, Equation (2.20) becomes:

$$L(\Pi') = \Gamma^{(2)} = \frac{\bar{D}}{Dt} \underbrace{\left(\frac{\partial^2 u_i' u_j'}{\partial x_i \partial x_j} \right)}_{\text{Term Ia}} - 2 \frac{dU}{dx_2} \underbrace{\frac{\partial^2 u_2' u_j'}{\partial x_1 \partial x_j}}_{\text{Term Ib}} \tag{2.21}$$

which is Goldstein's Equation[34].

Note that in deriving Equation (2.21) Goldstein first expands the left-hand

side of Phillip's equation about $U(x_2)$, dropping all the non linear terms. He then operates on the result with the mean convected derivative, Equation (2.19) and subsequently assumes that the fluctuation field is incompressible. The reason for neglecting the nonlinear terms which arise on the left-hand side of Phillip's equation is that the pressure in turbulent shear flows is very nearly uniform and therefore the nonlinear terms are thought to represent scattering of the acoustic waves by the fluctuating velocity field, as well as refraction of the waves by the part of the mean flow which is not unidirectional and transversely sheared. Goldstein[34] argues that such scattering/refraction terms are small compared to the source terms in $\Gamma^{(2)}$ above. We can write the Equation (2.20) with the mean convective derivative in the expression for $\Gamma^{(1)}$ carried through the differentiations with respect to x_i and x_j in the term Ia and II. The result is added to terms Ib and IIb, one obtains:

$$
\begin{aligned}
L(\Pi') = \Gamma^{(3)} = &\underbrace{-2\frac{\partial u_i}{\partial x_j}\frac{\partial u_j}{\partial x_k}\frac{\partial u_k}{\partial x_i}}_{\text{Term Ic}} \underbrace{-2\frac{\partial u_j'}{\partial x_k}\frac{\partial}{\partial x_j}(a^2\frac{\partial \Pi'}{\partial x_k})}_{\text{Term Id}} \underbrace{-u_k'\frac{\partial}{\partial x_k}(\frac{\partial u_i}{\partial x_j}\frac{\partial u_j}{\partial x_i})}_{\text{Term Ie}} \\
&+\frac{\bar{D}}{Dt}\Big(\underbrace{2u_j'\frac{\partial}{\partial x_j}(\frac{\partial u_i'}{\partial x_i})}_{\text{Term IIc}} + \underbrace{\frac{\partial}{\partial x_j}(a'^2\frac{\partial \Pi'}{\partial x_j})}_{\text{Term IIIa}} + \underbrace{a^2\frac{\partial \Pi'}{\partial x_i}\frac{\partial \Pi'}{\partial x_i}}_{\text{Term IVa}} + \\
&\underbrace{\frac{\partial \Pi'}{\partial x_j}(u_i'\frac{\partial u_i'}{\partial x_i}) + u_j'\frac{\partial}{\partial x_j}(u_i'\frac{\partial \Pi'}{\partial x_i})\Big)}_{\text{Term Vb}}
\end{aligned}
\tag{2.22}
$$

where it should be noted that the full velocity, u_i is used in terms Ic and Ie. Using Goldstein's assumptions in arriving at the source term $\Gamma^{(2)}$, we would drop all terms except Ic, Id and Ie in $\Gamma^{(3)}$. Of the remaining terms, Ic is now identical to the source term in Lilley's original equation (2.16). Now, note that in term Id, the quantity $\frac{\partial u_i}{\partial x_j}\frac{\partial u_j}{\partial x_i}$ can, by using Phillips equation (2.14), be set equal to

$$\frac{\mathrm{D}^2\Pi}{\mathrm{D}t^2} - \frac{\partial}{\partial x_j}(a^2 \Pi x_j) \tag{2.23}$$

Then, by comparing Terms Id and Ie with terms in the left-hand side wave operator of Lilley's equation and the linearized left-hand side of Equation (2.18), it is evident that one can make the same argument as Goldstein makes about the terms neglected in linearizing the left-hand side of Phillip's equation: they are wave propagation terms convected and sheared by the difference between the real flow, u_i and the parallel transversely sheared idealization of the flow, $U(x_2)$ and scattered by the fluctuations. Thus we might expect that they are also small like other scattering/refraction terms which have been dropped in writing the Goldstein's source term $\Gamma^{(2)}$.
A problem arises in two dimensional flows if terms Id and Ie are neglected because they represent scattering and refraction. We arrive at:

$$\Gamma^{(4)} = -2\frac{\partial u_i}{\partial x_j}\frac{\partial u_j}{\partial x_k}\frac{\partial u_k}{\partial x_i} \tag{2.24}$$

However, by writing out all the components of $\Gamma^{(4)}$ for two dimensional flow it is easily seen that this term is proportional to the divergence of the velocity field. Therefore since the parallel transversely sheared flow has zero divergence, if the fluctuations are assumed incompressible we have:

$$L(\Pi') = 0 \tag{2.25}$$

which is obviously too trivial.
Two additional remarks should be made regarding this argument. First, the arguments of Goldstein[ref] are meant to apply to three-dimensional flows

and thus it might be thought that the above critique, made on the basis of two dimensional flows, may appear to be unfounded. On the other hand, one might argue that the three-dimensional versione should reduce unambiguously to the appropriate version of the theory for two dimensions, which would suggest that the reason for neglecting terms used in arriving at Equation (2.22) is ad hoc and would have to be validated for each particular flow by showing that the neglected terms indeed have insignificant impact on the acoustic field compared to those retained.
This is unfortunate, in a way, since the source term, $\Gamma^{(2)}$ is in a very appealing form. As Goldstein shows, the source term has the same form as that for an externally applied force in a unidirectional transversely sheared flow, where the external force, f_i, is equal to

$$f_i = \frac{\partial}{\partial x_j} u_i' u_j' \tag{2.26}$$

and thus the right-hand side can be interpreted as an acoustic quadrupole of strength $u_i' u_j'$, as in Lighthill's theory. However we should not label sources as various order multipoles by simply counting the number of derivatives.

2.3 The formulation of Ffwocs Williams and Hawking equation

2.3.1 The wave equation

In the previous section, sound generated aerodinamically was considered with no solid bodies in the source region. Let us now consider a finite volume of space containing a disturbed flow and rigid bodies in arbitrary motion, the surrounding fluid being at rest. Bodies and flow generate sound. In that case it is certaintely possible to replace both flow and surfaces by equivalent

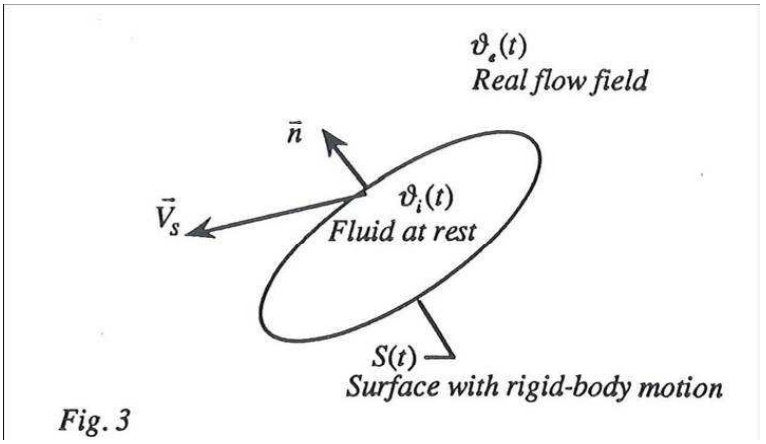

Figure 2.1: Sketch of Ffwocs Williams Hawking hypotesis.

acoustic sources, assuming that the whole medium is perfect at rest.
This is the foundation of the aeroacoustic analogy as extended by Ffwocs Williams and Hawking[17]. The key assumption is again that no flow-acoustics coupling occurs, or the acoustic field does not affect the flow, from which originates the sound. Consequently, this approach is no more valid when some resonant conditions induce an acoustic feedback on the flow.

When the aeroacoustic analogy can be used, the remaining problem is the determination of the equivalent sources.
To represent the real medium with flow and obstacles in a convenient way, Ffwocs Williams and Hawkings defined (figure (2.1)) an equivalent medium where the rigid bodies are replaced by mathematical surfaces. The inner volume of the surfaces is assumed to contain the ambient fluid at rest. In order to preserve the kinematics of the flow and the boundary condition of no cross-flow on the surfaces, a discontinuity must be imposed at the surface location, by introducing some mass and momentum sources in the equation of gas dynamics.

Mass and momentum equations are now written as:

$$\frac{\mathrm{d}\rho}{\mathrm{d}t} + \frac{\partial}{\partial x_i}(\rho V_i) = \rho_0 V_{Si}\delta(f)\frac{\partial f}{\partial x_i} \tag{2.27}$$

$$\frac{\mathrm{d}}{\mathrm{d}t}(\rho V_i) + \frac{\partial}{\partial x_i}(\rho V_i V_j - \sigma'_{ij}) = -\sigma'_{ij}\delta(f)\frac{\partial f}{\partial x_i} \tag{2.28}$$

In these equations, ρ, V_i are respectively the density and total velocity components of the flow, ρ_0 is the mean density, V_{Si} is the velocity field of a point on the surfaces, δ means the Dirac delta function, σ'_{ij} is the viscous stress tensor and $f(\vec{x}, t) = 0$ is an equation defining the kinematics of the surfaces. If the normal unit vector on the surfaces is $\hat{n}$, the boundary condition of no cross-flow is simply:

$$\vec{V} \cdot \vec{n} = \vec{V_S} \cdot \vec{n} \tag{2.29}$$

A formal procedure can now be used to derive an equation for the density fluctuation $\rho' = \rho - \rho_0$ in the following way from (2.27) and (2.28):

$$\begin{aligned} &\frac{\partial^2 \rho'}{\partial t^2} - c_0^2 \frac{\partial^2 \rho'}{\partial x_i^2} = \\ &= \frac{\partial^2 T_{ij}}{\partial x_i \partial x_j} + \frac{\partial}{\partial x_i}\left(\sigma'_{ij}\delta(f)\frac{\partial f}{\partial x_i}\right) + \frac{\partial}{\partial t}\left(\rho_0 V_{Si}\delta(f)\frac{\partial f}{\partial x_i}\right) \end{aligned} \tag{2.30}$$

Equation (2.30) is exact, because is a reformulation of the general fluid dynamics equations. ρ' and T_{ij} are zero inside the mathematical surfaces and equal respectively to the density fluctuations and the Lighthill tensor of the flow outside.

The statement of the generalized acoustic analogy follows:

The density fluctuations in the real fluid, in the presence of flow and rigid bodies, are exactly the same as those that would exist in an equivalent acoustic medium perfectly at rest and forced by three source distributions:

- a volume distribution $\frac{\partial^2 T_{ij}}{\partial x_i \partial x_j}$ in the outer region of the surfaces, due to the flow.
- a surface distribution $\frac{\partial}{\partial x_i}\left(\sigma'_{ij}\delta(f)\frac{\partial f}{\partial x_i}\right)$ due to the interaction of the flow with the moving bodies.
- a surface distribution $\frac{\partial}{\partial t}\left(\rho_0 V_{Si}\delta(f)\frac{\partial f}{\partial x_i}\right)$ due to the kinematics of the bodies.

As for Lighthill's equation, this result cannot be used directly to calculate the sound produced in practical situation. In fact, (2.30) is not exactly a wave equation, because the density fluctuation is also present in the supposed source terms. But it must reduce to the wave equation at large
According to the general definition of acoustic sources, the three equivalent source terms corresponding to the approximate form of equation (2.30) are respectively quadrupoles, dipoles and monopoles. distances from the source region, where the right hand side vanishes.

2.3.2 Solution of the wave equation

The acoustic analogy has the formal advantage of formulating the complicated problem of the noise generated by flows and rigid bodies in motion in a more standard one, governed by the inhomogeneous wave equation (2.30). Assuming that the sources of this equation are previously determined, the solutions is given by the Green's function technique[35]. For an unbounded medium at rest, the density fluctuation at a point $\vec{x}$ at time t is expressed as:

$$c_0^2\rho'(\vec{x},t) = \frac{\partial^2}{\partial x_i \partial x_j}\int_{-\infty}^{\infty}\int_{\Theta_\infty}\frac{\delta(t'-t+R/c_0)}{4\pi R}T_{ij}(\vec{y},t')d\vec{y},dt'$$
$$+\frac{\partial}{\partial x_i}\int_{-\infty}^{\infty}\int_{\Theta_\infty}\frac{\delta(t'-t+R/c_0)}{4\pi R}\left(\sigma'_{ij}\delta(f)\frac{\partial f}{\partial x_j}\right)(\vec{y},t')d\vec{y},dt'$$

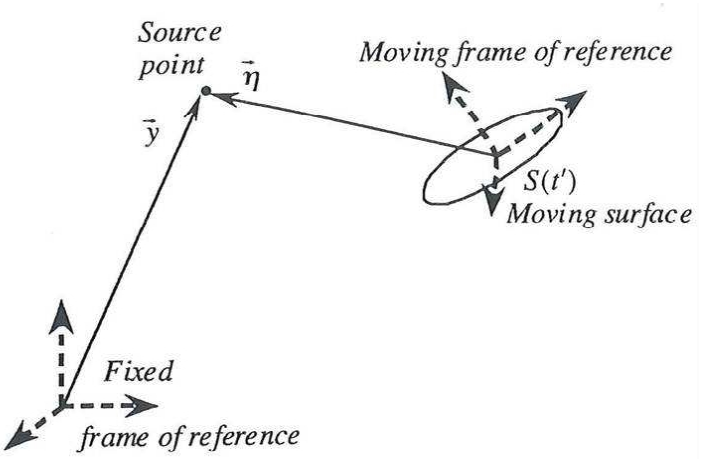

Figure 2.2: Moving frame of reference.

$$+\frac{\partial}{\partial t}\int_{-\infty}^{\infty}\int_{\Theta_\infty}\frac{\delta(t'-t+R/c_0)}{4\pi R}\Big(\rho_0 V_{Si}\delta(f)\frac{\partial f}{\partial x_i}\Big)(\vec{y},t')d\vec{y},dt' \quad (2.31)$$

with $R=|\vec{x}-\vec{y}|$. Because generalized functions are used, this equation holds anywhere in the unbounded space Θ_∞. The sources are described in a frame of reference of variables $(\vec{y},t')$, stationary with respect to the ambient fluid at rest outside the source domain. Then the sound is thought of as produced by stationary sources. It is more convenient to project the equation in a frame of reference fixed to the moving surfaces provided that we will use this kind of solution, in chapter 4, when we will treat propellers that correspond to sources in helicoidal motion.

If $(\vec{\eta},t')$ are the source coordinates in this moving frame of reference (figure (2.2)), (2.33) becomes:

$$c_0^2\rho'(\vec{x},t)=\frac{\partial^2}{\partial x_i\partial x_j}\int_{-\infty}^{\infty}\int_{\Theta_\infty}\frac{\delta(t'-t+|\vec{x}-\vec{y}(\vec{\eta},t')|/c_0)}{4\pi|\vec{x}-\vec{y}(\vec{\eta},t')|}T_{ij}(\vec{\eta},t')d\vec{\eta},dt'$$
$$+\frac{\partial}{\partial x_i}\int_{-\infty}^{\infty}\int_{\Theta_\infty}\frac{\delta(t'-t+|\vec{x}-\vec{y}(\vec{\eta},t')|/c_0)}{4\pi|\vec{x}-\vec{y}(\vec{\eta},t')|}\Big(\sigma'_{ij}\delta(f)\frac{\partial f}{\partial x_j}\Big)(\vec{\eta},t')d\vec{\eta},dt'$$

$$+\frac{\partial}{\partial t}\int_{-\infty}^{\infty}\int_{\Theta_\infty}\frac{\delta(t'-t+|\vec{x}-\vec{y}(\vec{\eta},t')|/c_0)}{4\pi|\vec{x}-\vec{y}(\vec{\eta},t')|}\Big(\rho_0 V_{Si}\delta(f)\frac{\partial f}{\partial x_i}\Big)$$
$$(\vec{\eta},t')d\vec{\eta},dt' \tag{2.32}$$

Here the relationship $\vec{y}=\vec{y}(\vec{\eta},t')$ defines a perfect solid-body motion. Now use can be made of the well-known property of the Dirac delta-function to perform the time integrals, which lead to the Ffowcs Williams Hawkings equation:

$$\begin{aligned}c_0^2\rho'(\vec{x},t) &= \frac{1}{4\pi}\frac{\partial^2}{\partial x_i\partial x_j}\int_{\Theta_\infty}\Big[\frac{T_{ij}}{R|1-\vec{M}\cdot\vec{R}/R|}\Big]d\vec{\eta}\\ &-\frac{1}{4\pi}\frac{\partial}{\partial x_i}\int_S\Big[\frac{P_i}{R|1-\vec{M}\cdot\vec{R}/R|}\Big]dS_{\vec{eta}}\\ &-\frac{1}{4\pi}\frac{\partial}{\partial t}\int_S\Big[\frac{\rho_0 V_n}{R|1-\vec{M}\cdot\vec{R}/R|}\Big]dS_{\vec{eta}}\end{aligned} \tag{2.33}$$

where $\vec{P}$ is the net force on the fluid from each surface element; V_n is the normal velocity field on surface, the normal unit vector pointing inwards; $\vec{R}=\vec{x}-\vec{y}(\vec{\eta},t)$; $\vec{M}$ is the Mach number of the sources, corresponding to the velocity in the stationary frame of reference; $(1-\vec{M}\cdot\vec{R}/R)$ is the Doppler amplification factor related to the projected motion on the line joining the source to the observer at $\vec{x}$ and the squared brackets [] mean that a quantity has to be evaluated at the retarded time, that is, at both position and time where and when the source emitted the signal heard at $\vec{x}$ at time t.

Now the sound is described as produced by moving sources. Equation (2.33) shows that sound radiation is strongly dependent of the Doppler effect and the convective amplification. Moreover, the intrinsic source behaviour is certainly easy to define in the moving axes. Then the main advantage of this description is to clearly distinguish the consequences of both the motion and the nature of the sources. Thus, the most important point that are related to a proper use of equation (2.33) are that the source intrisincs are to be

described in the moving axes and that the Doppler effects is defined by the motion of the sources in the fixed axes.

2.3.3 Far Field noise radiation

Only a small part of the energy in the source mechanisms is converted into acoustic waves. The remaining part corresponds to the localized reciprocal motion of the fluid. In order to extract the purely acoustic field from equation (2.33) it is necessary to place the observation point $\vec{x}$ in the far field, where the condition $\lambda/2\pi R << 1$, λ being a characteristic acoustic wave length, is satisfied.

Then, the only terms with the spherical divergence attenuation with the distance $1/R$ are retained in expanding the Ffwocs Williams Hawkings equation. Because $\vec{x}$ is also far from the source region, where the surrounding fluid is at rest, $c_0^2\rho'(\vec{x},t)$ can be identified as the exact acoustic pressure fluctuation $p'(\vec{x},t)$. We can rewrite the equation (2.33) as (see Goldstein reference):

$$\begin{aligned}
p'(\vec{x},t) = &\frac{1}{4\pi}\int_{\Theta_e}\Big[\frac{R_iR_j}{c_0^2\Delta R^3}\frac{\partial}{\partial t'}\Big(\frac{1}{\Delta}\frac{\partial}{\partial t'}\Big(\frac{T_{ij}}{\Delta}\Big)\Big)\Big]d\vec{\eta}\\
&+\frac{1}{4\pi}\int_{S}\Big[\frac{R_i}{c_0\Delta R^2}\frac{\partial}{\partial t'}\Big(\frac{P_i}{\Delta}\Big)\Big]dS_{\vec{\eta}}\\
&+\frac{1}{4\pi}\int_{\Theta_i}\Big[\frac{R_i}{c_0\Delta R^2}\frac{\partial}{\partial t'}\Big(\frac{\rho_0\Gamma_i}{\Delta}\Big)\Big]d\vec{\eta}\\
&+\frac{1}{4\pi}\int_{\Theta_i}\Big[\frac{R_iR_j}{c_0^2\Delta R^3}\frac{\partial}{\partial t'}\Big(\frac{1}{\Delta}\frac{\partial}{\partial t'}\Big(\frac{\rho_0V_i^*V_j^*}{\Delta}\Big)\Big)\Big]d\vec{\eta}
\end{aligned} \tag{2.34}$$

where, for convenience, we note $\Delta = |1 - \vec{M}\cdot\vec{R}/R|$ and Θ_i and Θ_e are the moving axes.

This formula is the most important one in practical applications. It shows that the unsteadiness of the source terms, expressed by time derivatives, is a necessary condition for noise to be heard in the far-field.

Just as example, let us consider the second source term in the right-hand side of (2.34):

$$\frac{\partial}{\partial t'}\left(\frac{P_i}{\Delta}\right) = \frac{1}{\Delta}\frac{\partial P_i}{\partial t'} - \frac{P_i}{\Delta^2}\frac{\partial \Delta}{\partial t'}$$

We can see that the unsteadiness, and then the noise itself, have two origins:

- the intrinsic unsteadiness of the source, defined in the moving frame of reference fixed to the source.
- the unsteadiness due to the motion of the source, expressed by the Doppler factor.

Furthermore

$$\frac{\partial \Delta}{\partial t'} = \frac{V_i^*}{c_0 R}\left(V_i^e - \frac{R_i R_j}{R^2} V_j^e\right) - \frac{R_i}{c_0 R}\Gamma_i$$

so that the Doppler unsteadiness can be split in turn into two contribution. The second one comes from the acceleration of the source; the first one exists, even for a non-accelerated motion, but it must be neglected as a higher order term in the far-field radiation.
So an important point is that a steady force does produce sound if accelerated. This is a well-known contribution of the noise radiated by high speed propellers, for example.
Performing a dimensional analysis of the dipole terms[reference] we can arrive to an expression for the acoustic intensities associated with the two terms of noise:

- intrinsic unsteadiness

$$n^2 \frac{\rho_0 (w/U_0)^2 U_0^6 c^4}{R_0^2 R^2 (1 - M_0)^4 c_0^3} \tag{2.35}$$

- unsteadiness due to motion

$$\frac{\rho_0 U_0^8 c^4}{R_0^2 R^2 (1 - M_0)^6 c_0^5} \tag{2.36}$$

M_0 being the characteristic Mach number (U_0/c_0), R the distance to the observer and w is an order of magnitude on the inflow variations on the blade (result from classical unsteady aerodynamics theories).
We can form the ratio:

$$\frac{Motion}{Intrinsic} = \frac{1}{n^2}\Big(\frac{U_0}{w}\Big)^2\Big(\frac{M_0}{1 - M_0}\Big)^2 \tag{2.37}$$

This ratio includes the effects of the Mach number and the rate of unsteadiness in the flow; n is an integer allowing the result to be varied with the multiples of the rotational frequency. It must be kept in mind that the unsteadiness due to motion is responsible for what is called the steady-loading noise of a rotor.
The eight-power law is obtained for the second-kind unsteadiness of the moving dipole
The characteristic flow Mach number strongly determines which kind of source is predominating. It also depends on the rate of unsteadiness in the oncoming velocity field.
If M_0 is not so high, the Doppler factor remains significant with positive values. In this case no singularity occurs in the Ffwocs Williams Hawkings equation and the result in (2.34) can be directly used in a computational approach.
At low Mach numbers the steady-loading noise can be neglected, i.e. for subsonic machines with thin blades the unsteady loading noise is the most significant sound source.
Conversely, at high Mach numbers, and lower frequencies, the intensity ratio can become large; for high speed propellers and rotors, the steady-loading noise is the dominant mechanism.

2.4 Final remarks

The discussion of acoustic analogies given here is far from exhaustive. With the exception of the theory of vortex sound (Powell[ref] and others) which requires a compact vorticity field (with a turbulent shear flow does not possess), most other works are variations of the theories discussed above.
Anyway, the acoustic analogy that we have discussed in this section, is the starting point for one of two models that we will use in next chapter for analyzing the noise generated in a subsonic jet: the Morris&Farassat model.
A simplified form of Navier-Stokes equations, the Euler equations, instead represents the starting point of the other model for subsonic jet noise discussed in next section: the Tam&Auriault model.
The FFwocs-Williams-Hawking, that are a rearrangement of Navier-Stokes equations as nonhomogeneus wave equations with source terms categorized in several ways, equations, instead will be the starting point for the analysis of propeller noise, discussed in chapter 4.

Chapter 3

Sources of aircraft noise: the Jet Noise

As stated in previous section Jet Noise is a large section of Aeroacoustics that focuses on the noise generation structures caused by aerodynamic jets. The work described in this chapter is in the framework of an italian project named CAST (Configurazioni Aerotermodinamiche innovative per Sistemi di Trasporto spaziale). CIRA (Centro Italiano Ricerche Aerospaziali) is one of the partners involved in the project. The research activity is devoted to the development of numerical tools for the prediction of the acoustic environment occuring during the ascent phase of space launcher. The problem can be conveniently split into three parts according to the involved noise generation mechanism:

- **Engine ignition**: in this phase the main noise source is the overpressure (blast wave) generated by the ignition of the powder grain and the chocking of the nozzle.

- **Lift off**: in this phase the main noise source is the supersonic jet and its interaction with the launch pad.

- **Transonic flight**: in this phase the main noise source (near-field pressure fluctuation) is the interaction between the shocks occurring on the launcher and the boundary layer.

The present chapter is focused on the noise generation and propagation mechanisms involved in the second flight condition. More precisely the activity carried out deals with the development of semi-analytical approaches in which the jet mean flow quantities and turbulence statistics computed through a steady RANS[1] jet plume simulation are used to compute the acoustic far-field levels by solving simplified wave propagation problems.
All these approaches provide viable alternatives to the solution of transient Navier-Stokes equations that, because of the geometrical/fluid complexities and involved Reynolds and Mach numbers, are not affordable for industrial application.

3.1 Semi-analytical approaches for jet noise

3.1.1 Motivations and theoretical overview

The interest of developing semi-analytical methodologies typically used for aeronautical applications is related to the necessity of developing the required know-how for future developments of more sophisticated approaches. Several semi-analytical models are available for all the source generation mechanisms in subsonic and supersonic jet flows. These are reviewed in the following paragraphs.

[1]RANS=Reynolds Averaged Navier Stokes equations

3.1.2 Subsonic jet flows

In subsonic jets, the small-scale turbulence is believed to be the dominant source of noise. Even though large-scale coherent turbulent structures and instability waves have been observed in a wide range of Reynolds numbers, these structures are not effective aeroacoustic sources. However, they play a crucial indirect role on the jet noise generation, by enhancing the turbulent mixing and the consequent jet spreading. The universal character of the small-scale turbulent fluctuations contributes to the succes of predictive models based on the acoustic analogy theory. These models describe the mechanisms of mixing-noise generation in subsonic jets. The same mechanism are present in supersonic jets, but in this case other phenomena predominate.

Jet noise models that fall under the semi-analytical (or semi-empirical) category are mainly based on steady RANS jet flow predictions. The idea of extracting from a RANS aerodynamic solution the statistical turbulent quantities required by an acoustic analogy model in order to predict the far-field noise radiated by a jet is very old. One of the earliest RANS-based mixing noise models is implemented in the NASA code MGB, from the initials of its inventors Mani, Gliebe and Balsa[36]. The MGB code uses a RANS mean flow solution to define local length scale,time scale, and source strength parameters for a source model. This is based on a simplified Lighthill quadrupole source term with an approximate high-frequency solution of Lilley's equation for propagation to the far-field. MGB predictions have been heavily used by industry and NASA for the last twenty years and, over time, its accuracy has been increased. More recently, Kharavan and co-workers[37][38] have removed many of the limitations of the method by reformulating both the propagation and noise source models into the jet-noise code MGBK. Methods of this kind are usually referred to as semi-empirical, since the RANS turbulence model itself is semi-empirical.
Tam & Auriault[39] have proposed a RANS-based prediction scheme for the

fine-scale turbulence mixing noise component of jet noise. In their formulation a modified $k - \epsilon$ turbulence model provides parameters for a semi-empirical space-time correlation function of turbulent fluctuations.
The aeroacoustic source term, however, is not based on Lighthill's analogy. By analogy with the gas kinetic theory, they postulated a relationship between the turbulence kinetic energy and the fluctuating pressure. An adjoint field was then used to project the near-field source onto the far field. Morris & Farassat[40] argued that the Tam & Auriault's model provides better results than previous Lighthill's type models, not because of some flaw in the acoustic analogy approach, but thanks to a better modelling of the turbulence statistics. RANS-based methods provide good predictions for generic axi-symmetric or rectangular nozzles, but they are often unable to account for nozzle design changes, such as the addition of chevrons[38]. In addition they do not perform well at the low and high-frequency ends of the acoustic spectrum. The fundamental limitation of the RANS-based approaches is in the non universal character of the turbulent fluctuations and to the difficulty in computing the space-time velocity correlations by means of RANS approaches.
A very interesting paper has been recently published by Bridges et Al.[41] where a comprehensive assessment of NASA semi-empirical jet-noise prediction capabilities is carried out.

3.1.3 Supersonic jet flows

When a supersonic jet nozzle operates at adapted ambient conditions, no shock cells are generated in the plume. In this case, the only noise generation mechanisms is associated with the small-scale turbulence mixing noise and Mach wave radiation. The mixture of these two mechanism is commonly referred to as supersonic turbulent mixing noise[42]. Two commonly observed

features of this noise generation mechanism are:

- the high directionality, with downstream predominant radiation between 25° and 45° from the jet flow direction.
- a broadband power spectral density spanning over about two frequency orders, with a very smooth peak separating a variation law as the square of the frequency on the left, from a variation law as the inverse of the frequency on the right.

When a supersonic jet is not operated at perfectly expanded conditions, a quasi-periodic shock cell pattern appears in the jet-plume. The interaction between the vortical disturbances in the jet stream and the shock fronts generates additional noise, referred to as shock associated noise. The main property of this noise component is that its spectral peak frequency decreases away from the downstream flow direction.
In addition, the associated acoustic power level exhibits an opposite directivity behaviour with respect to the mixing noise. As a consequence, the acoustic radiation in the jet rear arc, at observation angles greatest than 90∘, is commonly dominated by the shock associated noise. This behaviour has been described by a simple and elegant phased point-source array model by Harper-Bourne & Fisher[43].
They assumed that the source of shock associated noise is a synchronized array of periodic point monopoles located at a distance equal to the length of the shock cells. The phases of adjacent monopoles are assumed to be correlated by the time taken for turbulent eddies to be convected from one point source to the next. The resulting acoustic waves interfere constructively along observation angles which depend on the acoustic frequency, according to a behaviour analogous to that of a directional antenna. Starting from the basic concept of a phased array of sources, Tam&Tanna[44] developed a predictive analytical model of the broadband shock associated noise. By employing so-

phisticated mathematical techniques and elegant use of statistical models of vortical instability waves, they obtained a compact semi-empirical formula for the acoustic power spectral density that provides favourable comparisons with experimental data.

3.1.4 The Morris & Farassat model for subsonic jet flow

The semi-empirical mixing-noise model developed by Morris&Farassat[40] is based on the solution to Lighthill's acoustic analogy equation:

$$\frac{\partial^2 \rho'}{\partial t^2} - c_0^2 \frac{\partial^2 \rho'}{\partial x_i \partial x_i} = \frac{\partial_{ij}^2}{\partial x_i \partial x_j} \tag{3.1}$$

where T_{ij} is the Lighthill stress tensor[1][2] given by:

$$T_{ij} = \rho u_i u_j + \delta_{ij}[(p - p_0) - c_0^2(\rho - \rho_0)] \tag{3.2}$$

with primes denoting the perturbation about the basic state denoted by a subscript 0, c_0 is the speed of sound in the uniform medium surrounding the source region and u_i is the instantaneous velocity vector.

Since we are mainly interested on noise radiation at 90◦ from the jet axis, it is also assumed that the primary contributions to the Lighthill's stress tensor involve products of velocity fluctuations. The far-field noise spectral density is related to the Fourier transform of the autocorrelation function of the far-field pressure by the following expression:

$$S(\vec{x}, \omega) = \frac{1}{2\pi} \int_{-\infty}^{+\infty} \frac{< p'(\vec{x}, t) p'(\vec{x}, t + \tau) >}{\rho_0 c_0} e^{i\omega t} d\tau \tag{3.3}$$

where <> denotes an ensemble average. Because, in the far-field, $p' = \rho' c_0^2$, we obtain:

$$S(x,\omega) = \frac{1}{32\pi^3\rho_0 c_0^5 x^2}\int_{-\infty}^{+\infty}\iiint_{V(y_1)}\iiint_{V(y_2)} < \frac{\partial^2 T_{xx}}{\partial t^2}(\vec{y_1},t_1)\times\frac{\partial^2 T_{xx}}{\partial t^2}(\vec{y_2},t_2) > \times$$
$$\times e^{i\omega t} d\vec{y_1}, d\vec{y_2}, d\tau \tag{3.4}$$

where

$$t_1 = t - \frac{|\vec{x}-\vec{y_1}|}{c_0}$$
$$t_1 = t + \tau - \frac{|\vec{x}-\vec{y_2}|}{c_0} \tag{3.5}$$

and where T_{xx} is the component of Lighthill's stress tensor in the direction of the far-field observer and the variable x at the denominator of (3.4) is $x = |\vec{x}-\vec{y}| \simeq |\vec{x}|$.

If the turbulent statistics are assumed to be stationary and the usual far-field approximation is made, the integral in (3.4) become:

$$S(x,\omega) = \frac{1}{32\pi^3\rho_0 c_0^5 x^2}\int_{-\infty}^{+\infty}\iiint_{V(y_1)}\iiint_{V(y_2)} \times < T_{xx}(\vec{y_1},t)T_{xx}(\vec{y_2},t_0) > \times$$
$$\times e^{i\omega t} d\vec{y_1}, d\vec{y_2}, d\tau \tag{3.6}$$

where $\tau_0 = t + \tau + \hat{x}\cdot\frac{[(\vec{y_2}-\vec{y_1})]}{c_0}$. As noted by Lighthill and others[ref], it is better to include as many properties of the source as possibile before any modelling of the turbulent sources. In order to include the effects of source convection, the statistical properties of the sources may be described in a moving frame of reference; this also has the advantage that it is the temporal variation in this frame that controls the noise generation while, in a fixed reference frame, the temporal variation is dominated by the convection effects. Thus, the two-point cross-correlation function of the Lighthill's stress tensor, in a fixed reference frame, is:

$$R_f(\vec{y_1},\vec{\eta},\tau) =< T_{xx}(\vec{y_1},t)T_{xx}(\vec{y_2},t+\tau) > \tag{3.7}$$

with $\vec{\eta} = (\vec{y_2} - \vec{y_1})$, while in a moving reference frame, the correlation R_m can be supposed to take the following Gaussian form[3][17]:

$$R_m(\vec{y_1},\vec{\xi},\tau) = A^2\rho_s^2 u_s^4 e^{\frac{|\vec{\xi}|^2}{l_s^2-\omega_s^2\tau^2}} \tag{3.8}$$

where $\vec{\xi} = \vec{\eta} - \hat{i}\cdot c_0 M_c\tau$ (M_c convection Mach number and $\hat{i}$ unit vector in the direction of the mean flow), l_s is a characteristic length scale, ω_s a characteristic frequency in the moving frame, u_s a velocity scale that characterizes the turbulent velocity fluctuations, and A determines the magnitude of the correlation. The length and timescales may be obtained from the $k-\epsilon$ solution and we assume that:

$$\begin{aligned} \omega_s &= \frac{2\pi}{\tau_s} \\ \tau_s &= \frac{C_\tau k}{\epsilon} \\ l_s &= \frac{C_l k^{3/2}}{\epsilon} \end{aligned} \tag{3.9}$$

where the constants A, C_l and C_τ have to be determined empirically. We can therefore obtain the following expression for the noise spectral density:

$$dS(\vec{x},\omega) = \frac{A^2C_l^3}{C_\tau^3}\frac{\pi^2}{9\rho_0 c_0^5 x^2}\Big\{\rho_s^2 k^{7/2}(\frac{\omega}{\omega_s})^4 e^{\frac{-\omega^2}{4\omega_s^2}}\Big\}dV \tag{3.10}$$

The factor

$$(\frac{\omega}{\omega_s})^4 e^{\frac{-\omega^2}{4\omega_s^2}} \tag{3.11}$$

describes how each volume element contributes to a range of frequencies about the local characteristic frequency w_s.

The expression (3.10) is the final result achieved trough the Morris&Farassat model, based on acoustic analogy. It is also possibile to realise a further model which takes advantage of some aspects of theradically different approach proposed by Tam&Auriault and the method of Lighthill's acoustic analogy.

The starting point is (3.1). The Green's function of this wave equation is given by the solution of the equation:

$$\frac{\partial^2 G}{\partial t^2} - c_0^2 \frac{\partial^2 G}{\partial x_i \partial x_i} = \delta(\vec{x} - \vec{x_1})\delta(t - t_1) \tag{3.12}$$

and we seek a periodic Green's function such that:

$$G(\vec{x}, \vec{x_1}, t, t_1) = \int_{-\infty}^{\infty} \hat{G}(\vec{x}, \vec{x_1}, \omega) e^{[-i\omega(t-t_1)]} d\omega \tag{3.13}$$

Then, the Fourier transform of (3.12) is:

$$(\nabla^2 + k^2)\hat{G}(\vec{x}, \vec{x_1}, \omega) = \frac{\delta(\vec{x}, \vec{x_1})}{2\pi c_0^2} \tag{3.14}$$

The adjoint function $G_a((\vec{x}, \vec{x_s}, \omega))$ now satisfies the equation:

$$(\nabla^2 + k^2)\hat{G}_a(\vec{x}, \vec{x_s}, \omega) = \frac{\delta(\vec{x}, \vec{x_s})}{2\pi c_0^2} \tag{3.15}$$

and it is readily shown that:

$$\hat{G}(\vec{x_s}, \vec{x_1}, \omega) = \hat{G}_a(\vec{x_1}, \vec{x_s}, \omega) \tag{3.16}$$

Thus, the far-field density may be written, if the derivatives are transferred onto the adjoint function by integration by parts, as:

$$\rho'(\vec{x},t) = \int \dots \int \frac{\partial^2 G_a}{\partial x_{1i}\partial x_{1j}}(\vec{x_1},\vec{x},\omega)T_{ij}(\vec{x_1},t_1) \times e^{[-i\omega(t-t_1)]}d\omega dt_1 d\vec{x_1} \quad (3.17)$$

The noise spectral density defined by (3.3) takes the form:

$$\begin{aligned} S(\vec{x},\omega) = \frac{c_0^3}{\rho_0}\int \cdots \int \frac{\partial^2 G_a}{\partial x_{1i}\partial x_{1j}}(\vec{x_1},\vec{x},\omega_1)\frac{\partial^2 G_a}{\partial x_{2k}\partial x_{2l}}(\vec{x_2},\vec{x},\omega_2) \cdot \\ \cdot < T_{ij}(\vec{x_1},t_1)T_{kl}(\vec{x_2},t_2) > \times exp[-i\omega_1(t-t_1) - i\omega_2(t-t_2)] \\ \delta(\omega-\omega_2)d\omega_1 d\omega_2 dt_1 dt_2 d\vec{x_1} d\vec{x_2} \end{aligned} \quad (3.18)$$

Now, assuming that the two-point cross correlation of the Lighthill's stress tensor in a fixed frame of reference is given by:

$$< T_{ij}(\vec{x_1},t_1)T_{kl}(\vec{x_2},t_2) >= A_{ijkl}\rho_s^2 u_s^4 exp\left\{\frac{-|\xi|^2}{\bar{u}\tau_s} - \frac{1}{l_s^2}\left[(\xi-\bar{u}\tau)^2 + \eta^2 + \zeta^2\right]\right\} \quad (3.19)$$

where

$$\begin{aligned} \xi &= x_1 - x_2 \\ \eta &= y_1 - y_2 \\ \zeta &= z_1 - z_2 \\ \tau &= t_1 - t_2 \end{aligned} \quad (3.20)$$

considering the solution of (3.15), say:

$$G_a(\vec{x_1},\vec{x},-\omega) = -\frac{1}{8\pi^2 c_0^2}\frac{exp[ik|\vec{x_1}-\vec{x}|]}{|\vec{x_1}-\vec{x}|} \quad (3.21)$$

in the far-field and at $\theta = \pi/2$ with θ denoting the polar angle measured from the downstream jet axis, and considering the scaling laws of (3.9) we obtain:

$$dS(\vec{x},\omega) = \frac{\pi^2\sqrt{\pi}}{9\rho_0 c_0^5 x^2}\frac{A^2 C_l^2}{C_\tau^3}\rho_s^2 k^{7/2}\frac{(\frac{\omega}{\omega_s})^4}{1+\frac{4\pi^2\omega^2}{\omega_s^2}} \times \exp\Big[-\frac{\pi^2 C_l^2}{C_\tau^2}\frac{\omega^2}{4\omega_s^2}\frac{k}{\bar{u}^2}\Big]dV \quad (3.22)$$

This result is similar to the one obtained by TamAuriault and described in next section, except for the significant change in the frequency exponent that is 2 in Tam&Auriault model while is 4 in Morris&Farassat model.

3.1.5 Tam & Auriault model for subsonic jet flow

The reason why we describe two different models for the prediction of jet mixing noise is that there are some substantially difference between the model of Morris&Farassat and that one proposed by Tam&Auriault. First, the Morris&Farassat model is based on the Lighthill's acoustic analogy while Tam&Auriault proposed a model containing some heuristic arguments to describe the noise sources inspired by the kinetic theory of gases and used the linearized Euler equations to describe the propagation of sound generated by the model sources. In the Morris&Farassat model it is assumed that the source is compact and the two-point cross correlation function for the source can be modelled in a moving reference frame. The Green's function in the Morris&Farassat model is simply the free-space Green's function for the wave equation. In Tam&Auriault model there is no explicit assumption concerning the compactness of the source, the two point cross correlation function is defined in a fixed frame of reference, and the Green's function is obtained from the adjoint solution of the linearized Euler equations. A final difference between the two formulations is that the far-field noise depends on a model for the cross correlation of the Lighthill's stress tensor in Morris&Farassat

model, and on the cross correlation of the convective derivative of the source term in Tam&Auriault model.

About the question of how the fine scale turbulence in a jet generates sound, Tam&Auriault proposed a gas kinetic theory analogy. The use in turbulence of the analogy with gas kinetic theory is well established. We can regard the fine-scale turbulence as a distribution of small blobs of fluid moving randomly, in the same way as the motion of gas molecules in a moving frame fixed with the mean flow of velocity v.

Suppose that m is the mass of a molecule, and n is the number of molecules per unit of volume. Because of the random motion of the gas molecules, the gas exerts a pressure p on its surroundings. It is a simple matter to show that, following the standard kinetic theory of gases[47][48], p is given by:

$$p = \frac{1}{3}mn < v \cdot v >= \frac{1}{3}\rho < v^2 > \tag{3.23}$$

where v is the random molecular velocity, ρ is the density of the gas, and $<>$ is the ensemble average.

By analogy with the gas molecules, let u be the random velocity of the fine-scale turbulence measured in the mean flow moving frame. The fine-scale turbulence effectively exerts a pressure p_{turb} on its surroundings equal to:

$$p_{turb} = q_s = \frac{1}{3}\rho < v^2 >= \frac{2}{3}\rho k_s \tag{3.24}$$

where $k_s = \frac{1}{2} < v^2 >$ is the kinetic energy of the fine scale turbulence per unit mass. This pressure must be balanced by pressure and momentum flux of the surrounding fluid. The fluctuation of this pressure generates acoustic disturbances. It is argued that once sound is generated by these local pressure fluctuations, the propagation of the noise may be described by the Linearized

Euler equations with a source term on the right-hand side related to the fluctuating pressure gradient generated by the fine-scale turbulence. That is:

$$\bar{\rho}\Big[u_i' + \bar{u_j}\frac{\partial u_i'}{\partial x_j}\Big] + \frac{\partial p'}{\partial x_j} = -\frac{\partial q_s}{\partial x_i} \tag{3.25}$$

where the overbar denotes a mean quantity and the primes denote acoustic field variables. The sound waves satisfy the linearized equations of energy and continuity and the equation of state for a perfect gas:

$$p + \bar{u_j}\frac{\partial p}{\partial x_j} + \gamma\bar{p}\frac{\partial u_i}{\partial x_j} = 0 \tag{3.26}$$

The new approach of Tam&Auriault for describing the mean flow acoustic interaction, rather than converting the left-hand side operators into Lilley's equation, is to make use of the adjoint equation. In fact, it is shown[39] that the periodic Green's function for the LEE (Linearized Euler equations) is related to the solution of adjoint Euler equations by:

$$\begin{aligned}
\hat{p_1}(\vec{x_0}, \vec{x_1}, \omega) &= u_a(\vec{x_1}, \vec{x_0}, \omega) \\
\hat{p_2}(\vec{x_0}, \vec{x_1}, \omega) &= v_a(\vec{x_1}, \vec{x_0}, \omega) \\
\hat{p_3}(\vec{x_0}, \vec{x_1}, \omega) &= w_a(\vec{x_1}, \vec{x_0}, \omega)
\end{aligned} \tag{3.27}$$

where p_n for $(n = 1, 2, 3)$ are the Green's functions for sources, in cylindrical components, of the linearized momentum equations and u_a, v_a and w_a are the solutions of the adjoint linearized momentum equations that may be written in this way:

$$\bar{\rho}\Big\{i\omega u_a + \bar{u}\frac{\partial u_a}{\partial x}\Big\} + \gamma\bar{p}\frac{\partial p_a}{\partial x} = 0$$

$$\bar{\rho}\left\{ i\omega v_a + \bar{u}\frac{\partial v_a}{\partial x} - \frac{\partial \bar{u}}{\partial r}u_a \right\} + \frac{\gamma\bar{p}}{r}\frac{\partial(p_a r)}{\partial r} = 0$$
$$\bar{\rho}\left\{ i\omega w_a + \bar{u}\frac{\partial w_a}{\partial x} \right\} + \frac{\gamma\bar{p}}{r}\frac{\partial(p_a)}{\partial \phi} = 0$$
$$\left(i\omega p_a + \bar{u}\frac{\partial p_a}{\partial x} \right) + \left[\frac{1}{r}\frac{\partial(v_a r)}{\partial r} + \frac{1}{r}\frac{\partial w_a}{\partial \phi} + \frac{\partial u_a}{\partial x} \right] = -\frac{1}{2\pi}\delta(x - x_0) \quad (3.28)$$

The general solution is given, once known the Green functions, by the convolution of Green's functions with the source terms:

$$p'(\vec{x},t) = -\int\cdots\int \left\{ \nabla_1 \cdot \Big[u_a(\vec{x_1},\vec{x},\omega) q_s(\vec{x_1},t_1) \Big] - q_s(\vec{x_1},t_1)\nabla_1 \cdot \right.$$
$$\left. \cdot \Big[u_a(\vec{x_1},\vec{x},\omega) \Big] \right\} \times exp\Big[-i\omega(t-t_1) \Big] d\omega dt d\vec{x_1} \quad (3.29)$$

where

$$\nabla_1 \equiv \left(\frac{\partial}{\partial x_1}, \frac{\partial}{\partial r_1}, \frac{1}{r_1}\frac{\partial}{\partial \phi_1} \right)$$
$$u_a(\vec{x_1},\vec{x_0},\omega) = [u_a, v_a, w_a](\vec{x},\vec{x_0},\omega) \quad (3.30)$$

However, the divergence of the adjoint velocity is known from the equation for the adjoint pressure p_a, given by the fourth of (3.28). Also, q_s is zero at the source point for the adjoint solution, so that:

$$p'(\vec{x},t) = -\int\cdots\int \left(i\omega p_a + \bar{u}\frac{\partial p_a}{\partial x_1} \right)(\vec{x_1},\vec{x},\omega) q_s(\vec{x_1},t_1) \times$$
$$\times exp[-i\omega(t-t_1)] d\omega dt d\vec{x_1} \quad (3.31)$$

or

$$p'(\vec{x},t) = -\int\cdots\int \left(t_1 + \bar{u}\frac{\partial}{\partial x_1} \right)\{ p_a exp[-i\omega(t-t_1)] \} \times$$
$$\times q_s(\vec{x_1},t_1) d\omega dt d\vec{x_1} \quad (3.32)$$

Note that, at this stage of the analysis, the convective derivative acts on the adjoint solution. However, integration by parts yields:

$$p'(\vec{x},t) = -\int \ldots \int \Big(t_1 + \bar{u}\frac{\partial}{\partial x_1}\Big)\{p_a \exp[-i\omega(t-t_1)]\} \times$$
$$\times \frac{\mathrm{D}}{\mathrm{D}t_1}[q_s(\vec{x_1},t_1)]d\omega dt d\vec{x_1} \tag{3.33}$$

where the convective derivative is given by:

$$\frac{\mathrm{D}}{\mathrm{D}t_1} = +\bar{u}\frac{\partial}{\partial x_1} \tag{3.34}$$

Using (3.3), the spectral density for the intensity is then obtained by forming the autocorrelation for the pressure and taking its Fourier transform. The spectral density is then found to be given by:

$$S(\vec{x},\omega) = \frac{1}{\rho c_0}\int \ldots \int p_a(\vec{x_1},\vec{x},\omega)p_a(\vec{x_2},\vec{x},\omega) \times < \frac{\mathrm{D}}{\mathrm{D}t_1}\{q_s\vec{x_1},t_1)\}$$
$$\frac{\mathrm{D}}{\mathrm{D}t_2}\{q_s\vec{x_2},t_2)\} > \times \exp[-i(\omega_1+\omega_2)t + i\omega_1 t_1 + i\omega_2 t_2] \cdot$$
$$\cdot\delta(\omega-\omega_2)d\omega_1 d\omega_2 dt_1 dt_2 d\vec{x_1} d\vec{x_2} \tag{3.35}$$

It is necessary to make some assumption about the correlation function for the source terms. Basing on experimental measurements, Tam&Auriault assume that:

$$< \frac{\mathrm{D}}{\mathrm{D}t_1}\{q_s\vec{x_1},t_1)\}\frac{\mathrm{D}}{\mathrm{D}t_2}\{q_s\vec{x_2},t_2)\} >= \frac{q_s^2}{c^2\tau_s}\exp\Big\{-\frac{|\xi|}{\bar{u}\tau_s} - \frac{1}{l_s^2}\Big[(\xi-\bar{u}\tau)^2 +$$
$$+\eta^2+\zeta^2\Big]\Big\} \tag{3.36}$$

In addition, there is a crucial point in the formulation: the turbulence statistics are modelled in terms of the cross correlation of the convective

derivative of the source. When the sequence of integration given by Tam&Auriault is followed, it is straightforward to show that:

$$S(\vec{x},\omega) = \frac{4\pi^2\sqrt{\pi}}{\rho_0 c_0}\int\int\int |p_a(\vec{x_2},\vec{x},\omega)|^2 \times$$
$$\times \frac{q_s^2}{c^2\tau_s} l_s^3 \frac{\exp\left\{\frac{-\omega^2 l_s^2}{4\bar{u}^2}\right\}}{\left[1+\omega^2\tau_s^2\left(1-\frac{\bar{u}cos\theta}{a_\infty}\right)\right]} d\vec{x_2} \tag{3.37}$$

with θ denoting the polar angle measured from the downstream jet axis (it is assumed that the length scale l_s is small compared to total extent of the source region) and where we have used, as suggested by Tam&Auriault, that the difference between $p_a(\vec{x_1},\vec{x},-\omega)$ and $p_a(\vec{x_2},\vec{x},-\omega)$ is a simple phase factor such that

$$p_a(\vec{x_1},\vec{x},-\omega) \simeq p_a(\vec{x_2},\vec{x},-\omega)\exp\left[-i\left(\frac{\omega}{a_\infty}\right)cos\theta(\vec{x_1}-\vec{x_2})\right] \tag{3.38}$$

This implies that the sources have a limited spatial extent. That is, the length scale l_s is small compared to the total extent of the source region.

To obtain a closed-form result, it is necessary to determine $|p_a(\vec{x_2},\vec{x},-\omega)|$. Because at $\theta = \pi/2$ the effects of the mean flow are negligible, the equations for the adjoint functions may be reduced to a Helmholtz equation for the adjoint pressure:

$$\nabla^2 p_a + k^2 p_a = (\frac{i\omega}{2\pi c_0^2})\delta(\vec{x}-\vec{x_2}) \tag{3.39}$$

so that:

$$|p_a(\vec{x_2},\vec{x},-\omega)|^2 = \frac{\omega^2}{64\pi^4 c_0^4 x^2} \tag{3.40}$$

Then from (3.37) at $\theta = \pi/2$ and reminding that $q_s^2/c^2 = 4A^2\rho^2k^2/9$, the contribution to spectral density from an elemntal volume of turbulence is given by:

$$dS(x,\omega) = \frac{\sqrt{\pi}}{p\rho_0 c_0^5 x^2}\frac{A^2C_l^2}{C_\tau^3}\rho_s^2 k^{7/2}\frac{(\frac{\omega}{\omega_s})^2}{1+\frac{4\pi^2\omega^2}{\omega_s^2}} \times \exp\Big[-\frac{\pi^2C_l^2}{C_\tau^2}\frac{\omega^2}{\omega_s^2}\frac{k}{u^2}\Big] \qquad (3.41)$$

that is substantially the final result of Tam&Auriault model to be compared with the equivalent expression in (3.22) for Morris&Farassat model.

3.1.6 Shen model for supersonic jet flow

Compared with a subsonic jet, a supersonic jet is more efficient in generating noise. In addition to the well known mixing noise, there are two additional noise component commonly found in supersonic jets; they are termed Mach wave radiation and shock associated noise.

Mach wave radiation may be considered in hot, high subsonic jets or cold supersonic jets above Mach 2. It is generated by convected turbulent large structures with supersonic phase speed. Shock noise is associated with imperfectly expanded jets.

The shocks in an imperfectly expanded supersonic jet interact with the jet turbulence to produce a source of noise in addition to that due to the turbulent mixing. This source has two components, one of which consists of discrete tones, usually referred as screech tones and the other are with a more broadband character, usually referred shock associated noise. The former one, which involves an acoustic feedback from the source region to the nozzle, was studied in detail by Powell[56]. The second one, which is essentially due to the same source but without the acoustic feedback, has been studied by Harper-Bourne and Fischer[53].

In the following section we will study the broadband shock noise using a

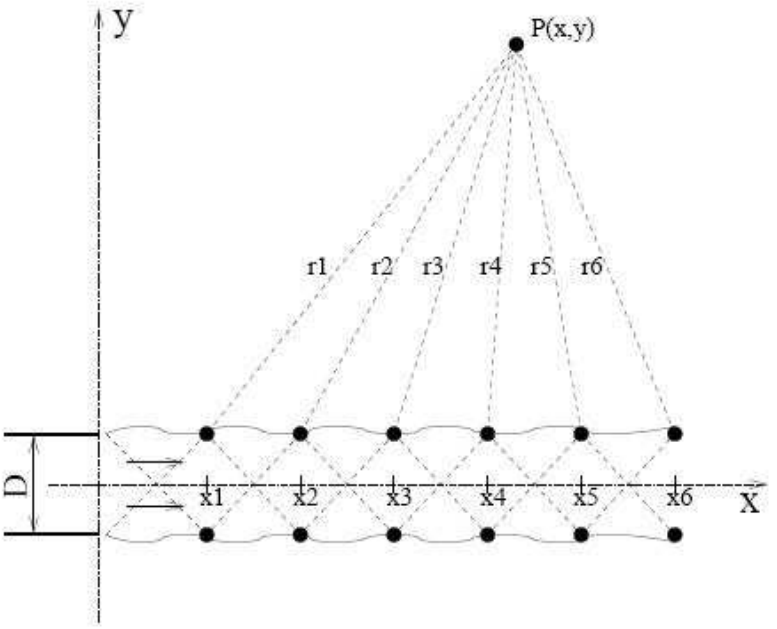

Figure 3.1: Schematic of phased array of shock cell noise sources in a jet flow. At the point P interference can occur depending on the phase difference between two adjacent sources. The relative phasing is set by the convection of turbulent eddies between the sources.

semi-analytical approach derived by Shen et Al.[52] from the Harper-Bourne model.

The Shen model is an improvement of a previous and well-known semi-empirical prediction model based on phased array noise sources developed by Harper-Bourne and Fisher[53] that allows reasonably accurate predictions of the main characteristics of broadband shock noise, in terms of peak frequency and noise spectral behaviour, for simple jets.

The premise of the model is that the shock noise is generated by the interactions of shock cells with coherent large turbulence structures represented by instability waves in the jet shear layer. A steady RANS solution is used

to calculate the shock cell structure and the turbulence statistics $(k-\epsilon)$. The concept of phased array is illustrated in figure (3.1). Assuming noise sources are concentrated at the tip of each shock cell at axial location x_n with $n = 1, 2, \ldots, N$; let be F_n(t) be the corresponding source function in time. At the far field location $r(x, y)$ the observed acoustic pressurefrom all sources is:

$$p(\vec{r}, t) = \sum_{n=1}^{N} \frac{1}{r_n} F_n(t - \frac{r_n}{c_0}) \tag{3.42}$$

Here r_n is the distance between the n_{th} source point and the far-field location. The autocorrelation of acoustic pressure at the far-field can be calculated as:

$$R(\vec{r}, t) = p(\vec{r}, t)p(\vec{r}, t + \tau) = \sum_{m=1}^{N} \sum_{n=1}^{N} \frac{1}{r_n r_m} F_m(t) F_n(t + \bar{\tau} - \frac{r_n - r_m}{c_0}) \tag{3.43}$$

Equation (3.43) represents a summation of correlations between source functions. Let $R_{mn}(t)$ be the correlation of source functions:

$$R_{mn}(\tau) = F_m(t)\bar{F_n}(t + \tau) \tag{3.44}$$

The source functions reflect the interactions between converting turbulence eddies and the stationary shock cell structure. The turbulent eddies, especially those with large scales, may pass through a number of shock cells before being fully dissipated. Therefore, there are similarities between source functions at different source points in a time-delayed fashion, that can be expressed as:

$$F_n(t) = F_m(t - \tau_{mn})G_{mn}(t) \tag{3.45}$$

where $\tau_{mn} = (x_n - x_m)/u_c$ and u_c is the eddy convection speed. $G_{mn}(t)$ is an arbitrary slow function of time. Substituting (3.45) into (3.44) relates $R_{mn}(\tau)$ to self-correlation $R_{mm}(\tau)$:

$$R_{mn}(\tau) = R_{mm}(\tau)\bar{G_{mn}} \tag{3.46}$$

where we made use of the mean value of $G_{mn}(t)$. Thus (3.43) becomes:

$$R(\vec{r}, \tau) = \sum_{m=1}^{N}\sum_{n=1}^{N} \frac{\bar{G_{mn}}}{r_m r_n} R_{mm}(\tau - \tau_{mn} - \tau'_{mn}) \tag{3.47}$$

where $\tau'_{mn} = (r_n - r_m)/c_0$. The far-field acoustics power spectral density can be calculated by taking the Fourier transform of the auto-correlation:

$$S(\vec{r}, \omega) = \frac{1}{2\pi}\int_{-\infty}^{+\infty} R(\vec{r}, \tau)e^{i\omega\tau}d\tau = \sum_{m=1}^{N}\sum_{n=1}^{N} \frac{\tilde{S}_{mn}(\omega)}{r_n r_m} e^{i\omega(\tau_{mn}+\tau'_{mn})} \tag{3.48}$$

with:

$$\begin{aligned} \tilde{S}_{mn}(\omega) &= \bar{G}_{mn}\tilde{S}_{mm}(\omega) \\ \tilde{S}_{mm}(\omega) &= \frac{1}{2\pi}\int_{-\infty}^{+\infty} R_{mm}(\tau)e^{i\omega\tau_{mn}} \end{aligned} \tag{3.49}$$

where S_{mm} is the power spectral density of a single source and S_{mn} the cross correlation between two source points. In Harper-Bourne and Fisher models, the source spectra are modelled as follows:

$$\begin{aligned} \tilde{S}_{mn}(\omega) &= C_{|m-n|}(\omega)\tilde{S}^{1/2}_{mm}(\omega)\tilde{S}^{1/2}_{nn}(\omega) \\ \tilde{S}_{mm}(\omega) &= \frac{\beta^4 D^2 L_s}{c_0} H_0(\frac{\omega L_s}{2\pi c_0}) \end{aligned} \tag{3.50}$$

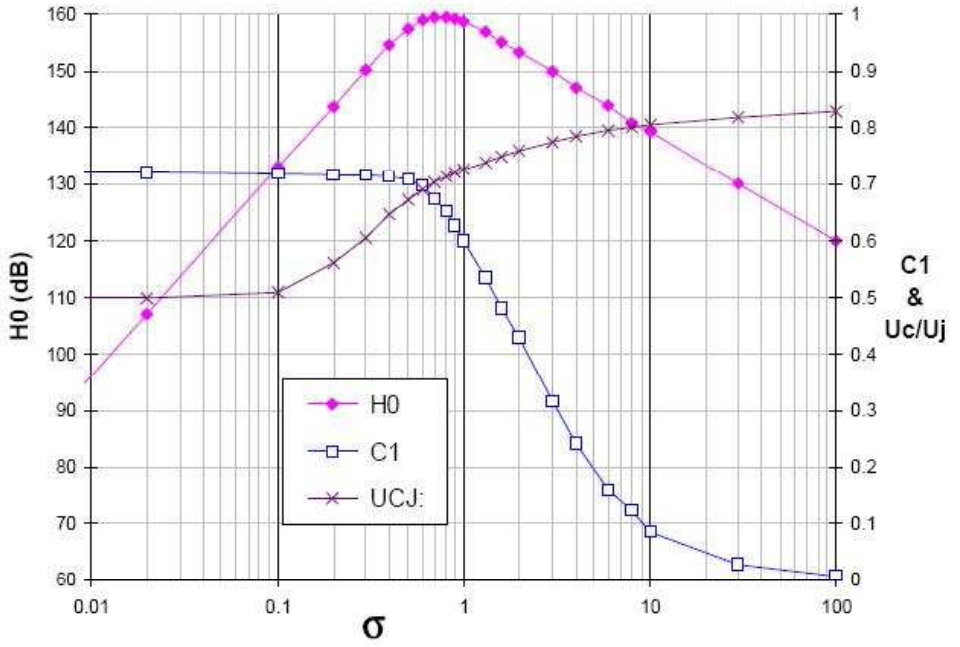

Figure 3.2: Universal generic parameters H_0 and C_1 as originally evalutated for unheated round jets[53].

The function H_0 can be regarded as the universal source spectrum of shock noise. The universal generic parameters, H_0 and C_1, as originally evaluated for unheated round jets, are presented in figure (3.2) against the Helmotz number $\frac{\omega L}{u_c}$[54].

The final expression for the power spectral density at the far field takes the following form:

$$S(r,\omega) = C_0 \sum_{m=1}^{N}\sum_{n=1}^{N} \frac{C_{|m-n|}(\omega)}{r_m r_n} \frac{\delta\bar{p}_m \bar{p}_n D_m D_n (L_m)^{1/2}(L_n)^{1/2}}{a_\infty} \times$$
$$\times (H_0)^{1/2} \left(\frac{\omega L_m}{2\pi a_\infty}\right) e^{i\omega(\tau_{mn}+\tau'_{mn})} \tag{3.51}$$

The pressure variation $\delta p'$ is an estimated pressure, normalized by the

ambient pressure, of the noise source and it can be extracted from the CFD solution by using the following formula:

$$\delta p' \approx \frac{k^2}{u_s \epsilon} \frac{\Delta p_s}{L_s} \tag{3.52}$$

where Δp_s is the steady pressure variation across a schock cell normalized with the ambient pessure, and L_s is the shock cell mutual distance.
The radial averages of p_s and $\sigma = \frac{k}{\epsilon} u_s$, with u_s denoting the eddy convection speed, are carried out by:

$$\begin{aligned} \bar{p}_s(x) &= \frac{\int_{R_0}^{R_{jc}} 2r p_s(x,r) dr}{R_{jc}^2 - R_0^2} \\ \bar{\sigma}(x) &= \frac{\int_{R_0}^{R_{je}} 2r \sigma(x,r) dr}{R_{je}^2 - R_0^2} \end{aligned} \tag{3.53}$$

Here R_0 is the inner boundary of the jet, R_{jc} is the radial location where the turbulent eddy viscosity reaches the maximum and R_{je} is the radial location at which the turbulent viscosity drops to 10% of the maximum value. At this point the averaged source strength in pressure, that appears in equation (3.52) can be defined for each shock cell as:

$$\delta p'_n \approx \frac{\sigma_n}{L_n} \Delta p_{s,n} \tag{3.54}$$

for $n = 1, \cdots, N$.

Considering that x_n is the axial location of the shock cell and that r_n is the distance between the n^{th} source point and the far-field location, the variables τ_{mn} and τ'_{mn} correspond respectively to $(x_n - x_m)/u_c$ and $(r_n - r_m)/a_\infty$ with u_c and a_∞ denoting the eddy convection speed and the ambient speed of sound. $D_m$is the local equivalent diameter and is defined as:

$$D_m = 2[R_{jc}^2(x_m) - R_0^2(x_m)]^{1/2} \tag{3.55}$$

C_{m-n} is the correlation coefficient for the adjacent source combination and is defined as:

$$C_{m-n}(\omega) = \frac{S_{mn}(\omega)}{S_{mm}^{1/2}(\omega) S_{nn}^{1/2}(\omega)} \tag{3.56}$$

This quantity has a vanishing behaviour at the high frequencies, but it is otherwise nearly constant. An useful formula for it is:

$$C_{m-n}(\omega) = C_1^{m-n2}(\omega) \tag{3.57}$$

A brief comment is necessary for describing the proper value of H_0 to put into (3.51). How we can see in the figure (3.2), H_0 is already expressed in Decibels: this means that H_0 is evaluated as $10log(\frac{H_{00}}{p_{ref}^2})$, this implies that in the expression (3.51), that is a power spectral density, we have to insert the value of H_00 as $H_00 = p_{ref}^2 \cdot 10^{H_0/10}$.

3.2 Numerical results

In this section we present the results for

- the subsonic jet noise prediction obtained by using the Morris&Farassat model[40] and the Tam&Auriault model[39]. The analysis is focused on the mixing noise at 90°.
- the supersonic jet noise prediction obtained by using the Shen model[54] (an update of Harper-Bourne and Fisher model) focusing on shock associated noise.

3.2.1 Subsonic jet flow

A demonstration of the RANS-based semi-analyitical prediction is made in this report for the low-Reynolds number case of Stromberg et Al.[45].
For this case we have used the values:

$$\begin{aligned} M &= 0.9 \\ Re &= 3600 \\ D_j &= 0.0079 \quad m \\ u_j &= 284 \quad m/s \\ p_\infty &= 0.018 \quad atm \end{aligned} \tag{3.58}$$

Figure (3.3) shows results obtained by using the model of Tam&Auriault. The noise intensity spectral density is plotted. The two lines correspond to two different RANS solutions generated by ZEN code (realised by CIRA), one utilizing the Myong-Kasagi $k-\epsilon$ model and the other one with Dash and Pope $k-\epsilon$ model.

The corresponding Sound Pressure Level (SPL) is given by:

$$SPL(dB) = 10log\left[\frac{4\pi S(x,\omega)}{\frac{p_{ref}^2}{\rho a_\infty}(\frac{D_j}{u_j})}\right] \tag{3.59}$$

where $p_{ref} = 2\mu Pa$ is the reference pressure. Figure (3.4) shows the two SPL curves obtained with the two different RANS solution compared with similar results obtained by Afsar et Al[49], on the same jet flow of Stromberg.

The comparison between the two calculation has to be done taking into account the directivity of SPL measured by Stromberg et Al.[45] and reported in Figure (3.5) showing that a difference of 12 dB is to be expected between the noise peak at 90° and the noise at 30°.

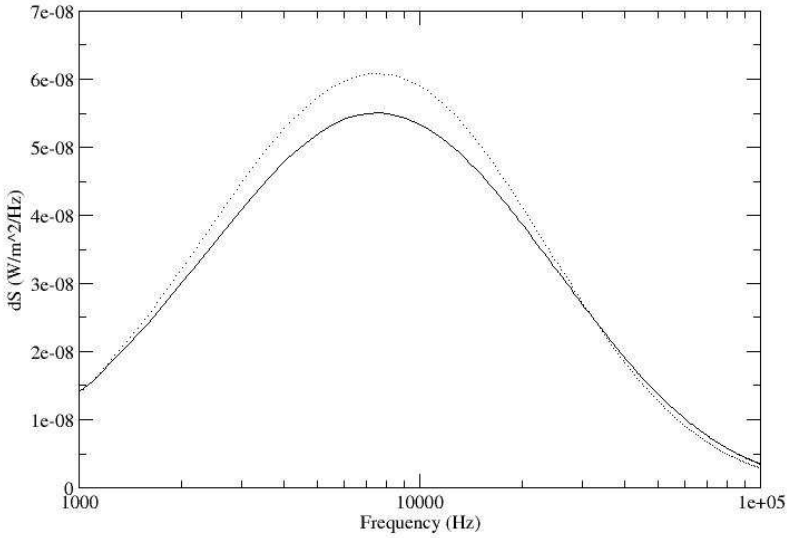

Figure 3.3: Sound spectral density obtained by applying the Tam&Auriault model to ZEN steady-RANS output. The solid line is the result obtained from Myong-Kasagi solution, while the dot line is the result obtained from Dash and Pope solution.

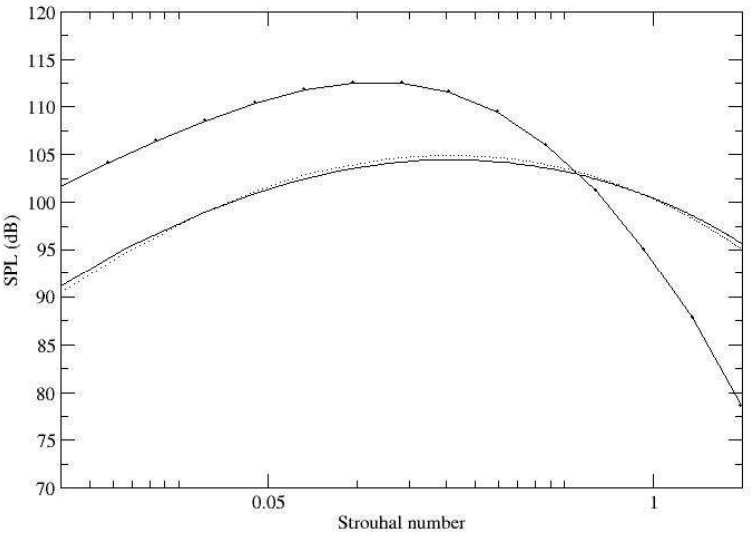

Figure 3.4: Sound Pressure level versus the Strouhal numer $St = (\omega \cdot D_j)/u_j$. The full line and the point line represent the ZEN-based results at 90 degrees obtained with Tam&Auriault model while the full line with the circles represents the sound pressure level prediction calculated by Afsar et Al.[54] at an observation angle of 30°.

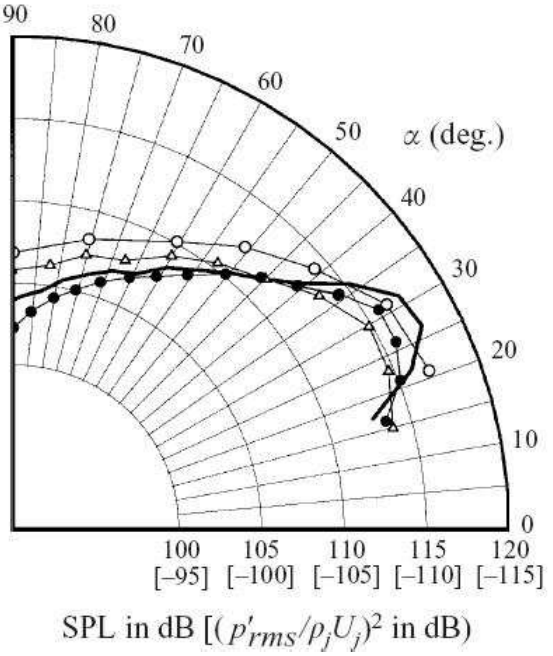

Figure 3.5: Overall Sound Pressure level directivity at a distance of $30D_j$ from the nozzle. The angle α is measured from the jet axis. The full circles are the Stromberg data, the blank circles are from Mollo-Christensen et Al. experiments data[50], the triangles are Lush experimental data[51] and lines are from Afsar et Al[49].

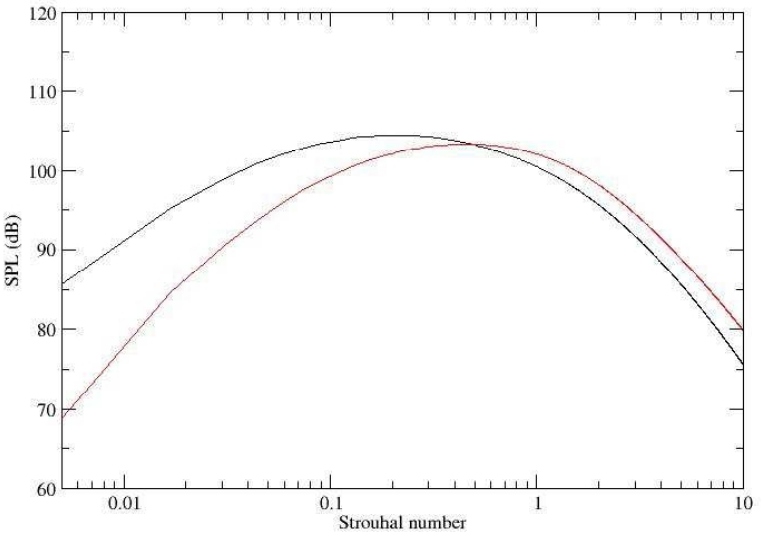

Figure 3.6: Comparison of noise spectra obtained with Tam&Auriault model (black line) and Morris&Farassat model (red line). The jet flow conditions are those of Stromberg.

The same noise prediction is carried out by using equation (3.22). Figure (3.6) shows the comparison between the Tam&Auriault results and the Morris&Farassat results. It can be observed that the noise peak value is similar, but a slight difference in the frequency peak occurs.

It is clear that the RANS-based semi-analytical results are not completely in agreement with the experimental data. However it is remarkable that the values for the SPL peak are coincident. In fact, with our prediction model, we obtain an SPL peak around 103 dB at 90° from jet axis, and, combining Figure (3.4) with Figure (3.5), it is clear that it is the same result obtained by Afsar et Al.[49].

The peak Strouhal frequency is not perfectly predicted: it is around

0.13 in the Afsar et Al. calculation and 0.2 in our calculation based on Tam&Auriault model. Moreover, the high frequency decay in Afsar et Al. prediction is faster than the one predicted with the present model, but the reason for this discrepancy can be due to two facts:

- The Tam&Auriault model is formulated for an observation angle of 90° while the Stromberg data and the Afsar et Al. results showed in Figure have been taken and calculated at 30°.
- The semi-analytical model strictly depends on three RANS statistical quantities, say A, C_l, C_τ, that in this case are chosen as $A = 0.773$, $C_l = 0.256$ and $C_\tau = 0.233$, as suggested by Tam&Auriault. Different values can significantly modify the prediction.

Concerning the model of Morris&Farassat, we can see that it predicts the same value of SPL peak as Tam&Auriault model, while there is a different prediction of Strouhal peak. The exponential decay is similar in the two models.

Globally, the agreement between the RANS-base mixing noise model and the experimental data and other numeric results can be intended as encouraging taking account that the choice of the turbulence model seems to no modify the acoustic results. On the other hand, the choice of the jet noise semi-analytical model yields a different peak frequency prediction but not a different SPL peak. Both models, however, predict an overestimated frequency peak.

3.2.2 Supersonic jet flow

The Shen model has been implemented in a fortran code in order to perform some preliminary validation test.
The test case is the noise generated by an under-expanded supersonic round

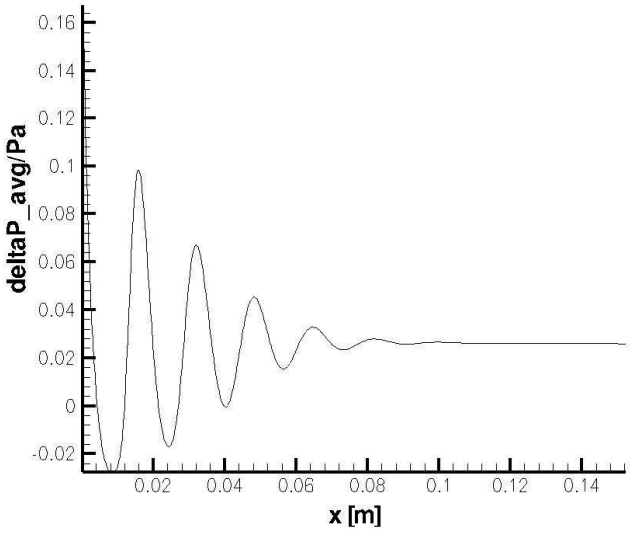

Figure 3.7: Radial average of p_s and σ and extraction for discrete source strength. For each shock cell is also indicated the location x_n, the spacing L_n and $\Delta\bar{p}_s, n$, that is the variation of radial average of pressure.

jet exhausting into a quiescent infinite medium, with a fully expanded jet Mach number $M_j = 1.2$ and with a nozzle diameter of 1.6 cm [54].
In Figure (3.7) the radial averages of the static pressure p_s for each shock cell are showm. The pressure variations and the shock cell spacing are extracted from the cells. In Figure (3.8) the radial average of σ are shown. The values of σ in the point x_n where are the shock cells correspond to the parameters σ_n.

Once the parameters are extracted according to equation (3.54) all the informations for calculating the power spectral density are available.
Figure (3.9)shows the far-field Sound Pressure Level evaluated at an angle of 90°. A primary peak of 100 dB at a frequency of 1.1 kHz can be observed.

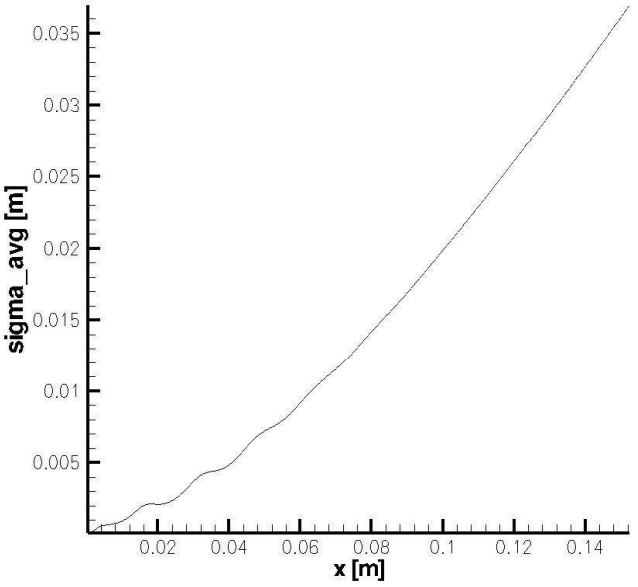

Figure 3.8: Radial average σ_n extracted at any shock position x_n.

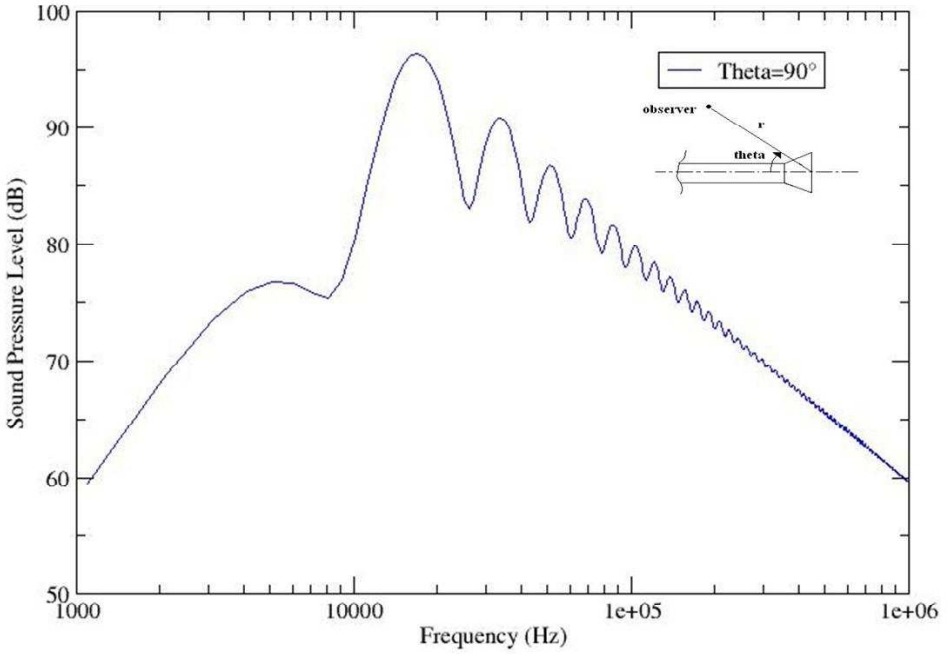

Figure 3.9: Sound Pressure Level at 90°. The peak is around 96 decibels.The angle θ is evaluated as showed on the right side on the top of the figure.

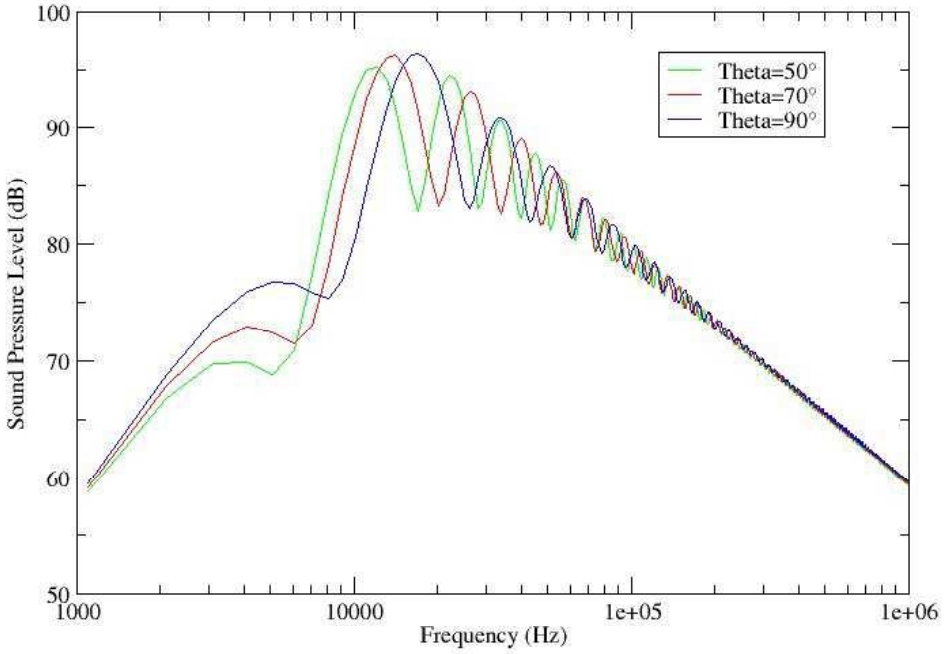

Figure 3.10: Sound Pressure Level calculated at 50°, 70° and 90°. The angle θ is evaluated as showed on figure (3.9).

In Figures (3.10) and (3.11)several Sound Pressure Levels at increasing angles are compared. It is visible that, increasing the angle θ, a frequency shift of the peak occurs. Moreover an increase of 2 or 3 decibels of the primary peak is observed when the angle increases.

The trend of the frequency peak as a function of the angle θ may be compared with the following formula, that gives the primary peak frequency resulting from the principle of constructive interference between the noise sources, that is:

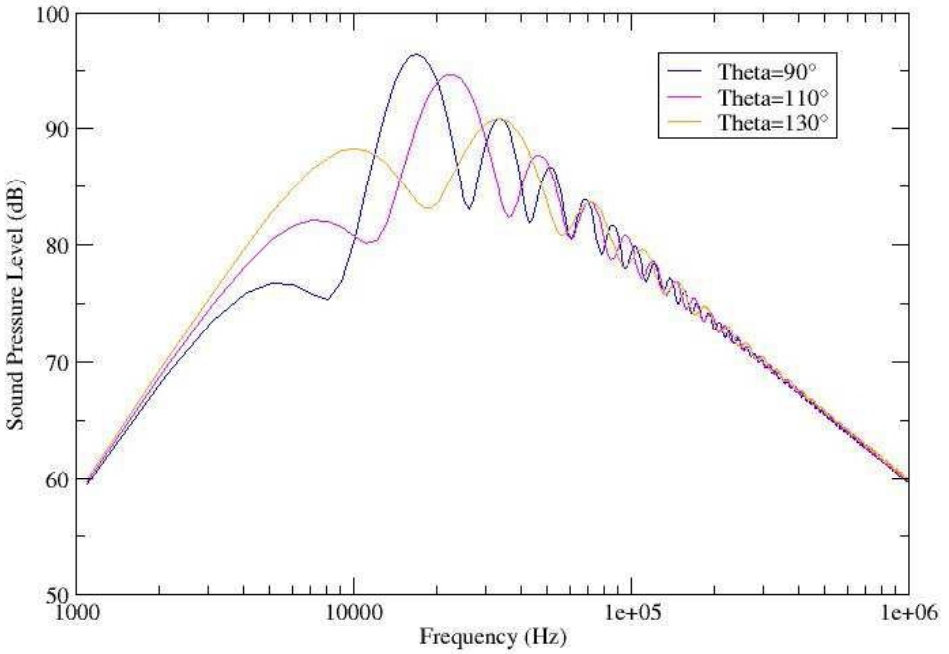

Figure 3.11: Sound Pressure Level calculated at 90°, 110° and 130°. The angle θ is evaluated as showed on figure (3.9).

$$f_p = \frac{u_c}{L_s(1 + M_c cos\theta)} \tag{3.60}$$

In equation (3.60) $M_c = u_c/c_0$ is the convection Mach number based on the ambient speed of soud. Comparison of equation (3.60) with our model is in reasonably good agreement: putting a reasonable average value of all the shock spacing cells as L_s and inserting the value of M_c and u_c, the formula (3.60) predicts an increasing of the frequency when the angle goes from 50° to 70° and then to 90°.
The agreement is qualitative but it is a verification of the model.
Furthermore, observing the dependence of Sound Pressure Level from the angle, our results are in agreement with the numerical ones obtained by Shen[52]: that is a little increase (1 or 2 dB) of SPL when we increase the angle from 50° to 70° and from 70° to 90°.

This trend is not in agreement with experimental data[55] that instead show a decrease of the SPL at increasing angles. The Shen model gives a good estimate for the value of SPL but it cannot represent the trend when the angle increase.
Finally, concerning the absolute value of SPL, Figure (3.12) compares our results with those of Norum&Brown[55] who measured the jet mixing noise at far-field. The mixing noise contains the broadband shock cell term and, as can be seen, the upper curve in the figure, corresponding to a flight Mach number of 0, is about 5 dB greater than our numerical prediction.

3.3 Description of the tool for subsonic case

In Figure (3.13) is shown the input file of the tool implemented for the verification of the Tam model. The first two lines specify the CFD input files, geometry and solution, in PLOT3D format. Then there are all the

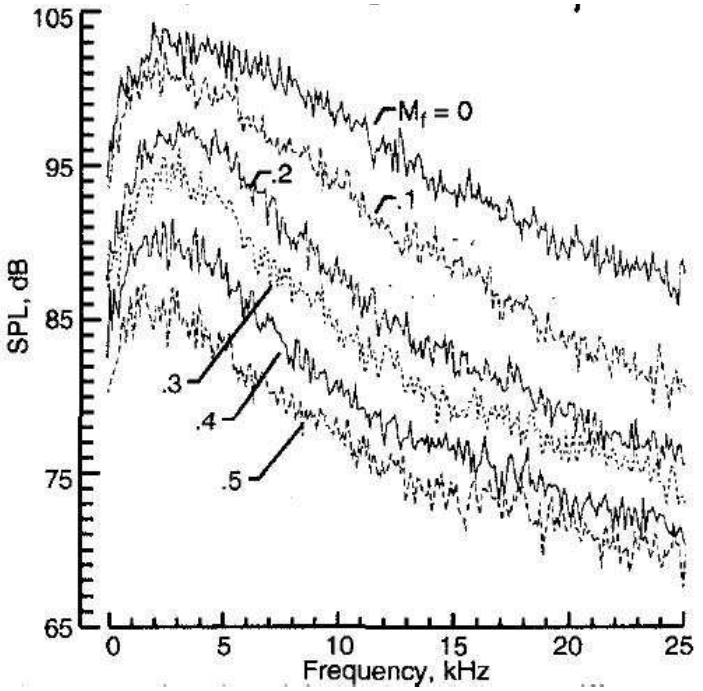

Figure 3.12: Far-field jet mixing noise spectra at different Mach flight speeds. The upper line corresponds to $M_j = 1.2$.

```
!-----------------------------------------------
!                 CFD INPUT FILE
!-----------------------------------------------
JET_DPMODEL.geo
JET_DPMODEL.res
!-----------------------------------------------
!                CFD PARAMETERS
!-----------------------------------------------
0.9d0    ............................. Jet Mach number
1.226d0  ............................. ambient air density [kg/m3]
288.15d0 ............................. ambient air temperature [K]
1.4d0    ............................. specific heat coefficient ratio
287d0    ............................. Boltzmann constant [J/kgK]
0.0079d0 ............................. Nozzle diameter [m]
!-----------------------------------------------
!             CFD TURBULENCE MODEL
!-----------------------------------------------
0.09d0   ............................. Cmu viscosity
!-----------------------------------------------
!             STATISTICAL PARAMETERS
!-----------------------------------------------
0.125d0 ........................... A stat TAM    #(MORRIS=0.773)
0.45d0  ........................... Cl     TAM    #(MORRIS=0.130)
0.125d0 ........................... Ctau   TAM    #(MORRIS=0.308)
!-----------------------------------------------
!             SPL OUTPUT FILE
!-----------------------------------------------
100d0 ............................. minimum frequency
300000d0 .......................... maximum frequency
1000 .............................. number of frequency

```

Figure 3.13: Input file for subsonic case.

CFD reference parameters necessary for the proper dimensionalization of the output variables of the ZEN code: the Jet Mach number, the ambient air density and temperature, the gamma coefficient, the Boltzmann constant and the nozzle diameter, according to Stromberg data[45], then there is the viscosity coefficient.

The following three lines specify the parameters used for the statistic model of two-correlation function and the last three specify the range of frequency (expressed in Hz).

3.4 Description of the tool for supersonic case

Figure (3.14) specifies the input file of the tool implementing the Shen model. The first two lines are the CFD input files, geometry and solution, in

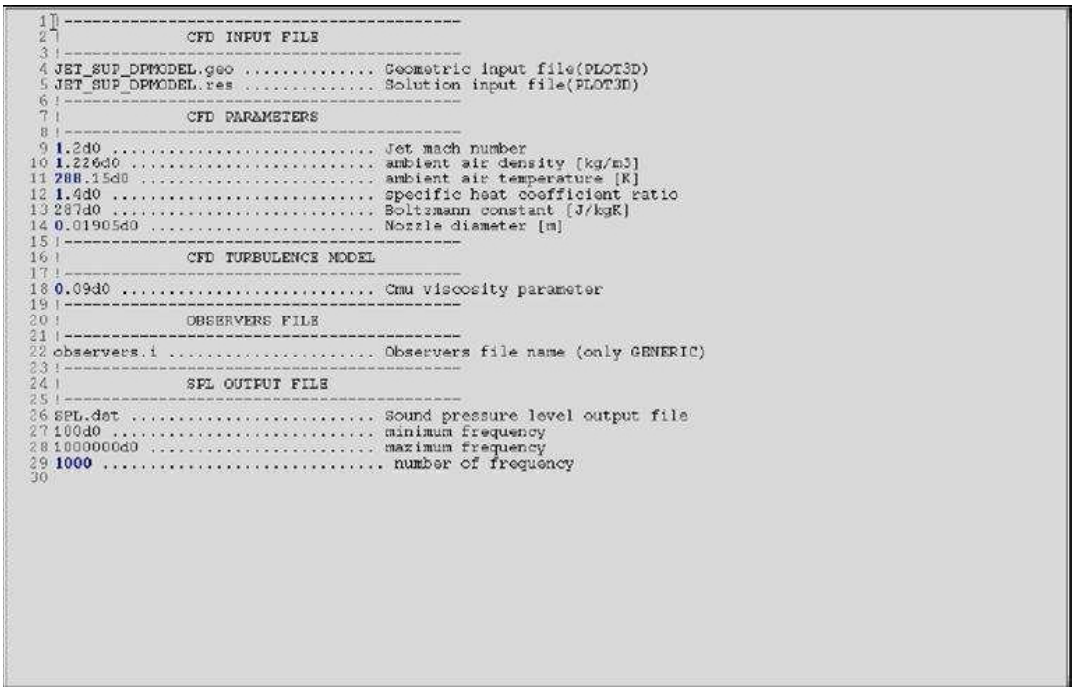

Figure 3.14: Input file for supersonic case.

PLOT3D format. Then, as for the subsonic case there are all the CFD reference parameters necessary for the proper dimensionalization of the output variables of ZEN code: the Jet Mach number, the ambient air density and temperature, the gamma coefficient, the Boltzmann constant and the nozzle diameter, following the data of Norum Brown[53]. Then there is the viscosity coefficient. The last five lines indicate the file in which are contained the location of microphones, the output file and the frequency range.

"Observers.i" (Figure (3.15)) is the input file in which we give the spatial coordinates of microphones. The first line there is the number of observers and the angle coordinates, after there are the cartesian coordinates.

"SPL.dat" (Figure (3.16)) is the file in which there is the final result, that is the SPL value and frequency range (for a certain microphone location).

```
5 ..................... Number of observers (x.z[m])(theta=130.110.90.70.50)
-1.22451 1.45932
-0.65155 1.79011
0  1.905
0.65155 1.79011
1.22451 1.45932

```

Figure 3.15: Observers file for supersonic case. The number of observers is on first line with the angle coordinates. In next lines are the cartesian coordinates for each microphone.

```
# observers number=           1
# x[m] -   -1.22451000000000       z[m] -    1.45932000000000
# SPLoa [dB]-    107.517966114988
   1099.90000000000        58.7216371406962
   2099.80000000000        66.8441003914690
   3099.70000000000        69.7740443638464
   4099.60000000000        69.8456514941984
   5099.50000000000        68.7842065874174
   6099.40000000000        70.9036744859168
   7099.30000000000        77.4916482314390
   8099.20000000000        84.2228973363205
   9099.10000000000        89.5197616847695
   10099.0000000000        93.0660130553608
   11098.9000000000        94.9073065878152
   12098.8000000000        95.1964433771733
   13098.7000000000        94.1090063340706
   14098.6000000000        91.8190602729736
   15098.5000000000        88.5347288555812
   16098.4000000000        84.7785661251621
   17098.3000000000        82.8405109006738
   18098.2000000000        85.4067400302309
   19098.1000000000        89.1807182912711
   20098.0000000000        92.0864137729406
   21097.9000000000        93.8577569057027
   22097.8000000000        94.5494738422052
   23097.7000000000        94.2583403878015
   24097.6000000000        93.0784220560863
   25097.5000000000        91.0976709809082
   26097.4000000000        88.4240433322654
   27097.3000000000        85.3397952369876
   28097.2000000000        83.0070174969977
   29097.1000000000        83.5293442291599
   30097.0000000000        85.9356023446350
   31096.9000000000        88.2131666327234
```

Figure 3.16: Output file for supersonic case.

Chapter 4

Noise from open rotors

4.1 Introduction

4.1.1 General properties

It is generally accepted that, in most cases, the major part of the aerodynamic noise of a rotor is generated by blade loadings. As a matter of fact, thickness noise is important as well of an helicopter, for example, and quadrupole sources (altough much less investigated) become very efficient at characteristic velocities near the speed of sound. In this section, the emphasis is on loading noise for subsonic machines; according to the dimensional analysis of part III, a particular attention will be paid to unsteady loadings.
It is remarkable that, in spite of the great variety of existing machines in aeronautics and in air-conditioning, the physical mechanism is nearly the same, so that of a rotor contains a broadband part and a discrete-frequency part at the blade-passing frequency(number of blades times rotational frequency) and harmonics. The latter is generally refered to as the rotational noise and is due to all periodic interactions between the rotor and the flow, whereas the former is due to random interactions with turbulence. Apart from this,

the various shapes of spectra simply involve differnces in blade number and rotating speed.
The characteristic rotational Mach number is also an important parameter, since high velocities induce more complicated sources and higher Doppler-amplification effects.
Roughly speaking, rotating machines, ducted as well unducted, can be arbitrarily classified by inspecting three parameters: the number of blades B, the rotation speed Ω and a characteristic radius R_0. This is shown on the figure (4.1) and suggests that the way a machine could be investigated depends on the corresponding areas in the planes (Ω, B) and (Ω, R_0).
For example, the main rotor of an helicopter is characterized by small blade number and rotating speed, than a very low fundamental frequency. This kind of rotor exhibits a strong rotational noise, which is perceived like a pulsation. The time-domain approach is well suited to describe the noise, when it would be irrelevant to a turbofan engine, for which te noise currently heard is a high-frequency screech or whistle.
In a different way, we can see that cooling fans are subsonic machines with low characteristic Mach numbers; this certainly allows for special assumptions, which cannot be made in the case of aeronautic machines, and leads to a differents balancing on sound sources, according to the general laws of noise variation with velocity. Typically, in this case, the blades can be best considered as compact sources essentially determined by the unsteady loadings.

In another context, the unit price of a small fan is not comparable to the price of an aircraft turbomachines. Consequently, the flow in the small fan is often only partially controlled and roughly pre-defined by one-dimensional arguments, whereas the turbomachine has to be well designed.
These are the reasons why people working on the noise from cooling fans or from aeronautic rotors may do very different jobs whith the same basic

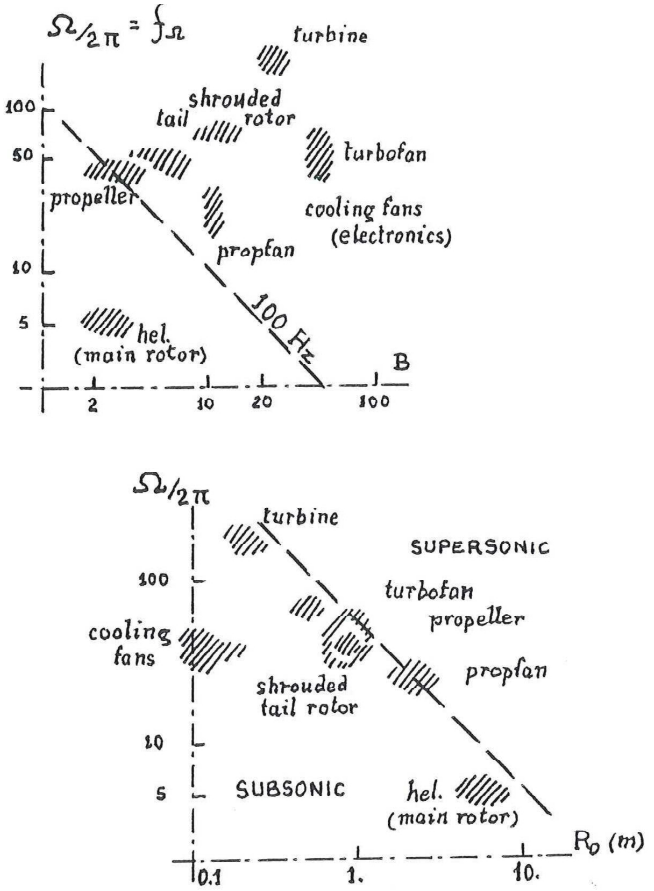

Figure 4.1: Different classes of rotating machines.

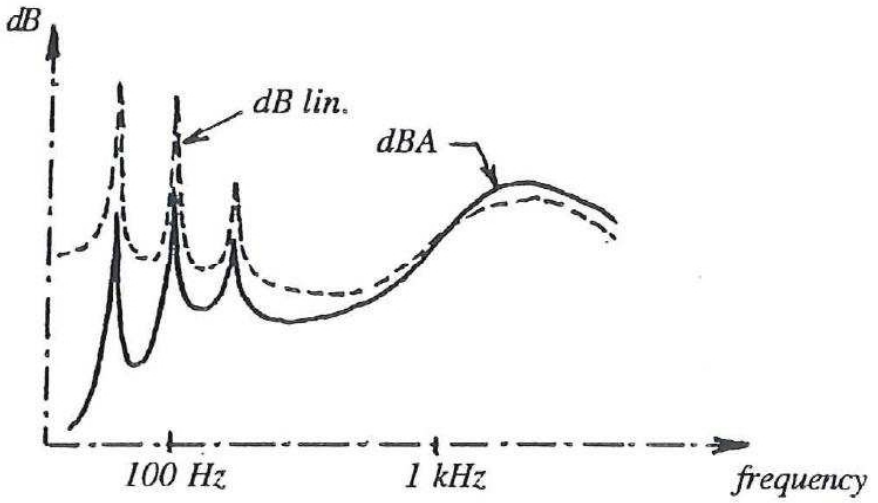

Figure 4.2: Shape of the noise spectrum of a small fan.

physical mechanisms.

In all cases, the need for noise reduction depends on the subjective nuisance,which in turns depends on two points: I) the relative levels of discrete-frequency and broadband contributions, II) the value of the blade-passing frequency tone in the range of human audition.

To illustrate our discussion, let us consider the spectrum of figure (4.2), which is representative of a small cooling fan. A rapid examination of the spectrum in the natural dB scale could lead to the conclusion that the discrete-frequency noise is more painful. Actually, because of the filtering of the dB-scale, more convenient to evaluate the subjective effects of noise, the broadband contribution above 1 kHz is the effective nuisance. In this case, the relevant task is to reduce the broadband noise (here associated with trailing edge emission). Of course, the converse conclusion would follow if the fundamental frequency were nearly 1 kHz, say, or if the tone levels exceeded the broadband level by 20 dB.

Only aeronautic machines are considered here. However, the general equa-

tions apply to any less sophisticated subsonic machine as well.

4.2 Acoustic properties of rotating sources

4.2.1 Compact sources in motion

A source region is said acoustically compact when retarded time variations over this regions are negligible in comparison with a characteristic period T of the source, considered in the moving frame of reference[35]. This condition, well-known in general acoustics for stationary sources, is more complicated for moving sources: it is expressed as:

$$T >> \left[\frac{L}{c_0 \bar{\Delta}}\right] \tag{4.1}$$

where L is a characteristic length scale of the source region and $\bar{\Delta}$ an average value of the Doppler factor.
Consider an emitting segment of length l moving at half the speed of sound, as depicted in figure (4.3). At time t the segment is in $A - B$. The sound received at the observation point E at this time comes from other locations of all points between A and B at previous times, say between A' and B'. A' and B' form an acoustic virtual image of the segment. Because the propagation distances R'_A and R'_B are different, the virtual length l' is different of l. If the segment is approaching E, $l' > l$ and if it is leaving $l' < l$.

So it appears that the motion artificially induces a spatial stretching of each source filament, and consequently that compactness cannot be correctly inferred if the motion is not taken into account. A source that would be compact at rest could become non compact at all when moving.
In a general way, a given source region of space is more compact when leaving the observer and less compact when approaching. When the considered

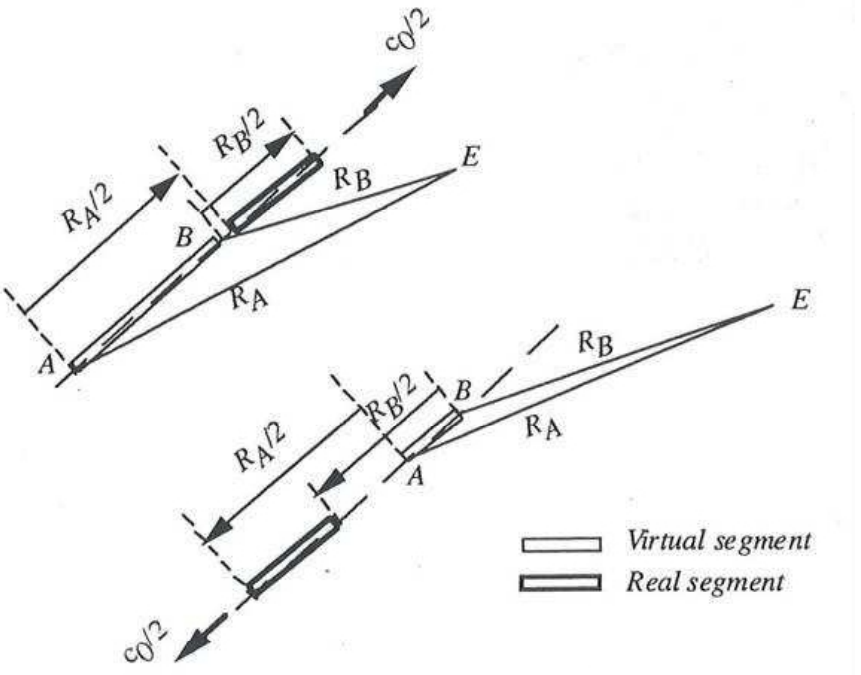
c0/2
RB/2
RA/2
RB
E
B
RA
A
E
RB
B
RB/2
RA/2
RA
A
Virtual segment
Real segment
c0/2

Figure 4.3:

source region is compact, it radiates in the same way as a point source, causing a great simplification of Ffowcs Williams-Hawkings equation. In this case, it exists an equivalent form of FW-H equation, demonstrated by Lowson for point sources in motion. By introducing the relative Mach number of the source in the observer direction $M_r = \vec{M} \cdot \vec{R}/R$, we have, for a dipole of force $-\vec{F}$ that:

$$p'(\vec{x}, t) = -\frac{1}{4\pi}\Big[\frac{R_i}{c_0 R^2 (1 - M_r^2)^2}\Big(\frac{\partial F_i}{\partial t'} + \frac{F}{1 - M_r}\frac{\partial M_r}{\partial t'}\Big)\Big] \tag{4.2}$$

where $\vec{F}$ is the total aerodynamic force induced by the fluid on the surface. For blade segments in normal operating conditions, $\vec{F}$ is often approximated to the net lift force. Lowson's formula (4.2) is often directly used to calculate the noise from cooling fans or other machines for which the blade chord length is acoustically compact. This requires that the blade motion occurs at relatively low Mach number.

4.2.2 Far-field radiaton of a rotating dipole

The major part of the noise radiated by subsonic rotating machines is due to equivalent dipoles. This is the first fundemental point related to the noise from open rotors or turbomachines. The second point is the rotating motion, for which the Doppler effect induces some specific behaviours, described in this section for a medium at rest.

First consider a blade segment of radius R_0 rotating at a constant angular frequency Ω. This segment acts as an acoustic dipole of strenght $\vec{F}$(t), $\vec{F}$(t) being roughly the instantaneous lift force, with a constant inclination γ relative to the rotation axis $\vec{e}_3$. A sketch of the circular trajectory of the source and the location of the observer $\vec{x}$ are defined on figure (4.4). If the blade segment is not acoustically compact, the following results apply to any com-

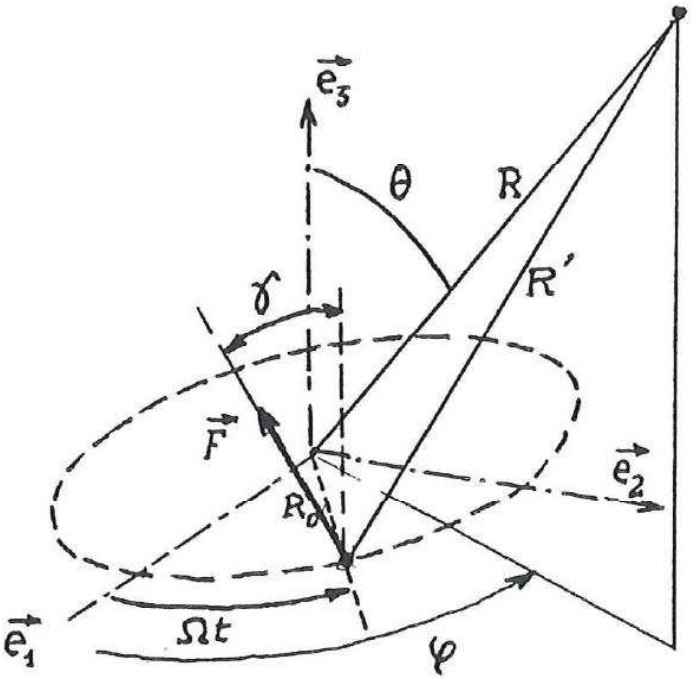

Figure 4.4: Frame of reference used in the calculations.

pact sub-segment with the local unsteady lift force instead of the total one.

$\vec{F}(t)$ is often assumed to be tangent to the cylinder of axis $\vec{e}_3$ and radius R_0 (i.e. with axial and tangential components only) in the practical applications overviewed in the literature, for this geometrical arrangement corresponds to the axial-flow machines of common use in aeronautic transports.
In order to calculate the noise at the point $\vec{x}$ in the far field for a known value of $\vec{F}(t)$, the Lowson's formula (4.2) is referred to. But the calculations require at first the solving of the retarded time equation:

$$t'_1 - t + \frac{R'}{c_0}\Big[1 + \Big(\frac{R_0}{R'}\Big)^2 - 2\frac{R_0}{R'}sin\theta cos(\Omega t'_1 - \phi)\Big]^{1/2} = 0 \qquad (4.3)$$

which, at each reception time t, defines the corresponding time of emission

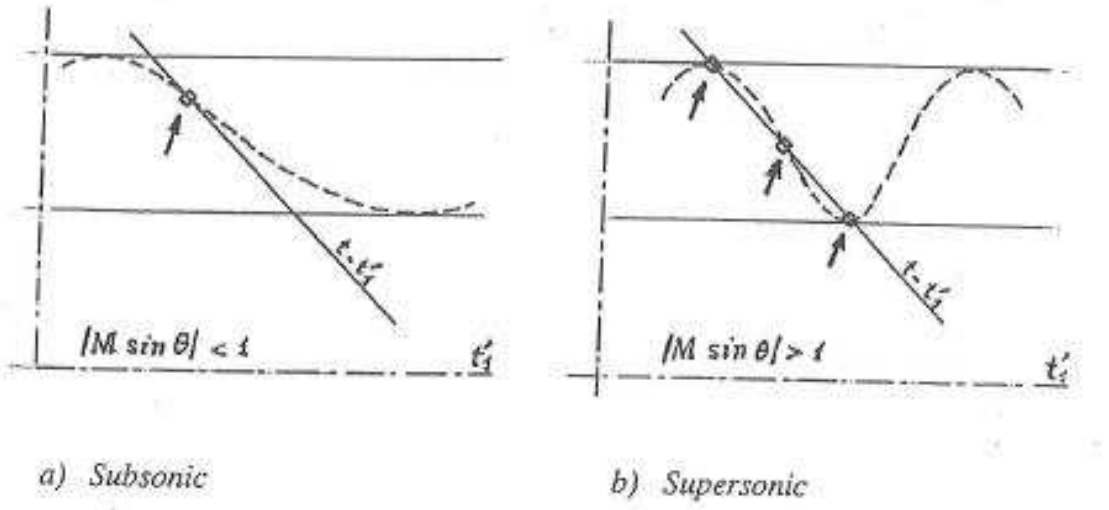

Figure 4.5: Solutions of the time retarded equation.

$t'_1(t)$ and then the retarded location of the source. This is the principal difficulty of solving the equation in the time domain.
It is easily shown that (4.3) admits one to three solutions depending on the rotational Mach number. The solving is illustrated on figure (4.5) by finding the intersection between the oscillatory part in the brace brackets in (4.3) and the function $t - t'_1$. When $|Msin\theta| > 1$, with $M = \Omega R_0/c_0$ the slope of the oscillatory part, can exceed (4.3) and three points of intersection can be obtained. This induces complications in the calculations (it would be so in the frequency domain approach as well). When the method is applied to a blade, the determination of the acoustic image of the blade is somewhat tedious that we won't do in this work.

In a lot of applications, and especially when investigating the discrete-frequency noise (tone noise) of a fan or a turbomachine stage, solving in the frequency domain is more appropriate. In this case we are interested not directly in the pressure signal $p'(\vec{x}, t)$, but in its Fourier transform $\hat{p}(\vec{x}, \omega)$. The time history of the pressure signal can always be restored thanks to the

inverse transform of $\hat{p}(\vec{x},\omega)$:

$$\hat{p}(\vec{x},\omega) = \frac{1}{2\pi}\int_{-\infty}^{\infty} p'(\vec{x},t)e^{i\omega t}dt \tag{4.4}$$

$$p'(\vec{x},t) = \int_{-\infty}^{\infty} \hat{p}(\vec{x},\omega)e^{-i\omega t}d\omega \tag{4.5}$$

In the following of this text, will be used the frequency domain approach. Nevertheless, when the time history is more important than the noise spectrum, as is the case for impulse acoustic signals such as the characteristic beating, called blade slap, of the main rotor of an helicopter, the time domain approach is the relevant one.
More precisely, the Fourier transform $\hat{p}(\vec{x},\omega)$ is:

$$\hat{p}(\vec{x},\omega) = \frac{1}{2\pi}\int_{-\infty}^{\infty} -\frac{1}{4\pi}\Big[\frac{R'_i}{R'^2 c_0(1-M_r)}\Big(\frac{F_i}{1-M_r}\Big]_{t'=t'_1} e^{i\omega t}dt \tag{4.6}$$

In (4.5) the change of variable $t \to t'_1(t)$ leads to an expression in which the retarted time becomes just a variable of integration. So the integral can be calculated without knowing the exact relationship (4.3) between t and t_1. In other words, this approach avoids the solving of the retarted time equation. The simplification arises becauses the rotating motion, and the retarted time equation as well, is periodic. Hence integrating by parts, replacing t'_1 by to simplify notations and elimitating terms that are negligible in the acoustic and geometric far field leads to:

$$\hat{p}(\vec{x},\omega) = \frac{i\omega}{8\pi^2 c_0}\int_{-\infty}^{\infty} \frac{\vec{F}\cdot\vec{R'}}{R^2} e^{i\omega(t+R'/c_0)}dt \tag{4.7}$$

In this relation, R' is a function of time. The exponential term is a phase modulation resulting from the motion of the source (the amplitude modulation is negligible in the far field). The result can be transformed by

applying the classical formula of the expansion of an exponential on the basis of Bessel functions. Introducing the Fourier transform of $F(t)$, say $\hat{F}(\omega)$, we obtain:

$$\hat{p}(\vec{x},\omega) = \frac{i\omega e^{i\omega R/c_0}}{4\pi c_0 R} \sum_{n=-\infty}^{\infty} (-i)^n e^{-in\phi} J_n\Big(\frac{\omega R_0 sin\theta}{c_0}\Big) \cdot$$
$$\cdot\Big\{cos\gamma cos\theta + \frac{nc_0 sin\gamma}{\omega R_0}\Big\}\tilde{F}(\omega + n\Omega) \tag{4.8}$$

(4.8) shows that the sound at angular frequency ω is the sum of all contributions from the source at the intrinsic angular frequencies $\omega + n\Omega$, n being any relative integer number. This frequency modulation in the far field is the consequence of the Doppler effect for a circular motion, in the same manner as the well-known frequency shift is the equivalent consequence for the rectilinear motion.

4.3 Discrete frequency noise of a rotor: general formulation

Now let the total force $F(t)$ on a compact blade segment be periodic with the fundamental period of rotation $2\pi/\Omega$. The Fourier series of F(t) is:

$$F(t) = \sum_{s=-\infty}^{\infty} F_s e^{-is\Omega t} F(s) = \frac{\Omega}{2\pi} \int_0^{2\pi/\Omega} F(t) e^{is\Omega t} dt$$

and its Fourier transform leads to:

$$\hat{F}(\omega + n\Omega) = \sum_{s=-\infty}^{\infty} F_s \delta(\omega - (s-n)\Omega) \tag{4.9}$$

In these conditions, a single blade segment can only produce sound at the rotational frequency and harmonics. So the acoustic pressure can be analyzed in the same way. Let us write:

$$p'(\vec{x},t) = \sum_{N=-\infty}^{\infty} p_N(\vec{x},t)p_N(\vec{x},t) = p_N(\vec{x})e^{-iN\Omega t}p_N(\vec{x},\omega) =$$

$$= \sum_{N=-\infty}^{\infty} p_N(\vec{x})\delta(\omega - N\Omega) \tag{4.10}$$

$p_n(\vec{x})$ is the complex amplitude of the acoustic pressure produced in the far field at angular frequency $\omega = N\Omega$. Now consider formula (4.8). Introducing the rotational Mach number $M = \Omega R_0/c_0$, the next formula follows:

$$p_N(\vec{x}) = \frac{iN^{iN\Omega R/c_0}}{4\pi c_0 R} \sum_{s=-\infty}^{\infty} e^{i(N-s)(\phi-\pi/2)} F_s J_{N-s}(NMsin\theta) \cdot$$

$$\cdot \Big\{ \cos\gamma cos\theta - \frac{N-s}{N}\frac{sin\gamma}{M} \Big\} \tag{4.11}$$

If each blade is assumed to be represented by a single blade segment, this result holds only for one blade. To derive the result for a rotor with B equally spaced blades, a similar expression has to be added for the (B-1) other blades, accounting for a time delay $2\pi/B\Omega$ between a blade travelling and the next one. Thus (4.11) is multiplied by the interference function of the rotor:

$$\sum_{j=0}^{B-1} e^{-i2j/B} \tag{4.12}$$

This function is zero if $N = mB$ and is exactly B if $N = mB$, so that the noise generated by the complete set of blade segments is at the blade passing frequency and harmonics $mB\Omega$. At the m^{th} harmonic, the full acoustic pressure can be written:

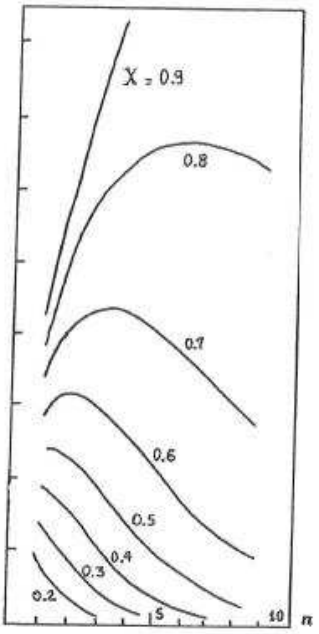

Figure 4.6: $nJ_n(nX)$ as a function of n for various values of X.

$$p_{mB}(\vec{x},t) = \frac{imB^2\Omega}{4\pi c_0 R}\sum_{s=-\infty}^{\infty} F_s e^{-i(mB-s)\pi/2} J_{mB-s}(mBMsin\theta)\cdot$$
$$\cdot\left\{cos\gamma cos\theta - \frac{mB-s}{mB}\frac{\sin\gamma}{M}\right\} e^{i(mB-s)[\phi-\Omega_s(t-R/c_0)]} \tag{4.13}$$

where:

$$\Omega_s = \frac{mB\Omega}{mB-s}$$

In practical applications, this expressions is to be integrated in the spanwise and chordwise direction, if necessary.

Some fundamental points are related to (4.13):

- First of all, periodic blade loadings generate a discrete frequency sound at the blade passing frequency and harmonics. The acoustic field of each tone or harmonic is the infinite sum of characteristic free-field radiation modes. The magnitude of one mode is proportional to a coefficient F_s of the Fourier series of $F(t)$ with a weighting factor defined by a Bessel function (The Bessel functions mean that, on the far-field point of view, rotation is responsible for a frequency modulation of the source, which is a consequence of the Doppler effect for circular motion). The complex coefficients F_s are the so-called blade loading harmonics.

- Each radiation mode rotates with the equivalent rotation speed Ω, defined by the phase term in (4.13)(note that this rotation speed is different from the rotation speed of the rotor). Then, as long as $s = mB$, the mode is called a spinning mode of radiation. A given spinning mode has a zero contribution to the far-field noise on the rotor axis and for another emission angle for which the brace bracket vanishes.

- The special case where $s = mB$ corresponds to the symmetric mode. This mode is the most efficient one in the sum if the related blade loading harmonic has a significant value,because of the Bessel factor J_0. Moreover, the symmetric mode is responsible for the on-axis radiation, and the corresponding noise vanishes in the plane containing the rotor.

  One can guess that very different directivity diagrams are possible,depending on the symmetric mode is produced or not by the source mechanism.

- The $s = 0$ mode defines the noise radiated by the steady part of the blade loadings (steady loading noise). It is important to notice that only this part is related to the total thrust of the rotor, which is of direct mechanical interest. Since che corresponding Bessel factor can

be very small, the steady loading noise alone may underestimate the total noise in all cases where unsteady loadings are present, which is very often the case. More precisely, the steady loading noise scales like the function $nJ_n(nX)$, X being less than 1 (see figure (4.6)).
It is weak and rapidly decreasing with frequency if X is small; this occurs if M is small or if the angle to the axis tends to zero. Conversely, it can be very important and rich in higher harmonics if X tends to unity. As a consequence, the steady loading noise is a very efficient mechanism for subsonic rotors only if the flow is nearly homogeneous, and in any case for high-speed propellers.
The steady loading noise has a zero efficiency on the rotor axis at an angle of emission $\Theta_0 = Arccos(tg\gamma/M)$, which does not depend on frequency. This angle is in the forward half-space,whereas the angle of maximum radiation is in the rearward half-space. As a consequence, if a significant noise level is measured on axis in an experiment, harmonic loadings are certainly generated.

- If mB is large enough, because of the decrease of Bessel functions with increasing order, the noise at the m^{th} blade passing harmonic is strongly dependent on the blade loading harmonics of order s such that:

$$mB(1 - M|sin\theta|) < s < mB(1 + M|sin\theta|) \tag{4.14}$$

In other words, a given blade loading harmonic of order s only determines the sound at the blade passing harmonics such that:

$$\frac{s}{1 + M|sin\theta|} < mB < \frac{s}{1 - M|sin\theta|} \tag{4.15}$$

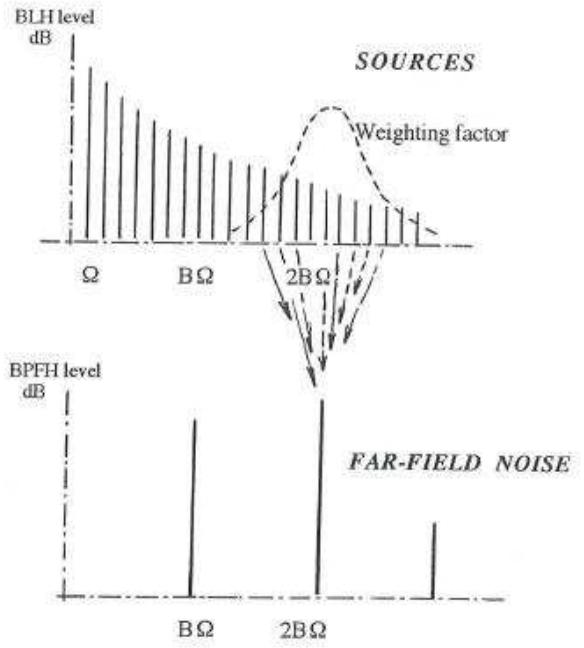

Figure 4.7: Range of blade loading harmonics contributing to the second discrete frequency in the noise spectrum.

The blade loading harmonic (BLH) preferentially feeds with energy the nearest blade passing frequency harmonic (BPFH) in the sound field. It can be noticed that $mBM|sin\theta|/|mB-s|$ is the maximal value of the equivalent rotational Mach number of the s^{th} spinning mode relative to the observation point. So, roughly speaking, only the spinning modes of radiation with supersonic relative speed contribute significantly to the far-field sound.

The energy transfer from the BLH's onto the BPFH's is illustrated in figure (4.7). The contribution of each BLH for a given BPFH is weighted by a Bessel function. An increase in the rotational Mach number makes the weighting factor wider and wider, allowing energy to be transferred even between frequencies well apart from each other. This is the reason why steady loading noise can be determinant at higher order harmonics for a high speed

rotor.

Finally, formula (4.13) is of easy use in practice for subsonic machines, since only a reasonable number of terms are needed in the infinite sum. For rotating machines with high rotational Mach number, some problems are to deal with and the time domain approach become more attractive.

4.4 An application of propeller noise model: PPLANE project

4.4.1 The PPLANE project

The PPLANE project is a direct follow up study to Out-of-the-Box project that aimed to identify potential new concepts and technologies for future air transport and focused on a number of radical changes to the system rather than taking incremental steps.

As a result of the Out-of-the-Box project, Pplane implements a systematic approach to radical and novel ideas for Personal Air Transport System (PATS). The project starts with the definition of several operational concepts and implements an optimisation model and several selection criteria to suggest and analyse new concepts for the personal air transport system of the future.

The main selection criteria include: "Security and Safety", "Automation and Control", "Environment" and "Human Factors". Horizontal areas such as technologies, regulation and affordability are considered in each of the above criteria. The resulting concepts are analysed and compared resulting in recommendations for implementation across Europe.

4.4.2 CIRA and PPLANE

The main objective for our activity in Pplane is to evaluate and score PATS vehicle propulsive systems and lifting architectures regarding their environmental performances. In order to this we have defined an ensemble of these PATS vehicle configurations to be submitted to the environmental assessment.

So it is necessary to define a list of input and output parameters in order to obtain a preliminary design of PAV configuration. These parameters are manipulated trough an user-friendly fortran code in order to easily interface them with the propeller analysis code.

4.4.3 Description of work

This section provides a description of the tool developed in task 5.2. The purpose of this tool is to manage a list of physical input and output data in order to have a preliminary but complete design of a PAV configuration where the term preliminary is to be intended as in the typical aeronautic practice. The tool has been named as *pplane_configuration*.
The choice of which physical variables had to be considered as input has been done following criteria in agreement with:

- PPLANE Partners Suggestions
- Aircraft Flying Certification Rules (FAR_{23})
- Literature data corresponding to regional propeller aircraft properly scaled.

The input parameters are listed in a single input file and gathered into several categories: kinematical inputs (cruise velocity, stall velocity, autonomy of the vehicle, height, etc...), aerodynamic inputs (friction coefficient,

Weights	Performance	Constructive	Statistic
Payload	Autonomy	Specific fuel consumption	Weight constants
Fuel fraction method	Height	Propeller efficiency	Wet surface
	Latitude	Lift/Drag ratio	Parasite surface
	Cruise velocity	Friction coefficient	Take off distance
	Stall velocity	Aspect ratio	
	Lift coefficient		

Figure 4.8: Input parameters for the definition of a personal plane.

wing aspect ratio, maximum lift coefficient in the different flight configurations, etc...), constructive inputs (propeller efficiency, specific fuel consumption, lift and drag ratio, etc...), statistics input (relations between take-off distance and wing surface, etc...) and weight evaluation inputs (payload weight, inputs for fuel fraction method, etc...).

The kinematical inputs have been selected using essentially the criteria I) and II) while the constructive inputs have been selected with the rule III) supposing our ideal PPLANE vehicle similar to a regional propeller aircraft and choosing parameters (as the aerodynamic efficiency or the specific fuel consumption) in the same range of those ones of a regional propeller aircraft.

In (4.8) are summarized all the inputs data required by the tool:

4.4.4 Mission profile

In a first step, the tool performs the weight evaluation. This is carried out by decomposing the mission profile into 8 phases:

By using the Steffen algorithm in connection with the fuel fraction method and operating on the weight ratios, the tool computes the values for the take-off weight, the empty weight and the fuel weight. The tool uses the statistic relation:

$$\mathrm{Log}W_{to} = A_1 + B_1 \mathrm{Log}(C_1 \cdot W_{to} - D_1) \tag{4.16}$$

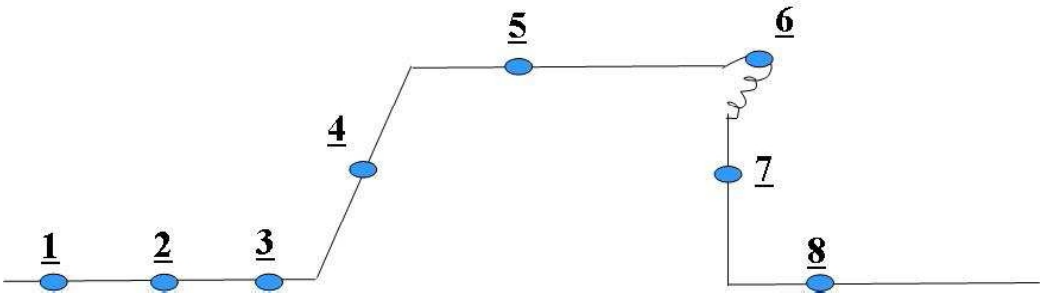

Figure 4.9: Mission profile phases.

Phase number	Phase name
1	Ignition
2	Taxi
3	Take-off
4	Rising and acceleration
5	Cruise
6	Loiter
7	Getting down
8	Landing, taxi and powering off

Figure 4.10: Definition of all the phases of a typical mission profile.

Where W_{to} is the take-off weight and the other parameters involved are statistic constants. After the determination of the weight, another critic parameter to be consider is the wing load.

It is possible to establish an upper limit for the wing load using the following relation :

$$v_{stall} = (\frac{2}{\rho})^{1/2}(\frac{W}{S})^{1/2}(\frac{1}{C_{Lmax}})^{1/2} \tag{4.17}$$

where ρ is the air density, W the weight, S the wing surface and W/S is the wing load. Using the rules previously mentioned, the stall velocity v_{stall}, in clear configuration and landing configuration, is inserted as input parameter.

Then, once fixed a maximum value for the stall velocity, and once obtained the weight from equation (4.17) we obtain an upper limit for the wing load and consequently a lower limit for the wing surface.

The stall velocity also provides an estimate, trough a statistic relation and considering the certification rules, of the landing distance:

$$L_{land} = 0.5136 \cdot v_{stall}^2 \tag{4.18}$$

this relation is expressed in U.K. units that means v_{stall} expressed in kts (1kts=1.852 Km/hr) and take-off distance in feet. A take-off distance input provides, trough a statistic relation, an estimate for the power P, once fixed the weight:

$$L_{takeoff} = 4.9 \cdot TOP_{23} + 0.009 \cdot \mathrm{TOP}_{23}^2 \tag{4.19}$$

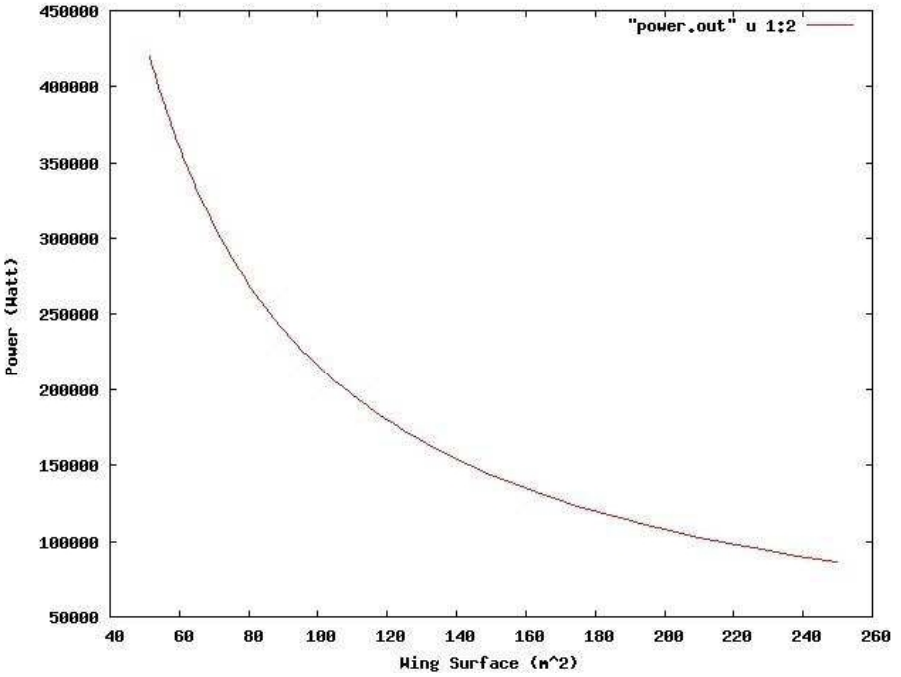

Figure 4.11: Power versus wing surface. The starting point in abscissa is determined by the lower limit of the wing surface.

with

$$TOP_{23} = \left(\frac{W}{S}\right)\left(\frac{W}{P}\right) \cdot \frac{1}{\sigma \cdot C_{Lmax}} \tag{4.20}$$

where TOP_{23} is defined by the flight certification rules FAR_{23} and $\sigma = \rho/\rho_0$, with ρ depending on height. Taking into account that we have already determined a lower limit for the wing surface it is possible to establish a relation between some tentative values for the wing surface and the corresponding power. The trend is showed in figure (4.11):

The last step is to determine the aerodynamic polar. We start from a statistic relation:

$$Log_{10}S_{wet} = C + D \cdot \mathrm{Log}W_{to} \tag{4.21}$$

U.K. units: W_{to} in lbs and S_{wet} in ft^2 with C and D denoting statistic constants, W_{to} is the the take-off weight. Once determined the wet surface, it is possible to calculate the parasite surface with another statistic relation:

$$Log_{10}S_{prs} = A + B \cdot \mathrm{Log}S_{wet} \tag{4.22}$$

U.K. units with A and B denoting statistic values depending on the friction coefficient and S_{prs} is the parasite surface. Finally we determine C_{D0} by using the simple relation

$$C_{D0} = \frac{S_{prs}}{S_{wet}} \tag{4.23}$$

The value of all the statistic constants derives from a list of tables that reported in[]. All the statistic parameters are taken taking in account the literature.

Once computed C_{D0} , it is possible to obtain the aerodynamic polar fixing a maximum possible value for the lift coefficient. Also in this case, the maximum value, in different flight configuration, comes from literature data. Finally varying the lift coefficient in a fixed range is possible to obtain different values for C_D and therefore the aerodynamic polar.

An example of aerodynamic polar is showed in figure (4.12).

4.4.5 Blade element theory

In order to have a prediction of the propeller noise, is necessary to have an estimate of the thrust provided by the blade.

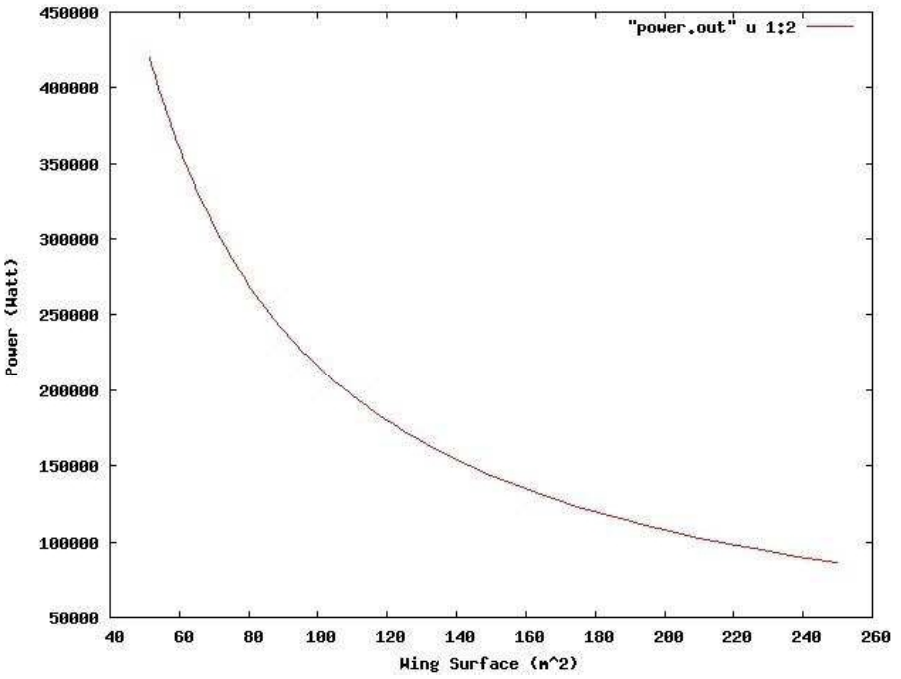

Figure 4.12: Aerodynamic polar. C_L in abscissa and C_D in ordinate. wing surface.

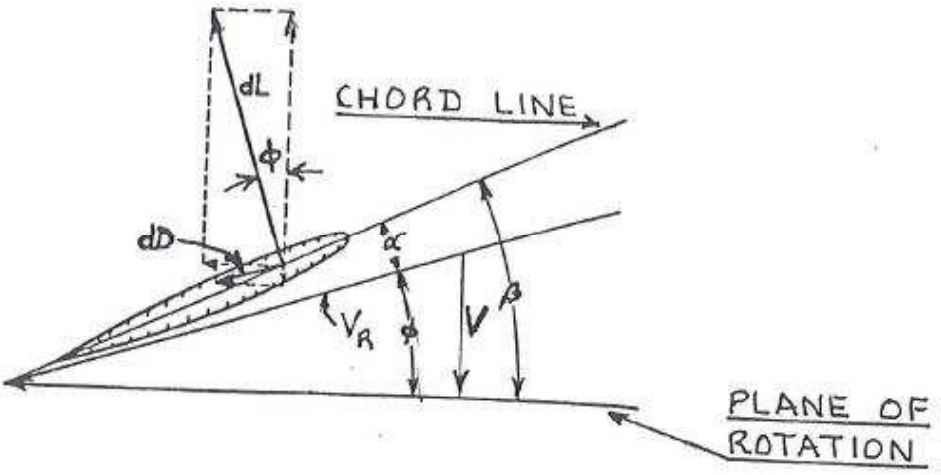

Figure 4.13: Definition of angles for a propeller blade element.

Starting from the output of the design tool, is possible to have, indeed, a minimum value for the thrust. For this, is necessary to remind some simple concept of blade element theory.

To begin, consider a blade element at r from the axis as shown in figure (4.13). The angle β is called the geometric pitch angle and v is called the advance speed. Since the airspeed at the element due to rotation only is Ωr, it is much less at the root of the blade than at the tip. However, the velocity of advance (=airspeed of airplane) is the same at both points. It follows that β should have to be sufficiently great to maintain an efficient angle of attack near the root of the blade[1].

Consider the forces acting on a blade element of width dr and chord c. The thrust is contributed by the component of lift and drag perpendicular to the plane of rotation. Hence:

[1]Usually the blade are twisted for this reason, but in our case, that is very preliminary, we don't enter in these details.

$$dT = dLcos\phi - dDsin\phi = \frac{1}{2}V_R^2 \cdot cdr(c_l cos\phi - c_d sin\phi) \tag{4.24}$$

where ϕ is the real angle seen from the blade profile and is given by $\phi = \beta - \alpha$, with α deriving from the effects of the forward and rotational velocities:

$$\alpha = \arctan\frac{v}{\Omega r} \tag{4.25}$$

If the number of blades is B, the total elemental thrust from simple blade element theory, omitting the c_d term and neglecting the induced velocity is:

$$BdT = BdLcos\phi = \frac{1}{2}Bc_l\rho(v^2 + \Omega^2 r^2)ccos\phi \tag{4.26}$$

Integrating this expression over the ray of the blade, we obtain the total thrust provided by the blades. This value corresponds to the left-hand side of the expression (4.27) and has to be put in comparison with the drag force acting on the wing, as we will show in next section.

A fortran tool has been realized in order to interfacing the preliminary design tool and the propeller noise analysis tool.
In this tool the value of the blade chord has to be considered as an input together with the rotational frequency of the blades. The advance velocity, the drag coefficient and the surface wing that compared on the right-hand side of the expression (4.27), are instead output coming from the preliminary design tool.

4.4.6 Propeller noise analysis

Once obtained a preliminary design of the aircraft, it is possible to extract from the design tool the parameters needed for the propeller noise analysis. In order to do this, is important to establish a relation between the drag force acting on the wing of the aircraft, with the minimun thrust that has to be provided by the blade. Substantially it has to be true that:

$$Th_{blade} \geqslant D_{wing} = \frac{1}{2}\rho \cdot v^2 \cdot S \cdot c_d^{wing} \tag{4.27}$$

where v is the forward velocity of the aircraft, S is the wing surface and c_d is the drag coefficient.
These three variables, together with the ρ, the air density, come from the design tool previously described. The values of these parameters constitutes a constrain for obtaining the minimum thrust provided by the blade.
A further constrain comes from M, the total Mach number. It is provided by the sum of the forward Mach and the rotational Mach number, that is:

$$M = M_f + M_{rot} = \frac{v}{a_0} + \frac{\Omega}{a_0} \tag{4.28}$$

where v is the forward velocity and Ω is the rotational frequency of the blade, that constitutes an input for our noise analysis. Combining equation (4.27) and equation (4.26) we obtain a direct comparison between the output coming from the design tool, that is the drag force acting on the wing, and the corresponding force needed on the blade.
Thus, once established different values for the drag force, is possible to calculate the force acting on the blade trough the (4.27) and finally the pressure level trough the (4.8).
In Figure (4.14) are showed different Sound Pressure Levels following differ-

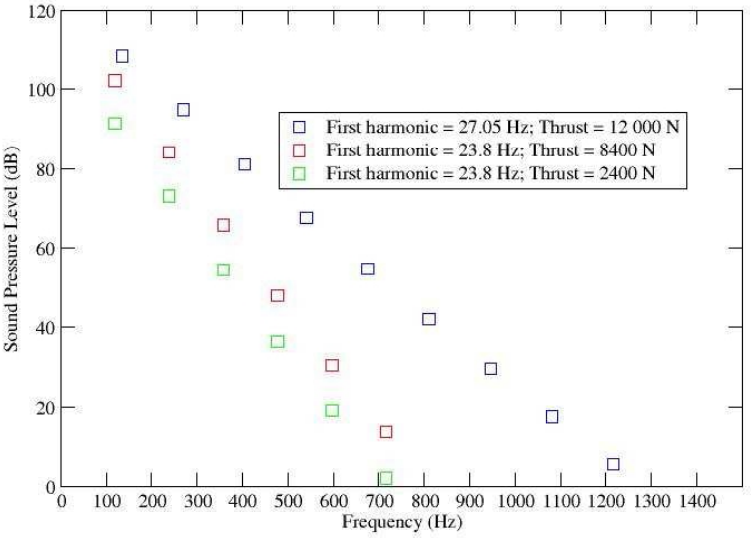

Figure 4.14: Harmonics for different thrusts.

ent thrusts. The input value of the minimun thrust has be obtained changing the wing surface or, in alternative, the rotational frequency. It is possible to observe that in all three predictions, the first harmonic is dominant in comparison to the other ones.

In addition, it is possible to observe that, obviously, greater is the thrust, greater is the Sound Pressure level. It is also visible that a change of rotational frequency produces an increasing of the SPL (caused by an increasing of the minimun thrust needed) and an increasing, obviously, of the first harmonic. The value of the harmonic corresponds to the product of the rotational frequency by the number of blades.

4.5 Concluding remarks

An analytical prediction for tonal propeller noise has been used. This analytical formulation is derived by the Fwocs-Williams Hawkings equations. The formulation predicts the sound pressure in a domain frequency and has as input the forces acting on the blade.
In order to extract the forces, in the framework of a CIRA project: Pplane, a preliminary design tool of a simple and small aircraft has been developed. This tool, compared with an interface tool (also developed in this framework) provides some input values for the thrust in order to calculate the forces acting on the blade. Once obtained the forces, is possible to apply the analytical formulation. Different SPLs are showed following different thrusts.
The tools developed will be used for propeller tonal prediction in the project pplane and constitute a branch of the analytical/semi-analytical/empirical overview developed in CIRA for describing all the noise sources of an aircraft.

Chapter 5

Landing gear noise

5.1 Introduction

Aircraft landing gear noise has been recognized in recent years as one of the major contributors to the total aircraft noise, especially at landing conditions.
Its prediction, however, remains one of the most difficult challenges in aeroacoustics, because of the complexity of the gear geometry and the surrounding flow field. Though significant progress has been made in computational power and numerical simulation methodologies in recent years, solving the flow field around a practical landing gear asssembly, and hence, computing the noise field, is still not a practically feasible task. This is very likely to remain so for many years to come and hence the developing of empirical approaches is one of the best option to use for having prediction tools.
The empirical approach described in this section is the Guo-method[57] and it is based on systematic testing and data analysis of the full-scale Boeing 737 landing gear.

5.2 Landing gear noise spectrum

The difficulty in landing gear noise prediction can be attributed to the large number of components in the gear assembly, which always have very different sizes, shapes and orientations. A precise understanding of how each of them generate noise and how they interact with each other is not practical and probably not necessary either. It is desirable and useful, however, to be able to catalog the gear components into groups according to the characteristics of their noise and to understand the relative importance of these groups in contributing to the total landing gear noise.

To explicitly separate the noise contributions of different component groups, a series of gear configurations with various degree of complexity was used in Boeing facilities. This enables to catalog the landing gear assembly into three groups, namely, the wheels, the main struts and the small features.

The last group includes all the small parts such as brake braces, hydraulic hoses and wires, as well as small geometry irregularities such as cutouts and steps. We choose to work with grouping because these three groups have very different characteristic length scales, and hence, generate noise in different frequency domains. The logic choices of the length scales are respectively the diameter of the wheels, the average cross section dimension of the main struts and the typical size of the small features.

By cataloging the gear components and separating their respective noise contributions, we can explicitly show the dominance of the small details in generating high frequency noise.

In low Mach number flows with rigid bodies, the noise is often scaled on the flow Mach number by the sixth power law. We will show that this indeed describes the low and mid frequency noise, but the spectra of the high frequency noise is better scaled by the seventh power law (corresponding to an eight law for the sound intensity or overall sound level), which is typical of

noise generated by turbulent flows themselves, instead of the unsteady forces on the surfaces of the bodies in the flow.

Furthermore, we find that the high frequency landing gear noise has spectral shapes that fall off approximately in proportion to the inverse square of frequency typical of turbulence generated noise. This may seem to contradict the commonly known sixth power law that attributes the noise sources to the unsteady forces on the bodies, and hence, in analogy to dipole sources. It is, however, readily explainable once it is recognized that high frequency noise sources are not likely to be compact, an assumption implied by the sixth power scaling law in aeroacoustic theories.

At low and mid frequencies the acoustic wavelength is relatively large compared with the typical dimension of the bodies with which the flow interacts. Thus, the bodies can be regarded as acoustically compact, complying with the dipole radiation analogy. At high frequencies when the acoustic wavelength is comparable to and/or smaller than the body dimensions, the bodies become acoustically non-compact. The dipole source due to the surface pressure fluctuations become a distribution with rapid phase variations. The noise radiation from such as dipole source distribution suffers severe mutual cancellation between the source elements, significantly reducing the radiation efficiency. As a result, the effects of the bodies are mainly to reflect the noise from the sources in the flow, acting as sounding boards. Thus, the radiation at high frequencies is essentially from the turbulent flow surrounding the landing gear, governed by the eighth power law. This physical reasoning is consistent with measurements taken from Boeing with a phased microphone array that identifies the high frequency sources to be a distribution in the wake of the gear.

For each of the three frequency domains, empirical formulas will be derived for the sound pressure as a function of the flow conditions, gear geometry and microphone locations. The implementation of such empirical prediction

is straightforward. In applying the Mach number dependence, however, it is important to point out that the Mach number should be the local flow Mach number just upstream of the landing gear, which can be noticeably different from the mean flow Mach number of the free stream far away from the aircraft. We will show that due to the installation effects of the wing, the local flow Mach number just upstream of a main landing gear can be 20 percent smaller than the free stream flow Mach number. This corresponds to a difference in noise of as much as 5.8 dB according to the sixth power law. Similarly, the local flow velocity just upstream of a nose gear can be noticeably higher than the free stream flow velocity because of the flow acceleration when passing the nose of the fuselage. This increase of flow velocity will lead to an increase in landing gear noise, which needs to be accounted for when predicting landing gear noise for airplanes.

The empirical prediction for each frequency domain correlates the noise not only to parameters such as flow Mach number and far field location, but also to geometry details such as the number of wheels and struts. For the high frequency component that is generated by the small details of the landing gear assembly, namely the hoses, wires, cutouts and steps, it is clearly not practical to have a precise description of the small features, because of their irregular shapes, sizes and locations. Nor is it necessary to define them precisely for noise prediction that is also affected by many other things. Instead, we will introduce a complexity factor[58] to characterize the aggregate effects of the small features and empirically relate the high frequency noise to this complexity factor. Intuitively, the larger the aircraft is, the more complex the landing gear needs to be. Thus the complexity factor can be related to aircraft gross parameters such as the maximum take off (or landing) weight. Though this is obviously not an unique definition to account for the high frequency landing gear noise generation, it does provide a practical approach for its prediction for commercial airplanes.

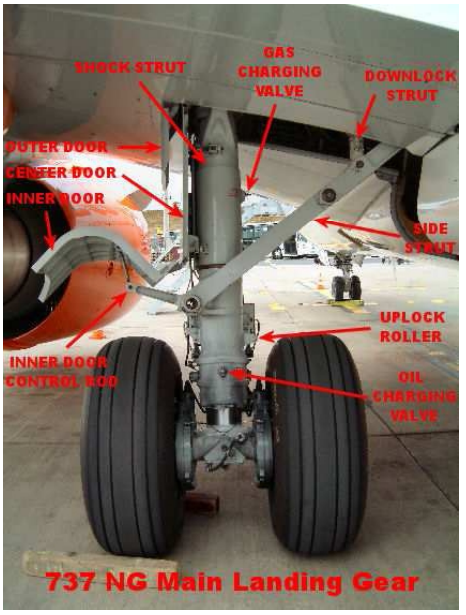

Figure 5.1: The Boeing 737 main landing gear.

5.3 Boeing Test facility and Data Acquisition

In order to derive and validate the empirical prediction for the landing gear noise, is necessary to have a wide range of experimental data.
The data used have been collected by Boeing in Boeing LSAF test facility and all the details are contained in this reference[57]. The objective of the test is to evaluate the noise from a full-scale landing gear with particular emphasis on the effects of geometry details on the far-field noise spectrum, and the relative noise contributions of the components in the gear assembly. To this end, the test used a full-scale Boeing 737 landing gear, which is typical of most Boeing landing gears. It has a main strut, a drag brace, a side brace, multiple hydraulic lines, and brakes. A photo of this landing gear is shown in figure (5.1).

The main difference between the Boeing 737 main landing gear and those for other Boeing airplanes is the number of wheels; the Boeing 737 has two

CONFIG	DESCRIPTION
A	Fully dressed with two large wheels
B	Clean with two large wheels
C	Clean without wheels
D	Fully dressed with two small wheels
E	Clean with two small wheels
F	Partially dressed with six wheels

Figure 5.2: Different configurations for the landing gear.

wheels while the other airplanes have either four or six wheel trucks on the main landing gear. For the purpose of examining the noise generated by small details on the landing gear, the Boeing 737 model is considered sufficient because it is typical of most Boeing landing gear small details.
To reveal the noise contributions from different parts of the landing gear, six variations of the landing gear configurations were tested, as showed in (5.2), defining the corresponding frequency domain ((5.3)).

In addition to the fully dressed configuration with all the small details, such as hydraulic hoses or electric wires, a clean configuration was tested that lacked the brake assembly and other dressing items.

5.4 Data analysis

For each of the six landing gear configuration summarized in (5.2), different Mach numbers were tested, starting from 0.18 to 0.24 with a 0.02 increment. The noise has been collected by an array of microphones. The flow conditions are mainly characterized by the generation in unsteady low Mach number

	COMPONENTS			FREQUENCY		
CONFIG	Wheel	Strut	Detail	L	M	H
A	■	■	■	■	■	■
B	■	■		■	■	
C		■			■	
D	■	■	■	■	■	■
E	■	■		■	■	
F	■	■	■		■	■

Figure 5.3: Effects on frequency range of each gear component.

flows with the presence of rigid, smooth bodies usually follows the sixth power law.

By using this scaling, the normalized OASPL (Overall Sound Pressure Level) is shown in figure (5.4) as a function of the microphone angles for two sets of data, one for the fully dressed gear (configuration A) with two wheels and the other for the partially dressed six-wheel configuration (configuration F). The results show satisfactory collapsing with variations of about one dB. The sixth power law can also be used to scale the sound pressure spectra. Figure (5.5) plots the Sound pressure level for the fully configured gear at the overhead location, with both the sixth power and the seventh power scaling. The seventh power scaling describes apparently better the high frequency data, while sixth power scaling collapse the data very well in the low and mid frequency domain. The seventh power scaling for SPL corresponds to an eighth power law for the OASPL or sound intensity, which is the well-known scaling for noise generated by turbulent flows.
At first glance, this seems to contradict the well-known result of noise radiaton, from unsteady forces on rigid bodies, which scales on the sixth power.

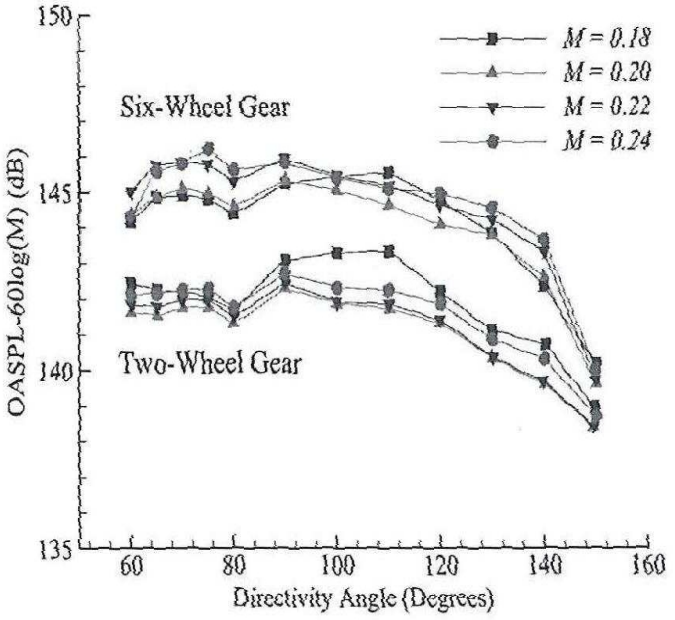

Figure 5.4: OASPL as a function of microphone angles for two different gear configurations at various Mach numbers.

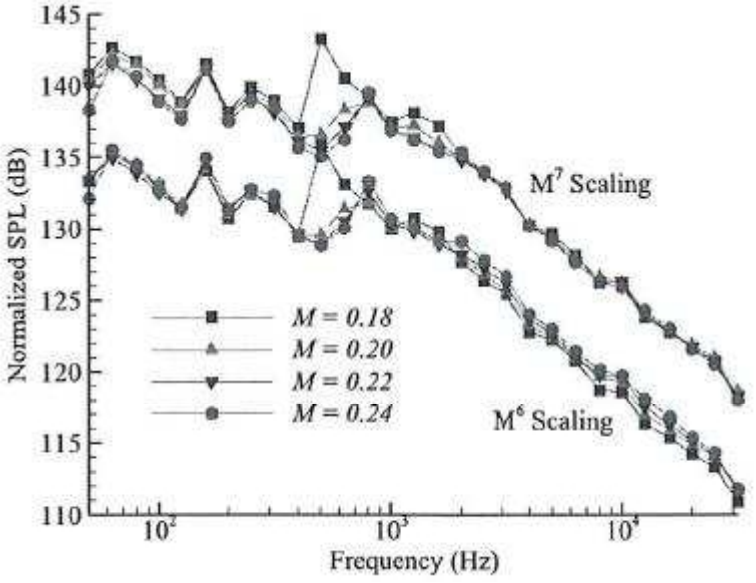

Figure 5.5: Comparison of different Mach number scaling on the SPL for the fully dressed gear configuration at overhead position.

In fact, it is readily explainable by the principles of aeroacoustics. As is well known, the sixth power law is applicable to bodies of compact dimension, in comparison with the acoustic wavelength.

Thus, the scaling is followed well at low frequencies where the acoustic wavelength is large making the bodies acoustically compact. In this case, the radiation is due to the dipoles furnished by the unsteady forces on the body surface. At high frequencies with short acoustic wavelength, the bodies become non-compact in relation to the wavelength. The surface pressure have significant phase variations within a wavelength so that their radiation suffers severe mutual cancellation.
As a result, the dipole radiation degrades to a quadrupole radiation and the bodies essentially reflect/diffract the noise from the unsteady flow, which scales on the eighth power law. The body surface are only sounding boards

that do not after the radiation efficiency of the unsteady flow. The almost perfect data collapsing shown in figure (5.5) with the seventh power law for the high frequency noise is precisely due to this physical mechanism.
Testing the configurations defined in (5.2) is a convenient way to derive functional dependencies of the gear noise on various parameters and to decompose the total landing gear noise into different spectral components. The spectral decomposition is feasible because the three groups of gear parts, namely, the wheels, the main struts and the small details, have distinctively different lengths. For the Boeing 737 landing gear, for example, the wheel diameter is about 1 meter. The typical cross section dimension of the main struts is about 0.1 meters and the typical size of the small parts is on the order of 1 centimeter. The typical lengths for the three component groups differ by decades, which, from the strouhal number argument, would lead to frequency domains separated by decades. If the wheels generate noise mainly in the range close to 50 Hz, the main struts would generate noise around 500 Hz and the small features around 5000 Hz. All three groups of course generate broadband noise, both because the high Reynolds number of the flow and because of the complex geometry of the gear assembly. Thus, the frequency domains may have some overlapping.

Figure (5.6) summarizes operations in the data analysis that can lead to various trend. The letters in the first column are the configurations defined in (5.2).
Take the operation F minus A, for example, which is the difference between the partially dressed six-wheel gear and the fully dressed two-wheel gear. The six-wheel gear is designed simply adding two sets of two-wheel trucks to the fully dressed two-wheel gear. The additional gear trucks do not have any of the small parts, which is why configuration F is namely partially dressed.

Thus, the difference between F and A would be purely the effects of the number of wheels. Since wheels generate noise mainly in the low frequency

OPERATION	EFFECTS
A-B	High frequency noise from details
C	Mid frequency noise from struts
B-C	Low frequency noise from wheels
A-D	Wheel size effect
F-A	Wheel number effect
D-E	High frequency noise from details
B-E	Wheel size effects

Figure 5.6: Effects on range frequency caused by different operation on landing gear

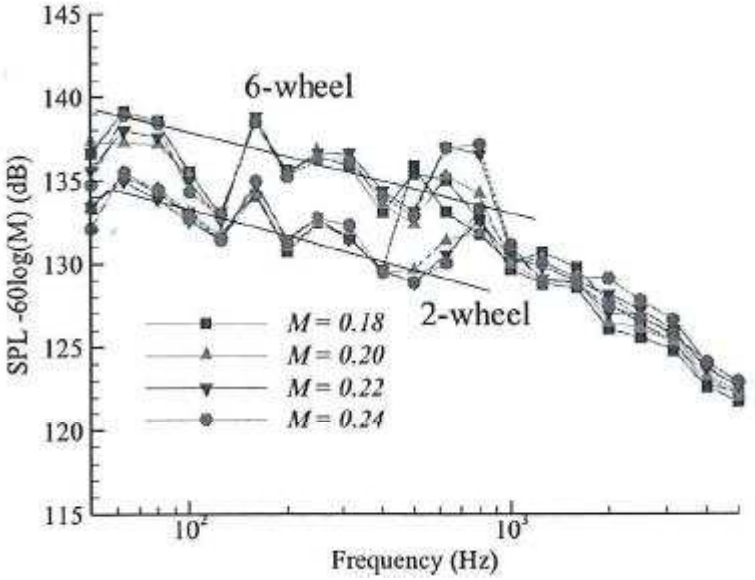

Figure 5.7: Effects of the number of wheels on the far field low frequency noise. Boeing experimental data.

domain, the difference in noise between these two configurations can be expected mainly in low frequencies. Experimental data showed in figure (5.7) seems to be confirm this.
Moreover, it is interesting to note that the difference showed in figure (5.7) is somewhere between 4 and 5 dB. On the basis of energy addition, the ratio 6/2 would give a noise difference of 4.8 dB. Thus it appears that the effects of the number of wheels can be simply taking care of by the energy addition; doubling the number of wheels simply adds 3 dB to the noise.

5.5 Guo empirical prediction

Based on the data analysis described in the previous section, an empirical prediction scheme is derived by Guo[]. The development procedure starts with identifying parameters that dominantly control the noise prediction and are covered by the database. Functional dependencies between the radiated noise and these parameters are derived by a combination of aeroacoustic theory and data analysis using linear regression and correlation analysis. The functional dependencies of the noise on some parameters, such as the flow Mach number, is guided by existing theories of flow noise, such as the acoustic analogy, which, for example, predicts a sixth power law of the noise on the flow Mach number. The law of spherical spreading also easily set the dependence of the noise on the radial distance of the microphone location, as is known for sound waves. Since the empirical tool is meant to be used for practical predictions, the Guo model is focused on the consistency with physics than the last-digit accuracy coming out of the data analysis. A good example of this is again the Mach number scaling. By strictly applying linear regression to the database, a power law of slightly less than six can be found for the overall sound pressure levels. Instead of use this, the choice is to be consistent with aeroacoustic theories and simply set the power law to six.

The difference between the two is insignificant for practical predictions.
The empirical prediction involves the summation of the three spectral components, namely, the low, mid and high frequency noise. The summation is on the energy basis according to

$$< p^2 >=< p_L^2 > + < p_M^2 > + < p_H^2 > \tag{5.1}$$

and

$$SPL = 10log[10^{SPL_L/10} + 10^{SPL_M/10} + 10^{SPL_H/10}] \tag{5.2}$$

where p is the sound pressure and SPL is the sound pressure level and with the subscripts L,M and H respectively indicating the low, the mid and the high frequency component and the symbol $< ... >$ means ensemble average. For each spectral component, the sound pressure level (SPL) is assumed to be a function in the general form of

$$SPL = OASPL + F(St) \tag{5.3}$$

where OASPL is a function defined by

$$OASPL = OASPL(M, R, \theta, l, N_s, N_w, \eta) \tag{5.4}$$

Here the flow is specified by the local flow Mach number M, which should be considered as the flow Mach number upstream of the landing gear. The far field microphone locaation is defined by the radial distance R and polar angle θ. No azimuthal angular variation is considered here because landing gear noise is of concern only in the overhead fly-over plane.
The landing gear components are characterized by the length scale l, which

are the diameter of the wheels, the mean value of the cross section dimensions of the main struts and the typical size of the small parts, respectively for the three groups of the gear components.
Also, N_s and N_w denote respectively the number of main struts and the number of wheels in the gear assembly. To account for the effects of the small details in the landing gear, which can significantly increase the high frequency noise as revealed in the test data discussed in previous section, has been introduced a complexity factor, denoted by η, and its contribution to the OASPL is also included in the identity (5.4). The frequency dependence in (5.3) is explicitily accounted for by the function F, which depends only on the Strouhal number St, defined by

$$St = fl/u \tag{5.5}$$

with f denoting the frequency and u being the local flow velocity. The length scale l should be chosen to be its respective value for each of the three components.
As defined in (5.4), the OASPL is computed as a function of flow and geometry parameters associated with a landing gear assembly, as well as the far field microphone locations. For all three components, the OASPL are expressed by the general form

$$\begin{aligned} OASPL = {} & 20log(l/R) + C_0 + C_1log(M) - C_2log(sin\theta) + C_3log(N_s) \\ & + C_4log(N_w) + C_5log(\eta) \end{aligned} \tag{5.6}$$

which involves six constants. These are derived by linear regression analysis of the test data for each of the three spectral components. The results are summarized in (5.8).

	Frequency domain		
	Low	Mid	High
C_0	145.7	168.5	185.3
C_1	60.0	60.0	70
C_2	4.3	2.4	9
C_3	0	10.0	10
C_4	10.0	0	0
C_5	0	0	10.0

Figure 5.8: C coefficient from the linear regression with Guo model.

These constants determine the functional dependencies of the overall noise on the geometry and flow conditions and measurement location. The spherical spreading law is closely observerd by all three components so that is simply assumed the same dependence for all three components. The normalized spectrum F in (5.3) is given for each of the three frequency components, and all three can be expressed in the general form,

$$F(St) = \sum_{n=0}^{5} B_n [log(St)]^n \tag{5.7}$$

where the Strouhal number St is defined by (5.3) and the four constants B_n (n=1,2,3,4) are given in (5.9).

These values are derived by applying linear regression analysis to each of the three frequency domain.

The Mach number dependence is given in (5.6) by the term involving C_1, which, as shown in table, is equal to 60 for the low and mid frequency com-

	Frequency domain		
	Low	Mid	High
B_0	-9.6866	-13.921	-13.389
B_1	1.9071	-5.9695	-10.892
B_2	-3.7577	-3.6107	-9.3852
B_3	0	0.6181	9.2856
B_4	0	0	0.4813
B_5	0	0	-2.4532

Figure 5.9: B coefficient from the linear regression with Guo model.

ponent and 70 for the high frequency domain, respectively corresponding to the sixth and seventh power law. The physics of such different scaling laws for the different frequency components is discussed in the previous section, reflecting the different source behavior.

5.6 Results

In figure (5.10)is showed the SPL predicted with the Guo empirical model for a typical Boeing 737. In figure are also showed the contribution derived from each component. It is visible the increasing contribute at high frequencies deriving from the small features of the landing gear, in agreement with the experimental data and with the physical mechanisms described in previous section.

Figure (5.11) describes the difference predicted by the model between 6-wheel landing gear and 2-wheel landing gear. Obviously the 6-wheel con-

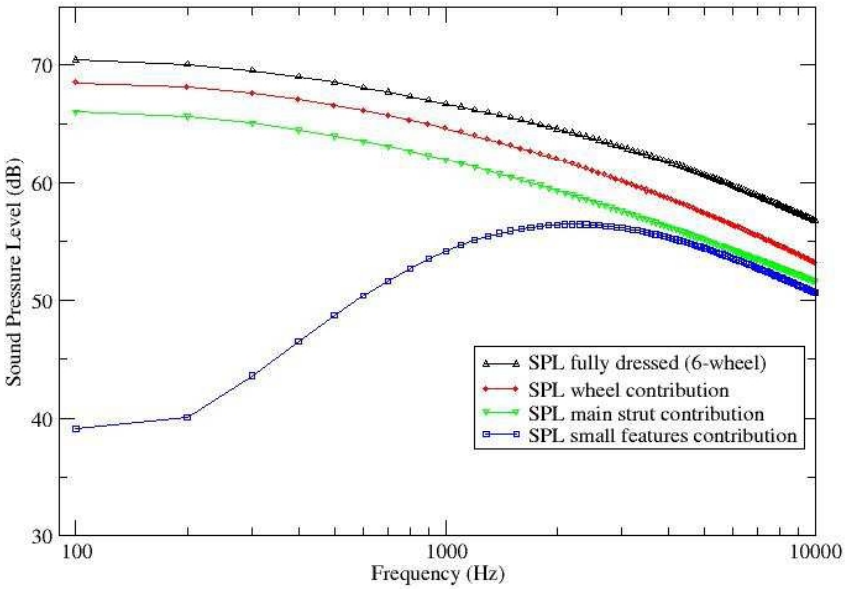

Figure 5.10: Fully dressed landing gear calculated with Guo model (triangles and black line). In red there is the wheel contribution, in green the main struts contribution and in blue the small details contribution.

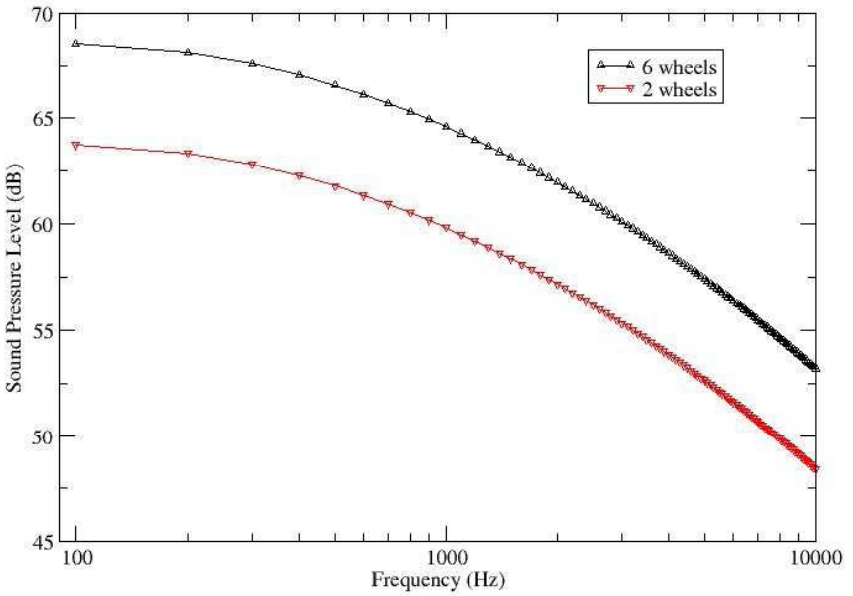

Figure 5.11: 6 wheel configuration, in black, and 2-wheel configuration, in red.

figuration is the noiser one. The difference between these configurations is given by the term $C_4 Log(N_w)$ and corresponds to a difference of 4.8 dB, in agreement with the experimental data described in figure (5.7).

SPL spectra for different microphone angles and for different Mach numbers are showed in figure (5.12). It is important to emphasize that the flow Mach number in the prediction scheme is that just upstream of the gear assembly. Since the test data, on which the prediction guo scheme is based, are for an isolated gear with no installation effects, the Mach number in the database is also the free stream Mach number. When applying the prediction to aircraft landing gears that are installed, the input Mach number, defined

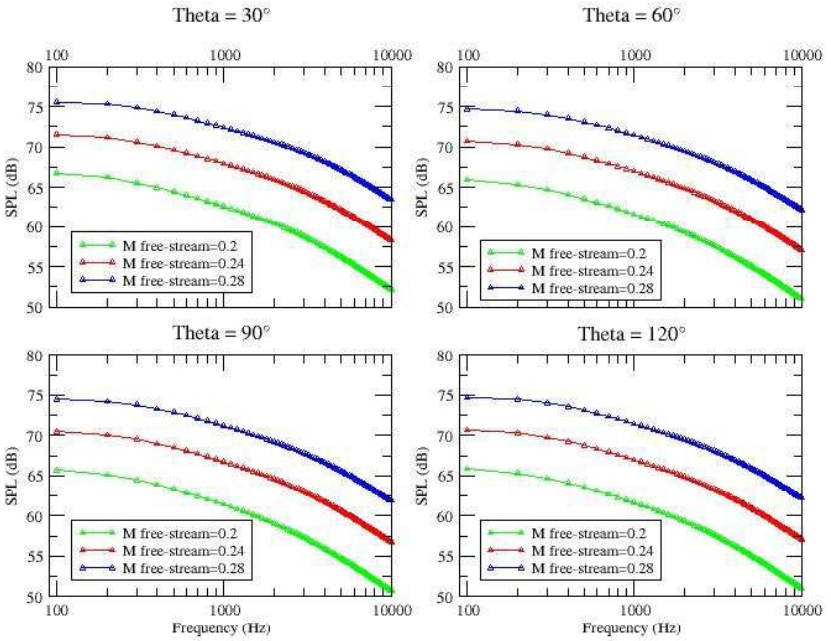

Figure 5.12: Sound pressure level for landing gear for different Mach numbers and different angle of observation.

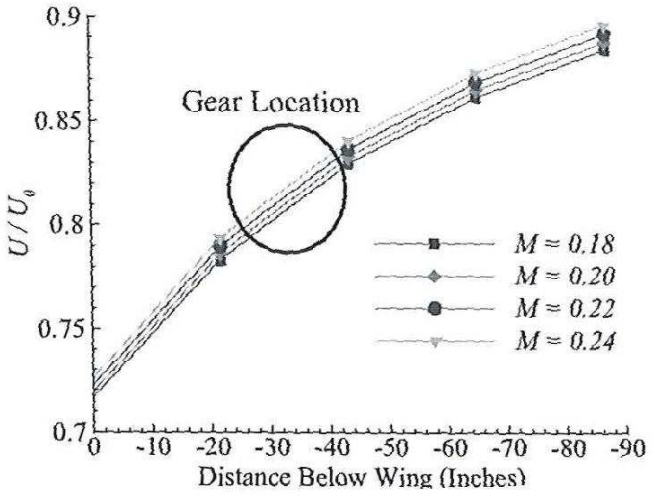

Figure 5.13: Mean flow velocity under the wing for the Boeing 737 aircraft.

as just upstream of the gear, is very often different from the free stream (or flight) Mach number.

For both the main landing gear and the nose gear, the installation effects may noticeable change the local flow. For the main gear, which is located under the wing, the high lift system slows down the flow under the wing, resulting in a smaller local Mach number than the free stream Mach number. For the nose gear, the local Mach number is higher because the flow is accelerated as it passes along the aircraft nose. To demonstrate the effects of this change of local flow conditions, figure (5.13) plots the flow velocity below the Boeing 737 airplane at 4 degrees of angle of attack with flaps deployed at 30 degrees, calculated by using a potential flow method. The velocity is normalized by the free stream velocity and is plotted as a function of the distance from the bottom of the aircraft.

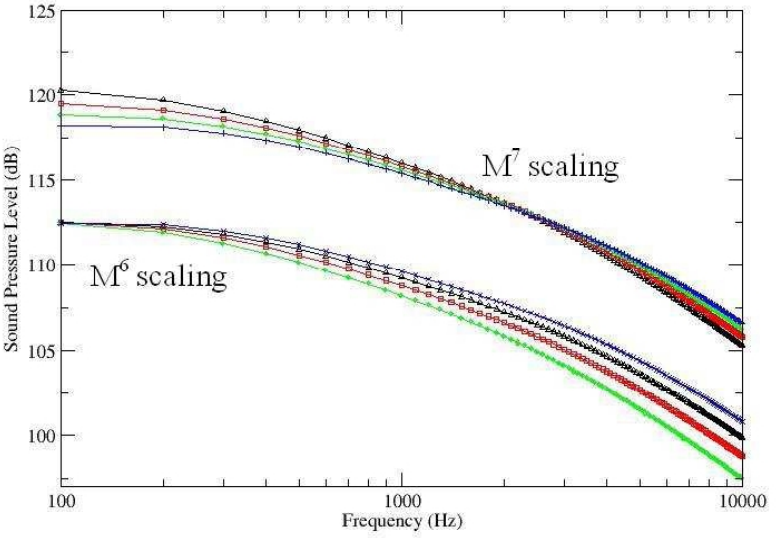

Figure 5.14: Sound pressure level Scaledwith sixth power law and with seventh power law, calculated for different Mach numbers trough the Guo prediction.

The location of the gear assembly is also indicated in the figure. As is shown, the velocity at the gear location is only about 80 percent of the free stream velocity. This variation can lead to significant error in noise prediction: based on the sixth power law, it corresponds to a difference in noise of about 5.8 dB.

Finally, in figure (5.14) is showed the SPl scaled with the Mach sixth power law and Mach seventh power law. As obvious, we can see how the sixth power law approximates better the SPL at low and mid frequencies while the Mach seventh power law gives a better approximations for high frequencies.

5.7 Concluding remarks

An empirical model for the analysis of the noise generated by landing gear has been described.

This empirical model, the Guo model, is derived from the analysis of experimental data taken in Boeing facilities. By testing a series of gear configurations with various degree of complexity, contributions of different gear components to the total noise are revealed.

The landing gear has been cataloged into three groups, namely, the wheels, the main struts and the small details, which generate noise respectively in the low, the mid and the high frequency domain. Parametric trends have been identified for each of the three spectral components in terms of the flow MAch number, gear geometry parameters and microphone locations.

At low and mid frequencies experimental data, and therefore the Guo model, denotes a sixth power law scaling on the flow Mach number, attributing the noise to the unsteady forces on the surfaces of the gear parts.

At low and mid frequencies noise from wheel and main struts is dominant, as confirmed by experimental data, while at higher frequencies there is a more relevant contribute from the small details.

This contribute is described into the Guo model trough a complexity factor, related essentially to aggregate effects (mass of aircraft). The purpose of the use of this empirical model is to predict the landing gear noise of other aircraft, changing the parameters of the model, and to constitute a branch of a suite for a complete noise analysis of the most relevant noise sources generated by an aircraft.

Chapter 6

Conclusion and future applications

The framework of this work is the aeroacoustic. The aeroacoustic is the unification of the fluid-dynamic and the acoustic: that is to say that the source sound is represented by a fluid.
A typical application of the aeroacoustic is the study of the noise generated by an aircraft. In this work, an overview on different kind of aircraft noise sources is provided. The purpose of this overview is to realize a suite in which to insert all the tools developed performing the noise analysis.
This analysis has been developed using analytical, semi-analytical or empirical models. The reason for this strategy is easily explainable.
The starting point for the solving of noise problem in aeroacoustic is to solve the Navier- Stokes equations. Often the numerical methods adopted for the solution of fluid-dynamics equations are too expensive from the computational point of view. For this reason is necessary to adopt a different strategy. The analytical or semi-analytical or empirical approaches lead us to obtain good results with a consistent reduction in computational time and without losing in accuracy.

The noise sources treated are the jet noise, the propeller noise and a component of airframe noise: the landing gear noise.
All these three kind of noise are relevant, or in cruise regime or in landing approach.
The model used for this analysis were: the Tam Auriault model and the Morris Farassat model for the jet mixing noise at subsonic regime, the Shen model for the shock associated noise at supersonic regime.
These models receive inputs from RANS equations, an averaged system of equation describing the turbulence, and using the acoustic analogy or other analytical methods, arrive to an expression for describing the sound pressure spectral density and the sound pressure level.
The propeller noise is described using the Ffwocs Williams Hawkings equations, that are an integral solution of the wave equation representing the acoustic analogy. The results obtained are in good agreement among them and also in comparison with experimenta data found in literature.
The propeller tonal noise has been analyzed in the framework of an international project, named Pplane, in which a concept of personal plane is required. For this reason the input parameters needed for the noise analysis, as blade geometry or thrust provided by the blades, are inserted taking into account some typical value for this size of aircraft.
The results obtained are in good agreement with a numerical solution of the Ffwocs Williams Hawkings equations done by Farassat and permits to have a prediction of the noiser harmonics generated by this kind of noise.
Finally the landing gear noise has been analyzed with an empirical model, the Guo model, based on experimental data of the Boeing. This model distinguishes three different sources: the wheels, the main struts and the small features (hoses, wires) that produces noise in different frequency domains. The results obtained with the Guo model will provide prediction for different sizes of aircraft.

Bibliography

[1] M. J. Lighthill, *On sound generated aerodynamically: I. general theory, Proceedings of the Royal Society of London, Series A: Mathematical and Physical Sciences*, Volume 211, pages 564-587, 1952.

[2] M. J. Lighthill, *On sound generated aerodynamically: II. turbulence as source of sound, Proceedings of the Royal Society of London, Series A: Mathematical and Physical Sciences*, Volume 222, pages 1-32, pages 1-32, 1954.

[3] H. H. Hubbard, *Aeroacoustic of flight vehicles: Theory and practice, Volume 1: Noise Sources*, Nasa Langley Research Center, 1991.

[4] D. Casalino et Al., *Aircraft noise reduction: a bibliography review*, Aerospace Science and Technology, 1-17, 2008.

[5] F. S. Archibald, *Unsteady Kutta Condition at High Values of the Reduced Frequency Parameter*, Journal of Aircraft,Volume 12, pages 545–550.

[6] B. Satyanarayana and S. Davis, *Experimental Studies of Unsteady Trailing-Edge Condition*, AIAA Journal, Volume 16, pages 125-129, 1978.

[7] D. G. Crighton, *Radiation Properties of a Semi-Infinite Vortex Sheet*, Proceedings of the Royal Society of London, Volume =A330, pages 185-193, 1972.

[8] S. A. Orszag and S. C. Crow, *Instability of a Vortex Sheet Leaving a Semi-Infinite Plate*, Studies in Applied Mathematics, Volume 49, pages 167-181, 1970.

[9] D. S. Jones, *Aerodynamic Sound Due to a Source Near a Half-Plane*, Journal of the Institute of Mathematics and its Applications, Volume 9, pages 114-122, 1972.

[10] D. G. Crighton and F. G. Leppington, *Radiation Properties of the Semi-Infinite Vortex Sheet: the Initial Value Problem*, Journal of Fluid Mechanics, Volume 64, pages 393-414, 1974.

[11] S. Davis, *Theory of Discrete Vortex Noise*, AIAA Journal, Volume 13, pages 375-380, 1975.

[12] M. S. Howe, *Contributions to the Theory of Aerodynamic Sound, with Application to Excess Jet Noise and the Theory of the Flute* , Journal of Fluid Mechanics, Volume 71, pages 625-673, 1975.

[13] M. S. Howe, *The Influence of Vortex Shedding on The Generation of Sound by Convected Turbulence* , Journal of Fluid Mechanics, Volume 76, Number 4, pages 711-740, 1976.

[14] M. S. Howe, *A Review of the Theory of Trailing-Edge Noise*, Journal of Sound and Vibration, Volume 61, Number 3, pages 437-465, 1978.

[15] M. S. Howe,*On the Generation of Side-Edge Flap Noise*, Journal of Sound and Vibration, Volume 80, Number 4, pages 555-573, 1982.

[16] J. E. Ffowcs Williams and L. H. Hall, *Aerodynamic Sound Generation by Turbulent Flow in the Vicinity of a Scattering Half-Plane*, Journal of Fluid Mechanics, Volume 40, pages 657-670, 1970.

[17] , *Sound Generated by Turbulence and Surfaces in Arbitrary Motion*, Philosophical Transactions of the Royal Society of London, Series A, Volume A264, Number 1151, pages 321-342, 1969.

[18] D. G. Crighton and F. G. Leppington, *Scattering of Aerodynamic Noise by a Semi-Infinite Compliant Plate*, Journal of Fluid Mechanics, Volume 43, pages 721-736, 1970.

[19] D. G. Crighton and F. G. Leppington, *On the Scattering of Aerodynamic Noise*, Journal of Fluid Mechanics, Volume 46, pages 577-597, 1971.

[20] D. M. Chase, *Noise Radiated from an Edge in Turbulent Flow*, AIAA Journal, Volume 13, Number 8, pages 1041-1047, 1975.

[21] K. L. Chandiramani, *Diffraction of Evanescent Waves, with Applications to Aerodynamically Scattered Sound and Radiation from Unblaffed Plates*, Journal of the Acoustical Society of America, Volume 55, Number 1, pages 19-29, 1974.

[22] , S. W. Rienstra, *Sound Diffraction at a Trailing Edge*, Journal of Fluid Mechanics, Volume 108, pages 443-460, 1981,

[23] R. K. Amiet, *Noise Due to Turbulent Flow Past a Trailing Edge*, Journal of Sound and Vibration, Volume 47, Number 3, pages 387-393, 1976.

[24] , S. Moreau and M. Roger, *Effect of Airfoil Aerodynamic Loading on Trailing Edge Noise Sources*, AIAA Journal, Volume 43, Number 1, pages 41-52, 2004.

[25] , S. Moreau and M. Roger, *Competing Broadband Noise Mechanisms in Low-Speed Axial Fans*, AIAA Journal, Volume 45, Number 1, pages 48-57, 2007.

[26] T. F. Brooks and T. H. Hodgson, *Trailing Edge Noise Prediction from Measured Surface Pressures*, Journal of Sound and Vibration, Volume 78, Number 1, pages 69–117, 1981.

[27] J. C. Hardin, *Noise Radiation from the Side Edges of Flaps*, AIAA Journal, Volume 18, Number 5, pages 549-552, 1980.

[28] M. R. Khorrami et Al., *Unsteady Flow Computations of a Slat with a Blunt Trailing Edge*, AIAA Journal, Volume 38, Number 11, pages 2050-2058, 2000.

[29] C. K. W. Tam and N. Pastouchenko, *Gap Tones*, AIAA Journal, Volume 39, Number 8, pages 1442-1448, 2001.

[30] N. Molin et Al., *Prediction of Low Noise Aircraft Landing Gears and Comparison with Test Results*, AIAA Paper, May 2006.

[31] J. E. Ffowcs Williams and G. Maidanik, *The Mach Wave Field Radiated by Supersonic Turbulent Shear Flows*, Journal of Fluid Mechanics, Volume 21, pages 641-657, 1965.

[32] O. M. Phillips, *On the Generation of Sound by Supersonic Turbulent Shear Layers*, Journal of Fluid Mechanics, Volume 9, pages 1-28, 1960.

[33] G. M. Lilley, *On the noise from jets*, AGARD CP-131, 1974.

[34] M. E. Goldstein, *A Generalized Acoustic Analogy*, Journal of Fluid Mechanics, Volume 488, pages 315-333, 2003.

[35] M. Roger, *Aeroacoustics*, Lecture note of Ecole Centrale de Lyon, Lyon, 2000.

[36] T. F. Balsa, P. R. Gliebe, *Aerodynamics and noise of coaxial jets*, AIAA Journal 15 (11), 1977, pages 15501558.

[37] A. Khavaran, E. A. Kresja, *On the role of anisotropy in turbulent mixing noise*, AIAA Paper 98-2289.

[38] A. Khavaran, J. Bridges, *Modelling of turbulence generated noise in jets*, AIAA Paper 2004-2983.

[39] C. K. W. Tam, L. Auriault, *Jet mixing noise from fine-scale turbulence*, AIAA Journal 37 (2), 1999, pages 145153.

[40] P. J. Morris, F. Farrasat, *Acoustic analogy and alternative theories for jet noise prediction*, AIAA Journal 40 (4), 2002, pages 671680.

[41] J. Bridges, A. Khavaran and C. A. Hunter, *Assessment of current jet noise prediction capabilities*, 2008, AIAA-2008-2993.

[42] C. K. W. Tam, *Jet noise generated by large-scale coherent motion*, H. H. Hubbard (Ed.), Aeroacoustics of Flight Vehicles: Theory and Practice, Volume 1: Noise Sources, NASA Langley Research Center, Hampton, VA, 1991, pages311390.

[43] M. Harper-Bourne, M. J. Fisher, *The noise from shocks waves in supersonic jets. Noise mechanisms*, AGARD-CP-131, 1974, pages 1111113.

[44] C. K. W. Tam, H. K. Tanna, *Shock associated noise of supersonic jets from convergent-divergent nozzles*, Journal of Sound and Vibration 81 (3), 1982, pages 337358.

[45] J. L. Stromberg, D. K. McLaughlin, T. R. Troutt, *Flow field and acoustic properties of a Mach number 0.9 jet at a low Reynolds number*, Journal of Sound and Vibration, Volume 72, Sept. 22, 1980, pages 159-176.

[46] J. Varnier, V. Koudriavtsev, A. Safronov, *Simplified approach of jet aerodynamics with a view to acoustics*, AIAA Journal, Vol. 44, Number 7, July 2006.

[47] R. P. Feynman, R. B. Leighton, and M. Sands, *The Feynman Lectures on Physics*, Vol. 1, AddisonWesley, New York, 1963, Chap. 39.

[48] H. W. Liepman and A. Roshko, *Elements of Gasdynamics*, Wiley, New York, 1957, Chap. 14.

[49] M. Z. Afsar, A. P. Dowling and S. A. Karabasov, *Comparison of jet noise models*, 12th AIAA/CEAS Aeroacoustic Conference, AIAA 2006-2593.

[50] Mollo-Christensen E. , Kolpin M. A. , Martucelli J. R. , 1964 *Experiments on jet flows and jet noise far-field spectra and directivity patterns*, J. Fluid Mech. , Vol. 18, pages 285-301.

[51] Lush P. A., 1971, *Measurement of subsonic jet noise and comparison with theory*, J. Fluid Mech., Vol. 46 , pages 477-500.

[52] Shen, H. et al., *An investigation of Shock cell noise from Model engine nozzles*, AIAA-2008-2839,2008.

[53] Harper-Bourne, M. and Fischer, M. J., *The Noise from Shock Waves in Supersonic Jets*, AGARD, CP-131, pages 1-13, 1973.

[54] Harper-Bourne, M., *On Modelling the near-field noise of the high-speed jet exhausts of combact aircraft*, AIAA 2002-2424, 2002.

[55] Norum, T. D., Brown, M. C., *Simulated high speed flight effects on supersonic jet noise*, AIAA 1993.

[56] Powell, A., *On Mechanism of choked Jet noise*, Proc. Phys. Soc. B., Volume 66, pages 1039-1056,(1953).

[57] Y. P. Guo et Al., *An empirical model for landing gear noise prediction*, 10^{th} AIAA/CEAS Aeroacoustics Conference, 2004-2888.

[58] Burley C. L. et Al., *ANOPP landing-gear noise prediction with comparison to model-scale data*, International Journal of Aeroacoustics, Volume 8, Number 5, pages 445-476, 2009.